

A STUDY OF THE SPECTRA OF LIGHT
SCATTERED FROM SIX LIQUID
BENZENE DERIVATIVES

Submitted by Hazel C. Craddock for the Degree of Ph.D.
of the University of Kent at Canterbury, March 1969.

This thesis is dedicated to my fiancé, Mr. E.C. Lucas,
without whom it would never have been written.

CONTENTS

List of acknowledgements.	page
Preface.	
<u>Chapter 1.</u> General Introduction.	1.1
Section 1. The Liquid Phase.	1.1
Section 2. Experimental techniques for examining liquids.	1.8
<u>Chapter 2.</u> Theory of light-scattering from liquids.	2.1
Section 1. General Introduction.	2.1
Section 2. The Isotropic Spectrum.	2.9
Section 3. The Anisotropic Spectrum.	2.26
<u>Chapter 3.</u> Experimental work.	3.1
<u>Chapter 4.</u> Experimental Results and Discussion.	4.1
Section 1. Experiment I. Preliminary experiment.	4.1
Section 2. Experiment II. Detailed investigation of the scattered light spectra of the six liquids.	4.11
Chlorobenzene.	4.20
Bromobenzene.	4.32
Nitrobenzene.	4.40
Aniline.	4.48
Benzonitrile.	4.54
Benzoyl chloride.	4.61
<u>Chapter 5.</u> Interpretation of results.	5.1
List of references	
Appendix A. Computational analysis of spectra.	
Appendix B. Thermal defocussing in liquids.	

ACKNOWLEDGEMENTS

I wish to acknowledge with much gratitude the invaluable assistance and encouragement of Professor J.G.Powles and Dr. D.A.Jackson during the course of this work.

In addition I should like to thank Prof. G. Rickayzen, Mr.S.E.Binns, and Mr.E.C.Lucas for many useful discussions, and Mr.B.Simic-Glavaski for assistance with some of the experimental work.

I should also like to thank the computer staff for their help and co-operation, and the workshop staff and glassblower for their technical work in the construction of the apparatus. Finally I should like to thank the Science Research Council for the provision of a research studentship.

PREFACE

A study has been undertaken of the spectra of light scattered from six benzene derivatives, chlorobenzene, bromobenzene, nitrobenzene, aniline, benzonitrile and benzoyl chloride. The sources used were He-Ne lasers (20-90 mW), operating in multimode at 6328\AA . The spectra were resolved using a Fabry-Perot interferometer with several spacers. The maximum frequency-change which could be examined was about 20 cm^{-1} ($6 \times 10^{11}\text{ Hz}$), and the minimum was limited by the laser linewidth to about $1 \times 10^9\text{ Hz}$. The scattering angle was 90° . The spectra were recorded over a temperature range from the melting point of the liquids to the boiling point or 160°C .

Light-scattering is caused by thermal fluctuations in parameters which affect the optical dielectric constant of the liquid. The dielectric constant ^{fluctuation} tensor may be written as the sum of a scalar part and a symmetric tensor of zero trace

$$\epsilon_{ik} = \bar{\epsilon} \delta_{ik} + s_{ik} \quad \dots\dots(0.1)$$

where $\bar{\epsilon}$ is scalar dielectric constant. The spectrum of scattered light may be separated experimentally into spectra corresponding to these two parts, by using different directions of polarization of the incident beam. Since the wavelength of light is very much greater than the intermolecular separation, the fluctuations may be considered from a macroscopic viewpoint.

The intensity corresponding to the scalar part is caused principally by isobaric entropy fluctuations and adiabatic pressure fluctuations. The former decay by thermal conduction and give rise to a spectral line at the incident frequency which is too narrow to be measured here. The pressure fluctuations are Debye phonons permeating the liquid. The choice of scattering angle fixes the wave-number of the observed phonons, and these cause a symmetrical Brillouin doublet in the scattered light spectrum. The

Brillouin splitting, of order 5×10^9 Hz, may be related to hypersonic velocity, and the linewidth to sound absorption coefficient. The temperature-variation of these parameters and a comparison with corresponding ultrasonic results, gives evidence for sound dispersion regions at or below the frequency-region 5×10^9 Hz. Varying the temperature changes the characteristic times for different processes in the liquids.

There is evidence for a structural dispersion in aniline, where there is hydrogen-bonding, at about 6×10^9 Hz at 10°C , and thermal dispersion in chlorobenzene and bromobenzene at frequencies below 5×10^9 Hz. The accuracy of hypersonic velocity measurement of 1-2% is inadequate to distinguish small dispersions which may be present in some liquids at hypersonic frequencies. To interpret the results unambiguously it is important to have adequate ultrasonic data. The spectral intensity distribution in all liquids was found to agree closely with that predicted by Montrose et al.*

The intensity corresponding to the symmetric tensor part of eq.(0.1) is due to fluctuations in the orientation of polar molecules, and the existence of shear stress waves in the liquids. The spectrum is centred at the incident frequency and of complex shape, sometimes extending to about 100 cm^{-1} (3×10^{12} Hz). Different parts of the spectrum have different widths characteristic of the processes causing scattering. The use of the Fabry-Perot interferometer limits measurements to the central region of the spectrum, giving the longest decay time, although estimates of shorter times may sometimes be made. The temperature-variation of the intensity in part of the spectrum may give evidence for the process causing that part.

*Montrose et al., 1968, J.Acoust.Soc.Am., 43, 117.

These results show that the central region of the spectrum in all cases is largely, but not entirely, determined by molecular reorientation, and is closely associated with the mechanism of shear viscous flow.

Nitrobenzene, and possibly aniline, show anomalous behaviour in that shear waves also contribute to the central region of the spectrum, decaying by molecular reorientation. There is no conclusive evidence for scattering from shear-waves in the other liquids, although this may contribute to the broader wings of the spectrum.

ERRATA

1. P. 1.4, line 8, after "where ρ is number density", insert " ρ_0 is average number density, T_0 average temperature, p pressure, and k Boltzmann's constant. The brackets $\langle \rangle$ imply an ensemble average over all states of the system."
2. P. 2.34, line 20, after "in the liquids considered here" replace the rest of the sentence by "there is an appreciable contribution to the induced polarizability in directions other than the major axis for permanent dipole moment and moment of inertia."
3. Replace "bulk" by "longitudinal" in the following lines: p. 4.16, lines 2,12,15, p. 4.17, line 3, p. 4.24, title of fig. 4.10, p. 4.26, lines 2, 16, p. 4.37, title of fig. 4.17, p. 4.41, line 18, p. 5.1, line 23, p. 5.2, lines 5,6,9,12,18.

CHAPTER 1

SECTION 1. The Liquid Phase.

At present, the liquid phase is the least clearly understood of the three phases of matter. There are a large number of unresolved theoretical and experimental questions, and the work of the theoreticians, which involves very complicated mathematics, while sometimes giving the main features of the experimental results, is as yet unable to predict the values of most experimental parameters with any accuracy.

There are several reasons underlying this. One is that for the liquid phase there is no convenient zero-order approximation. In a rarefied gas, to zero-order approximation, the intermolecular interactions are neglected and the thermal energy of the molecules is entirely kinetic. This leads, for example, to the equation of state for a perfect gas. The effects of collisions may be included by assuming that the molecules are hard spheres. This means that the intermolecular interactions are zero in between collisions, and there is a well-defined mean-free-path. Results thus obtained are corrected, but not altered in essence, by the introduction of more sophisticated assumptions. In a solid, it is assumed that each atom occupies a well-defined lattice-site in the position of minimum potential energy in the field of its neighbours. Except in glasses, the structure is spatially periodic, on average, for long time-periods. It is assumed that the thermal energy is entirely potential; the atomic motion is vibrational, and may be described by a spectrum of Debye waves or phonons

permeating the solid. In contrast, the liquid phase is one in which there is continual ~~diffusion and vibration of all the molecules~~, both translational and rotational motion. There is no long-range order, and short-range order persists only for short times. The molecules never become separated by a sufficient distance to have a negligible effect on each other's motion, so a mean-free-path cannot be defined. Each molecule is in the continuously varying field of many neighbours. However, an insight into the molecular motion may be gained by considering the time-scale on which different types of motion occur. It may be observed that the liquid responds as a fluid to slowly-varying disturbances; for example it flows with characteristic shear viscosity under the application of a stress gradient. If, however, an alternating stress of high frequency (of the order 10^{12} - 10^{13} Hz) is applied, the liquid responds like a solid, and exhibits a shear rigidity, with a modulus which does not differ markedly from that observed in the solid state. An early concept put forward to incorporate this situation was that of Frenkel (1), who suggested that the molecule remained in a fixed position relative to its nearest neighbours for a characteristic time τ , during which it executed vibrational motion, and after which it diffused to another position. This idea leads, for example, to the experimentally observed variation of the self-diffusion coefficient with temperature.

$$D \sim \exp(-W/kT) \quad \dots\dots(1.1)$$

where W is the activation energy required to leave the fixed site, and

D the self-diffusion coefficient. The liquid state may be described by a number of relaxation times, which characterise the response of individual molecules or macroscopic parameters to different types of disturbance from equilibrium. The classical hydrodynamic theory may then be modified to include elastic effects at high frequencies. Such theories predict (5) that in the case of shear stress, the appropriate time is the Maxwell viscoelastic relaxation time, of order 10^{-12} sec., given by

$$\tau_M = \eta / G \quad \dots\dots\dots(1.2)$$

where G is modulus of shear rigidity for very high frequencies, and η is low-frequency coefficient of ^{shear}viscosity. For disturbances faster than this, the diffusional motion of the molecules cannot follow the applied stress, so their response is limited to forced vibration. The liquid may be described macroscopically by such parameters as pressure, entropy, density, which have average values equal to their equilibrium values. However, at any point in the liquid, these parameters are varying in time about their equilibrium values, as the thermal energy is being exchanged continuously between one degree of freedom and another. So the field surrounding a given molecule is continuously varying. These difficulties arise even with atoms. If the molecules are anisotropic so that the intermolecular forces are non-central, or of complex internal structure, the situation is complicated yet further.

The two most fruitful techniques which have been applied to the study of the liquid state, are the method of statistical thermodynamics, approaching the problem from a macroscopic viewpoint, and the method of molecular distribution functions, from the microscopic. The fluctuations

in thermodynamic quantities may be Fourier analysed spatially, and in the long wavelength limit of such fluctuations, the two approaches must lead to the same conclusions. The approach of statistical thermodynamics may be used to calculate the fluctuations in the liquid in terms of measured experimental parameters. For example, the mean square density fluctuation is related to the isothermal compressibility by

$$\frac{kT}{\rho_0} \left(\frac{\partial \rho_0}{\partial P} \right)_T = \langle \rho^2 \rangle - \rho_0^2 \quad \dots\dots(1.3)$$

where ρ is number density. If required, the liquid structure may be introduced via a structure factor ξ , or set of such structure factors.

The distribution function approach considers the statistical averages of microscopic parameters of individual molecules, their variation with time, and the probability of their values being related to those of neighbouring molecules. The molecular motion may be described by a whole series of space- and time-dependent correlation functions of position, velocity, stress, etc. These make it possible to take the ensemble average of a desired quantity over a large number of molecules, and hence obtain macroscopic parameters. For example, the radial distribution function is particularly important. It gives the probability that, at a given moment, there is a molecule at \underline{r} and another at \underline{r}' . It is given by

$$g(\underline{r} - \underline{r}') = 1/\rho_0 \left\langle \sum_{i \neq j} \delta(\underline{r} - \underline{r}_i) \delta((\underline{r}' - \underline{r}) - (\underline{r}_j - \underline{r}_i)) \right\rangle \quad \dots\dots(1.4)$$

The correlation function for number density $\rho(\underline{r})$ is closely related to it. ($\rho(\underline{r})$ is the average number of molecules in $d\underline{r}$ at \underline{r})

The correlation function for $\rho(r)$ is given by

$$\langle \rho(r) \rho(r') \rangle = \rho_0^2 (g(r-r') + \delta(r-r')) \quad \dots\dots\dots(1.5)$$

A typical form of $g(r-r')$ at different temperatures is shown in fig. 1.1. This illustrates the decrease in short-range order with increase in temperature, and the increase in "free volume" surrounding a molecule. Clearly such a function will be angle-dependent for polar and anisotropic molecules.

The density-density correlation function may also be used to calculate the mean-square fluctuation in number density. In the long-wavelength limit, the result is directly comparable with eq. (1.3). The comparison gives: (ref. (5))

$$\frac{1}{\rho_0} \left(\frac{\partial \rho_0}{\partial p} \right)_T = \frac{1}{kT} \lim_{q \rightarrow 0} \left[1 + \rho_0 \int (g(r) - 1) \exp(i\mathbf{q} \cdot \mathbf{r}) d\mathbf{r} \right] \quad \dots(1.6)$$

At a given temperature, such distribution functions depend on the intermolecular potential. However, since many-body interactions must be taken into account and the pair potential is not unambiguously known even for atoms, little progress has been made in calculating one from the other. A more generally useful approach is to measure important distribution functions and predict experimental quantities from these, or vice versa.

Another important distribution function is the time-dependent radial distribution function. This is the probability that there is a molecule at \underline{r} at time zero, and the same or another molecule at \underline{r}' from it at time τ later.

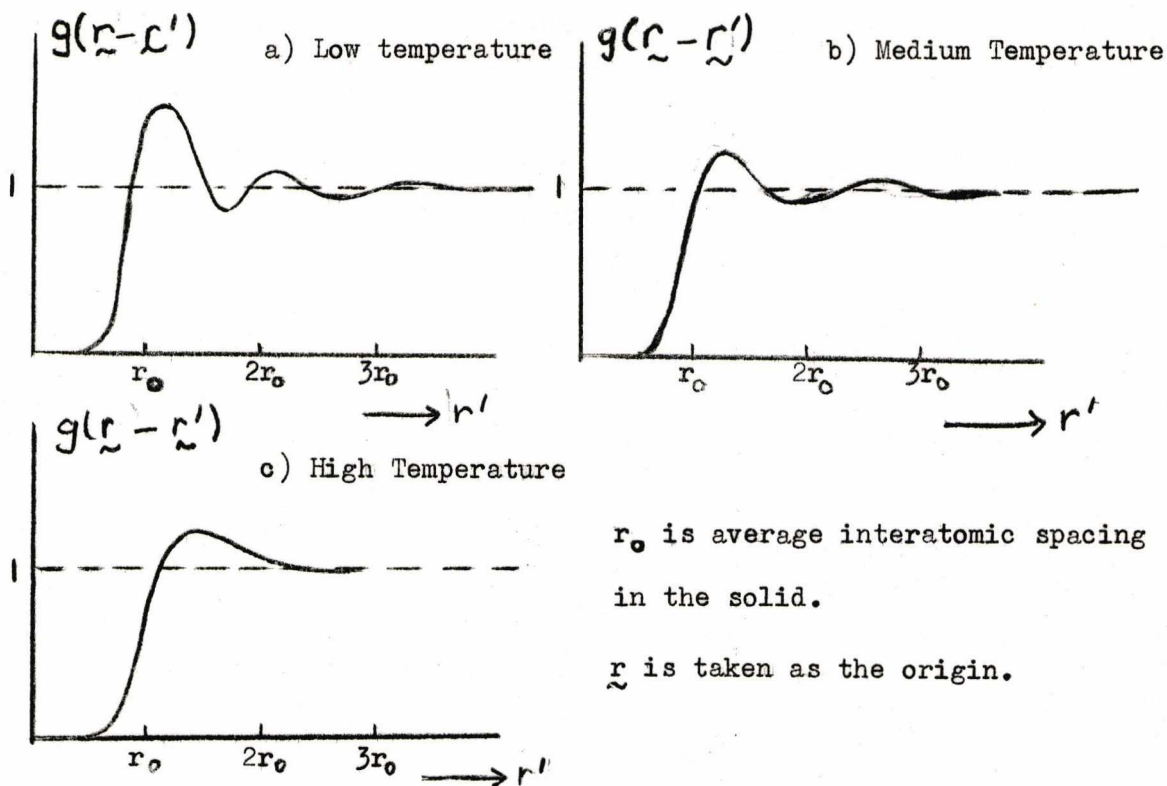


Fig. 1.1 Radial distribution function and its variation with temperature. Schematic diagram for atomic liquid.

* * * * *

The time-dependent distribution function is given by

$$G(\tilde{r}', \tau) = \frac{1}{n} \left\langle \sum_{i,j} \int d\tilde{r} \delta(\tilde{r}' + \tilde{r}_i(0) - \tilde{r}) \delta(\tilde{r} - \tilde{r}_j(\tau)) \right\rangle \dots (1.7)$$

The time-dependence of this function clearly depends on the motion of the molecules. It may consist of several terms, corresponding, for example, to diffusion and vibration. It may sometimes be usefully divided into a "self" ($i=j$) term and a "distinct" ($i \neq j$) term, particularly for experimental methods where it is possible to study the motion of single molecules. The "self" term will decrease approximately exponentially with τ in the case of simple diffusion, but will have an

oscillatory component if the molecule also vibrates.

In the light of this discussion, it is useful to consider some of the different experimental techniques which are in current use for obtaining information about liquids, and discuss the information each is likely to give. These techniques will be considered in turn, and then reviewed with relation to the information which may be obtained from light-scattering.

SECTION 2. Experimental Techniques for Examining Liquids.

i) Scattering techniques.

The comparison of results obtained from different scattering techniques has been dealt with by Egelstaff (2,3,4,5) among others. His basic concept is the scattering function $S(\underline{Q}, \omega)$, which is the probability of the scattering radiation imparting a momentum $\hbar \underline{Q}$ and energy $\hbar \omega$ to the liquid. Functions of energy and momentum may be obtained by Fourier transforming functions of space and time. (Van Hove 1954, (6)). For example, $S(\underline{Q}, \omega)$ is closely related to the double Fourier transform of $G(\underline{r}, \tau)$.

In all scattering experiments, \underline{Q} is fixed by the wavenumber of the incident radiation and the angle of observation, according to the equation

$$Q^2 = k^2 + k_0^2 - 2kk_0 \cos \Theta \quad \dots\dots\dots(1.8)$$

where k_0, k are the wave-numbers of the incident and scattered radiation respectively, and Θ is the scattering angle. The total intensity may be recorded at each angle, giving $S(\underline{Q})$, the structure factor, where

$$S(\underline{Q}) = \int_0^\infty S(\underline{Q}, \omega) d\omega = \left[1 + \rho \int (g(\underline{r}) - 1) \exp(i\underline{Q} \cdot \underline{r}) d\underline{r} \right] \quad \dots\dots(1.9)$$

showing the relation between this quantity and the radial distribution function. Spectral analysis of the intensity may be made at each value of \underline{Q} , to give $S(\underline{Q}, \omega)$.

$S(\underline{Q}, \omega)$, like $G(\underline{r}, \tau)$, may be divided into "self" and "distinct" terms. The "self" term reflects motion of a single molecule, and the "distinct" term collective motion which may involve large numbers of

molecules. High Q techniques ($Q > 1/d$, where d is average molecular separation) enable the study of the motion of single molecules. Low Q techniques make it possible to study both long-wavelength collective modes and the long wavelength components of random fluctuations of single particle parameters. To cover the entire range of Q, ω , a wide variety of scattering techniques are needed. Rather than attempt to obtain $G(r, \tau)$ by Fourier transformation, for which it is necessary to know $S(Q, \omega)$ over the entire range of Q, ω , it is often more feasible and useful to relate $S(Q, \omega)$ to correlation functions of the transport coefficients. For example, Egelstaff (3) has related the "self" part of $S(Q, \omega)$ to the velocity correlation function, and for a particular value of $|Q|$, has shown that the effects of diffusion, lattice vibration, rotation and internal vibration may be separated, using results for water.

X-rays are of the correct wavelength to study single atoms (very high Q), and if a study is made of the variation of total intensity with angle ($S(Q)$), the radial distribution function may be obtained. However, they have insufficient resolution to give relaxation times. (57). Mossbauer γ -rays also have very high Q , but the energy resolution is so high that only very slow diffusion times in very viscous liquids may be measured. (58) Neutron scattering covers a wide range of Q and ω , whereas light-scattering has a wide energy-resolution, but is concerned only with low Q -values, or the macroscopic limit of the distribution function approach. Neutron scattering may be divided into "coherent" and "incoherent" scattering. For incoherent scattering, the intensity and phase of radiation scattered from one molecule are completely unrelated to those from the next. Coherent scattering relates to lower momentum collective motion, but may not be extended

to values of Q used in light-scattering.

The reorientation of single molecules may be studied by incoherent neutron scattering, and such relaxation times for reorientation, if available, may be compared with light-scattering relaxation times from the orientational part of the spectrum. However, two difficulties arise in making such a comparison. The orientational self correlation function, which is the probability that if the direction Ω_0 defines the molecular orientation at time zero, the direction Ω does so at time t , may be expanded as a series of spherical Legendre polynomials.

$$P(\Omega_0, 0 / \Omega, t) \propto \sum_{l=0}^{\infty} \sum_{m=-l}^l Y_{l,m}^*(\theta_0, \phi_0) Y_{l,m}(\theta, \phi) \cdot f_l(t) \dots\dots\dots (1.10)$$

where angles (θ_0, ϕ_0) and (θ, ϕ) define the directions Ω_0, Ω .

Incoherent neutron scattering measures all the Legendre components of this function, whereas light-scattering measures only the $l=2$ components. Also light-scattering measures long-wavelength fluctuations in dielectric constant, and it is not obvious that times for the decay of such fluctuations are identical to those obtained for a single molecule.

The energy range available to light-scattering is quite high, again incorporating a variety of techniques. It includes the recently developed "self-beating spectrometer" (7) for measuring the width of the central Rayleigh line, which is due to thermal diffusion, and less than 10^6 Hz or 10^{-5} cm^{-1} (resolution $> 1:10^8$), and the Raman spectrometer, which observes lines shifted by several hundred cm^{-1} (about 10^{13} Hz). The range under consideration in this work is that limited by the Fabry-Perot interferometer, which is about $0.01 - 10$ cm^{-1} , or $3 \times 10^8 - 3 \times 10^{10}$ Hz. The value of Q is defined by the wavelength of the light and the

angle of observation, being given by

$$1/Q = \lambda_S = \lambda_0 / (2n \sin \Theta/2) \quad \dots\dots\dots (1.11)$$

where λ_S = wavelength of sound

λ_0 = wavelength of light in free space

n = refractive index of medium

Θ = scattering angle.

This formula is derived directly from eq. (1.8) in the case of negligible energy transfer.. ($|k| = |k'|$). The value of λ_0 being several thousand Angstrom units, λ_S also is many times longer than the intermolecular separation, and fluctuation theory, involving macroscopic concepts, is appropriate. The light is scattered as a result of fluctuations in the refractive index, which reflect those of density, temperature, and stress in the medium, and include such motions as the passage of thermal phonons through the liquid, the diffusion of entropy fluctuations, and the variation in orientation of molecules or groups of molecules.

Hence it is important, in a survey of techniques which lead to results directly comparable with those of light-scattering, to consider ways of measuring these last parameters other than scattering techniques.

ii). Nuclear magnetic resonance.

In this method the molecular motion is studied by its effect on the atomic nucleus. A constant magnetic field defines the nuclear spin states, and the temperature the distribution of nuclear spins among them. The population distribution is disturbed (for example, by the application of a 90° r.f. pulse) and its relaxation towards equilibrium observed. The most common interaction inducing relaxation in the liquids we are concerned with is the magnetic dipole-dipole interaction between nuclei possessing spin $\gg \frac{1}{2}$. Contributions to the relaxation from nuclei within the same molecule and those in others may be separated. Since the interactions between the nucleus and other degrees of freedom of the system are negligible compared with that between the magnetic moments and the main magnetic field, the molecule rotates as a whole without affecting the alignment of the nuclei. The molecular motion varies the relative positions and orientations of nuclei, and hence the magnetic interaction between them, and it is this varying magnetic field which induces transitions between the nuclear spin states. So from the relaxation of the nuclei, by postulating a suitable model, times for reorientation and translation of the molecule as a whole may be derived.

A similar technique is that of nuclear quadrupole resonance, where the electric quadrupole moment of the nucleus interacts with varying electric field gradients at the site of the nucleus. This technique also yields molecular reorientation times in suitable cases.

Like light-scattering, both these techniques pick out the $l=2$ term in the expansion (1.10).

iii). Dielectric relaxation.

In this method the response of molecules with a permanent dipole moment to an applied electric field is studied. Since this interaction has an angle-dependence of $\cos \theta$, (where θ is the angle between dipole and field), this method picks out the $l=1$ term in expansion (1.10). Reorientation times of order 10^{-11} s., which are often observed, correspond to wavelengths in the microwave region. The frequency is varied, and the wavelength for maximum dielectric loss determined. The polar molecules may be studied in mixtures with molecules of small dipole moment, or as pure solute, to observe the effects of the different intermolecular interactions, or the temperature may be varied. The width of the distribution of relaxation times gives an estimate of the complexity of the movements needed for reorientation to occur.

For example, Curtis et al. (8) discuss the dependence of the reorientation times on rigidity, shape, dipole moment and shear viscosity for a number of polar molecules.

Such an experiment differs from a light-scattering experiment in a number of ways. One is that it studies the response of the permanent dipole moment to an externally applied field, whereas light-scattering observes random fluctuations in the induced polarizability. The axes for induced polarizability and dipole moment are not necessarily coincident, and one axis for reorientation may be preferred. Also, if the angle-dependent intermolecular interactions are strong, the external electric field, in partially aligning the molecules, will cause the local field surrounding a molecule to differ from its value in the unperturbed situation, particularly at frequencies below the relaxation. Like nuclear

magnetic resonance, this method measures the relaxation time for single molecules, rather than fluctuations in a macroscopic variable. These considerations will be discussed further in connection with the experimental results in chapter 4.

iv) Ultrasonics.

This extensively developed field is another method of examining the behaviour of extremely long wavelength density fluctuations. It gives similar information to that obtained by examining the light scattered from thermal phonons in liquids, with two basic differences. The first is that the ultrasound is generated in the liquid by a vibrating quartz crystal, rather than being a spontaneous fluctuation due to the thermal energy. The second is a consequence of this; that this technique has a limited frequency range. In the past this has been due to the difficulty of generating waves above about 10^7 Hz, although recently oscillation of a quartz radiator at 10^{10} Hz has been obtained. (9). However, the absorption of sound at these frequencies is so great that the investigation of hypersound by this method has so far proved impossible. (Using incident light of a single wavelength, the light-scattering technique can examine a range of frequency of about 10^9 - 10^{10} Hz.)

A large amount of ultrasonic data on the velocity and absorption of sound-waves has been collected; indeed, this made possible the first classification of liquids. (10). From the results, values for parameters such as the modulus of elasticity and shear and bulk viscosity have been obtained. The frequency regions where dispersion of the sound waves and ~~maxima~~ maxima in the absorption occur are of particular interest to workers in the field. At very low frequencies, when an external pressure gradient is applied, the liquid attains equilibrium under the new conditions, each degree of freedom taking a characteristic time τ . As the frequency is increased above $1/\tau$ for the slowest process, the corresponding

degree of freedom can no longer follow the alternating pressure gradient and will "freeze out", so that the velocity changes from its low-frequency value. A number of possible causes for dispersion have been considered. Energy may be exchanged with the internal degrees of freedom of the molecules. This gives rise to a relaxing, or frequency-dependent specific heat. Alternatively, energy may be exchanged with structural reorganization in the liquid, which is expressed through a relaxing volume or shear viscosity. Dispersion has also been observed in molecules exhibiting rotational isomerism. For a detailed study of dispersion, see Herzfeld and Litovitz (11). Further information is obtained from considerations of whether a single relaxation time will describe the observed data, or whether a distribution of such relaxation times is needed. cf Kono et. al. (12) The existence of a distribution of relaxation times may indicate that a complex process, possibly involving several molecules, is necessary for the energy transfer to occur.

Dispersion regions in some liquids occur within the frequency range available to ultrasonic techniques. However, in many liquids, no dispersion has been observed within this frequency range, although values of the absorption at low frequency may be used to predict the approximate dispersion range, assuming likely causes for the dispersion. For example, Herzfeld and Litovitz, ch.11, p. 407, predict a dispersion in benzene at about 1×10^9 Hz due to relaxing internal specific heat. This is precisely the region accessible to light-scattering. However, equations predicting such regions are based on some model of the liquid, and the results are only approximate. Information about the propagation of hypersound in high frequency regions helps to clarify these matters,

although some dispersion effects only change the low-frequency sound velocity by a fraction of a percent and may pass unnoticed. The occurrence of a maximum in the curve of absorption against frequency may be a more sensitive test of the existence of such dispersion regions. The relaxation of shear and volume viscosity, has a Maxwell relaxation time (assumed equal for the two cases), of

$$\tau_M = \eta/G = \eta'/B \dots\dots\dots(1.12)$$

- where η = shear viscosity
- η' = volume or bulk viscosity
- G = modulus of rigidity
- B = modulus of compressibility

This gives a dispersion in the region of 10^{12} Hz for simple liquids (calculating from ultrasonic data for chlorobenzene) which is beyond the frequency range available to light-scattering techniques using visible light.

It is possible that as well as sustaining longitudinal pressure waves, liquids may, at high frequencies, sustain transverse shear stress waves. Such waves would be very heavily damped, and impossible to study using ultrasonic techniques. However, the refractive index would be changed by such variations in shear stress, so light scattering is a possible method for detecting such waves, if they exist spontaneously, and measuring their properties.

v). Review of results from different experimental techniques.

The spectrum of scattered light contains information about several different processes in the liquid. These will be summarised below.

a) Collective processes involving many molecules. These propagate as waves and Doppler shift the frequency of the scattered light according to their velocity. The width and shape of the peaks ^{in the scattered light spectrum} centred on these frequencies depend on the decay-time of the mode and the means of decay. Two such modes have been discussed.

ai) Longitudinal thermal sound waves, existing spontaneously in the liquid. Their velocity and absorption, and the variation of these with frequency (which may be varied by changing θ , and hence Q), may be measured. The variation of velocity and absorption with temperature may also be obtained. Such results are directly comparable with those of ultrasonics. The width of the scattered light peaks gives the lifetime of the propagating mode. If dispersion may be observed, the relaxation time τ_{dis} gives the time of response to a pressure gradient, of the dispersive mode coupled to the lattice vibration. If the dispersion is caused by a relaxing viscosity, τ_{dis} may be compared with reorientational relaxation times to give information about the structural relaxation process.

aii) Transverse thermal shear waves. Again the velocity and absorption may be measured. Light-scattering appears to be the only technique suitable for observing these waves. The lifetime of the mode may be obtained from the width of the corresponding peak. If these decay by molecular reorientation, their lifetime may be compared with times for reorientation of single molecules, and also structural relaxation times

which may be rate-determining in molecular reorientation processes. (cf Montrose and Litovitz (1968), (13)).

b) Single particle processes or self-scattering. Certain parameters affecting the dielectric constant vary spontaneously and randomly in space. These fluctuations have a spatial Fourier component of wave-number Q . Their decay is governed by the motion of single molecules. Two such processes give rise to components in the scattered light spectrum.

bi) Local isobaric entropy fluctuations. These give rise to the central Rayleigh line. They decay by thermal diffusion, which is a slow process (about 10^{-6} sec.) and the Rayleigh line is too narrow for its width and shape to be studied with the apparatus used in this work, so it will not be considered further.

bii) Fluctuations in orientation of the molecules. These give rise to that part of the depolarised background to the scattered light spectrum which is the Fourier transform of the correlation function for orientation; this is centred on the incident frequency. This is complex in shape, but it is fairly clear that parts correspond to molecular orientational diffusion and vibration. Times for these processes may be obtained and compared with those from n.m.r., dielectric relaxation and incoherent neutron scattering, subject to the limitations already discussed. They may also be compared with results from the collective modes as indicated above.

The depolarised spectrum contains light scattered due to effects aii and bii above, and may not easily be separated into the two parts. This is further discussed in chapters 2 and 4.5

CHAPTER 2.Theory of light-scattering from liquids.

The theory will first be examined from the standpoint of statistical thermodynamics, which leads to some general features of the results, but does not take into account microscopic effects such as the different types of frequency-dependent relaxation. It will then be reconsidered in more detail from two standpoints. Firstly the spectrum of light scattered from the scalar part of the fluctuations in dielectric constant will be considered, and from now on this will be called the isotropic spectrum. Secondly the light scattered from the shear part of the fluctuations will be treated, and will be referred to as the anisotropic spectrum.

i). General introduction.

The light-wave incident on a molecule may induce several effects. It may cause transitions between the rotational, vibrational or electronic energy levels, with clearly defined energy change. (Inelastic scattering). It will cause the molecule to oscillate as a dipole, and the energy of the light is changed only by a small amount due to the motion of the molecule. (Quasi-elastic scattering). The inelastic scattering is Raman scattering and will not be considered in this work.* The dipolar response of the molecule to the electric field is the basis of Rayleigh scattering.

* * * * *

*The vibrational and electronic lines remain distinct in the liquid state. The rotational levels are smeared out and contribute to the anisotropic spectrum of the quasi-elastic scattering.

If light of wavelength λ illuminates a large number of identical molecules, uniformly distributed, the sum of the radiated fields leads to a non-zero intensity in the forward direction only. Scattering in other directions only occurs when there are inhomogeneities in the distribution of the molecules, differences in their polarizability, or generally, variation in some parameter affecting the dielectric constant. Rayleigh originally considered a dilute gas of non-interacting particles of size much less than λ , separation much greater than λ , and obtained the formula (ref. (59))

$$i / I \propto \frac{\rho_0 \alpha^2}{\lambda^4 r^2} (1 + \cos^2 \theta) \quad \dots\dots (2.1)$$

for unpolarized incident light, where

i = intensity of scattered light

I = intensity of incident light

ρ_0 = number of particles per unit volume

α = polarizability of one particle

r = distance of observer from scattering region

θ = angle of scattering.

For the case of liquids, the assumption of non-interacting particles is clearly untenable, so Einstein (15) applied the same considerations to a system of non-interacting spheres of liquid, each large enough to contain many molecules but of dimensions much less than λ , and of dielectric constant $\Delta\epsilon + \epsilon_0$ slightly different from the average, ϵ_0 . He showed that

$$\langle \Delta\epsilon^2 \rangle \propto \alpha^2 \quad \dots\dots (2.2)$$

could be substituted into equation (2.1), and the scattering formula was

essentially the same. This holds except near the critical point, where the very high compressibility means that the correlation range for density fluctuations is no longer much less than the wavelength, and the assumption of independent fluctuations is invalid.

Hence the scattering intensity may be obtained by considering the different parameters causing fluctuations in the dielectric constant. The time-variation of these fluctuations, (which in every case is very slow compared with the time-variation of the electric field of the light wave) modulates the frequency and gives rise to the observed spectrum. It should be noted that the total scattered intensity due to inhomogeneities in the medium is extremely small, being smaller than the incident intensity by a factor of about 10^{-6} . The presence of large particles of dust, size comparable to λ , gives rise to scattering of such intensity that the Rayleigh scattering may be negligible in comparison.

We assume that the liquid is dust-free. There are several possible contributions to fluctuations in the optical dielectric constant, all of which, if applicable, arise spontaneously due to the exchange of thermal energy between modes within the liquid. These are listed below.

- a). Fluctuations in concentration, which arise in liquid mixtures and decay by diffusion. These would give rise to a line at the incident frequency in the isotropic spectrum, of width governed by the diffusion time. Since pure liquids are being considered in this work, this contribution will be ignored.
- b). Fluctuations in density.
- c). Fluctuations in temperature.
- d). The possibility of different internal structures of the molecule,

causing a variation in polarizability from one molecule to the next. This might well be important in complex or flexible molecules. It seems likely that there would be no correlation of this between one molecule and the next, but it would have a similar effect to fluctuations in concentration, and additional dispersive effects on the other modes if the internal structure were coupled to the surroundings.

e). Independent and statistical fluctuations in the orientations of anisotropic molecules.

f). Fluctuations in stress. The stress tensor may be divided into two components;

$$\sigma_{\alpha\beta} = \sigma'_{\alpha\beta} + \sigma\delta_{\alpha\beta} \quad \dots\dots\dots (2.2)$$

where $\sigma_{\alpha\beta}$ is stress tensor

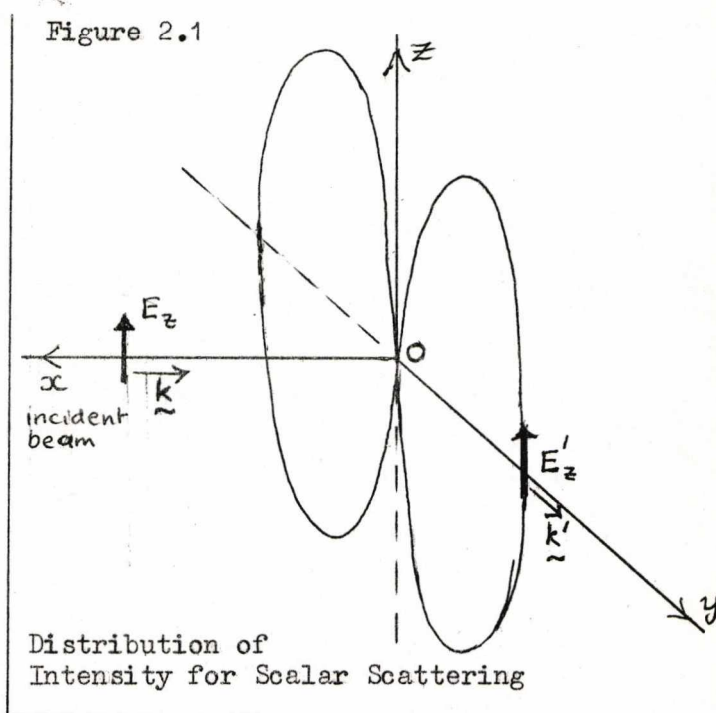
$\sigma'_{\alpha\beta}$ is pure shear stress tensor,

$\sigma = \frac{1}{3} \sum_{\alpha} \sigma_{\alpha\alpha}$ is scalar stress, which is equal to the hydrostatic pressure and of opposite sign.

The scalar stress, or pressure fluctuations, have already been accounted for in contributions(b) and (c), as will be shown below. The fluctuations in shear stress arise from the non-central forces between the molecules and include the shear waves mentioned in chapter 1.

The time variation of these different fluctuations will be governed by different processes, and if they decay with sufficiently different times, they should be separable in the light-scattering spectrum. Also their effects on the polarization of the scattered light will be different. Fluctuations which are scalar in nature (effects a,b,c,d) will have a polarization vector parallel to the incident electric field,

and the scattered light will be correspondingly dipolar in intensity distribution and polarization. See figure 2.1. There is no scattered intensity in the z-direction, and the scattered light observed in the y-direction is completely polarized in the z-direction. In contrast, fluctuations



which cause anisotropy of the dielectric constant (ϵ and the pure shear part of f), give rise to that part of the polarization which is not parallel to the incident electric field. As a result, there will be light scattered in the z-direction, and light polarized in the x-direction observed along 0-y. The scalar and anisotropy contributions may be separated by observing the light scattered first along 0-z and then along 0-y, or by analysing the light scattered along 0-y into the components of polarization parallel to x and z. The anisotropic spectrum may thus be separated from the isotropic, and the ratio of the total intensity in the two spectra is a measure of the molecular anisotropy. A more detailed separation of the effects within the two spectra is more difficult.

The relationship between the intensities in the spectra and the molecular anisotropy is given by the following equations: (Cabannes, (53)), (36)

$$\Delta^2 = \frac{5\rho_u}{(6-7\rho_u)} (\rho_0 k T \beta_T) \dots\dots\dots (2.3)$$

where Δ^2 is molecular anisotropy, β_T isothermal compressibility, ρ_u is the depolarization ratio for unpolarized incident light, defined as the ratio of the intensity of light polarized in the x-direction to that polarized in the z-direction observed along 0-y (incident light in the x-direction as in fig. 2.1).

The same quantity may also be obtained using light polarized in the z-direction by measuring the ratio of the total intensity of light scattered in the z-direction to that scattered in the y-direction.

It may also be obtained from the depolarization ratio for polarized incident light ρ_v (defined as above, but for vertically polarized light) from the relation

$$\rho_u = \frac{2 \cdot \rho_v}{1 + \rho_v} \quad \dots\dots (2.4)$$

The light is completely depolarized when $\rho_u = 6/7$, or $\rho_v = 3/4$.

For a perfect gas, Δ^2 is related to the principle polarizabilities of a single molecule, $\alpha_1, \alpha_2, \alpha_3$, via the relation

$$\Delta^2 = \frac{1}{2} \cdot \frac{(\alpha_1 - \alpha_2)^2 + (\alpha_2 - \alpha_3)^2 + (\alpha_3 - \alpha_1)^2}{(\alpha_1 + \alpha_2 + \alpha_3)^2} \quad \dots\dots (2.5)$$

In a liquid, Δ^2 measures the anisotropy of the polarizability tensor, but this is affected by, for example, the anisotropy of the local field as well as the polarizabilities of individual molecules. (See, for example, Kielich (36).)

Landau and Lifshitz, in ref. (60), § 91, evaluate the depolarization ratios for the components of an arbitrary polarizability tensor

$$\alpha_{ik} = (1/3) \bar{\alpha} \delta_{ik} + s_{ik} + a_{ik} \quad \dots\dots (2.6)$$

where $\bar{\alpha}$ is scalar polarizability (measured as departure from the mean)

s_{ik} is a symmetrical tensor of zero trace

a_{ik} is an antisymmetric tensor.

The scattered light may be written as a superposition of scalar, symmetric and antisymmetric scattering. Landau and Lifshitz calculate the scattering intensities and depolarization ratios for each type of scattering, and show that, for vertically polarized incident light, where the scattered light is observed in the x-y plane (see fig.2.1), the values of I_v (vertically polarized) and I_h (horizontally polarized), at scattering angle θ are as given in the table below.

TABLE 2.1

Scattering type	I_v	I_h	$\rho_v(90^\circ)$
Scalar	$(3/2)E\sin^2\theta$	0	0
Symmetric	$(3/20)S(3+\sin^2\theta)$	$(9/20)S$	$3/4$
Antisymmetric	$(3/4)A\cos^2\theta$	$(3/4)A$	∞

Here the intensities have been normalized to unity when integrated over all directions. The values of A,E,S are given by

$$\left. \begin{aligned} E &= \int \overline{\alpha_1 \alpha_2^*} \cdot dV \\ S &= \int \overline{s_{ik,1} s_{ik,2}^*} \cdot dV \\ A &= \int \overline{a_{ik,1} a_{ik,2}^*} \cdot dV \end{aligned} \right\} \dots\dots\dots (2.7)$$

The suffices 1,2 imply that α_{ik} has been measured at different points in space. The bar denotes averaging over the motion of the particles.

The scalar component gives the isotropic spectrum, and the other two components the anisotropic spectrum. The total depolarization ratio is then given by

$$\rho_v(\text{tot}) = \frac{(3/10)S + (1/2)A}{(E) + (2/5)S} \dots\dots\dots (2.8)$$

The depolarization ratio of the anisotropic spectrum alone is given by

$$\rho_v(\text{anis}) = \frac{(3/5)S + A}{(4/5)S} \dots\dots\dots (2.9)$$

Hence if the shear scattering is purely symmetric, so that $A=0$, then $\rho_v(\text{anis})$ takes the value $3/4$, or $\rho_u(\text{anis})$ becomes $6/7$. Where the scattering involves only a small change in frequency, and the incident frequency does not lie close to a range in which the scattering medium is absorbing, the polarizability tensor of the molecules may be replaced by the dielectric constant tensor of the medium. This is essentially symmetric, and hence one would expect $\rho_u(\text{anis})$ to have the value $6/7$ in most light-scattering experiments. The theories discussed in Section (iii) all assume the polarizability tensor to be symmetric, and most experimental results justify the assumption.

* * * * *

The two spectra will now be discussed in more detail. In the section on the isotropic spectrum, fluctuations in scalar parameters contributing to the mean dielectric constant will be considered. In that on the anisotropic spectrum, contributions to the off-diagonal elements of the dielectric constant tensor will be discussed.

ii). The Isotropic Spectrum.

Landau and Lifshitz, in their book "Statistical Physics" (14), evaluate the probability of the occurrence of statistical fluctuations in different quantities, and the mean-square values of fluctuations of thermodynamic parameters. The mean values of entropy, pressure, specific volume and temperature are given by S_0 , P_0 , V_0 , T_0 respectively. The probability of a fluctuation from the mean, designated by ΔS , ΔP , ΔV , ΔT is given by (ref. (14), p 351, eq. 111.3)

$$w \propto \exp \left[(\Delta P \Delta V - \Delta T \Delta S) / 2kT_0 \right] \dots\dots\dots (2.10)$$

considering the minimum work necessary to produce a reversible change. They also show that the probability distribution for fluctuations of a single variable, x , is given by

$$w(x) dx = \frac{1}{\sqrt{2\pi \langle x^2 \rangle}} \exp \left(-x^2 / 2 \langle x^2 \rangle \right) \dots\dots\dots (2.11)$$

(p 346, eq. 109.4). This equation is derived by expanding $S(x)$ in a Taylor series about its mean equilibrium value, and assuming that the probability of a departure from S_0 is proportional to $\exp(-\Delta S/k)$. ΔP , etc., may be expressed in terms of partial differentials which relate directly to macroscopic variables, and hence the expression $\langle \Delta P \Delta V - \Delta T \Delta S \rangle$ may be evaluated. It is possible to write this expression in two ways, one containing a term in $\langle \Delta S^2 \rangle$ and a term in $\langle \Delta P^2 \rangle$ only, with no terms containing $\langle \Delta S \Delta P \rangle$, and the other with terms in $\langle \Delta V^2 \rangle$ and $\langle \Delta T^2 \rangle$ only, and no terms in $\langle \Delta V \Delta T \rangle$. This implies that eq. (2.10) becomes the product of two Gaussians of similar form to eq. (2.11), from which it may be seen that the pairs of variables (V, T) and (S, P) are statistically

independent, or

$$\left. \begin{aligned} \langle \Delta V \cdot \Delta T \rangle &= 0 \\ \langle \Delta S \cdot \Delta P \rangle &= 0 \end{aligned} \right\} \dots\dots\dots (2.12)$$

Also, by direct comparison of equations (2.10) and (2.11), it is possible to evaluate the mean-square values of fluctuations of the parameters.

The results are

$$\langle \Delta T^2 \rangle = kT_0^2 / C_v \dots\dots\dots (2.13)$$

$$\langle \Delta V^2 \rangle = -kT_0 \cdot (\partial V / \partial P)_T = -kT_0 V_0 \beta_T \dots\dots\dots (2.14)$$

$$\langle \Delta S^2 \rangle = kC_p \dots\dots\dots (2.15)$$

$$\langle \Delta P^2 \rangle = -kT_0 (\partial P / \partial V)_S = -kT_0 / (V_0 \beta_S) \dots\dots\dots (2.16)$$

where β_T, β_S are isothermal and adiabatic compressibility respectively, and C_v, C_p are specific heats ^{per mole} at constant volume and pressure. An associated result is the mean square fluctuation in density, ρ ,

$$\langle \Delta \rho^2 \rangle = kT_0 \rho_0^2 \beta_T / V_0 \dots\dots\dots (2.17)$$

As has already been shown, the intensity of light scattered depends on the mean square value of fluctuations in the dielectric constant. These fluctuations may be described either in terms of V (or ρ), T , or in terms of S, P .*

* * * * *

*The state of a system is specified by at least three thermodynamic variables, not two. However, Coumou et al (17) took density, pressure and temperature, and showed that the fluctuations in pressure apart from those accounted for in the density fluctuations were negligible, and hence a representation in terms of density and temperature only is adequate.

The first procedure gives

$$\langle \Delta \epsilon^2 \rangle = \left(\frac{\partial \epsilon}{\partial \rho} \right)_T^2 \langle \Delta \rho^2 \rangle + \left(\frac{\partial \epsilon}{\partial T} \right)_\rho^2 \langle \Delta T^2 \rangle \dots \dots \dots (2.18)$$

or
$$\langle \Delta \epsilon^2 \rangle = kT_0 \left[\left(\frac{\partial \epsilon}{\partial \rho} \right)_T^2 \rho_0^2 \beta_T / v_0 + \left(\frac{\partial \epsilon}{\partial T} \right)_\rho^2 T_0 / c_v \right] \dots \dots (2.19)$$

and the second gives

$$\langle \Delta \epsilon^2 \rangle = \left(\frac{\partial \epsilon}{\partial S} \right)_P^2 \langle \Delta S^2 \rangle + \left(\frac{\partial \epsilon}{\partial P} \right)_S^2 \langle \Delta P^2 \rangle \dots \dots \dots (2.20)$$

This second division is experimentally very useful, because the fluctuations in pressure are propagating fluctuations, like adiabatic sound-waves permeating the liquid, and hence the light scattered from them is Doppler-shifted, whereas the fluctuations in entropy at constant pressure are slowly-decaying and non-propagating, and so give rise to a very narrow line at the incident frequency in the scattered light spectrum. The two may thus be conveniently separated experimentally. * However, in calculating the intensity in these two components from first principles, the assumption is often made that the variations in dielectric constant depend on the density fluctuations only. This is equivalent to neglecting the second term in eq. (2.19). The density-density correlation function is then used to obtain the scattering from both pressure and entropy fluctuations. (For example, Montrose et al, (16)). Coumou et al (17) have considered this assumption experimentally, and Fabelinskii (18) gives an approximate formula from which the neglected term may be calculated from experimental quantities. (ref (18), ch.1, p.29). He shows that the scattered intensity from temperature fluctuations in benzene amounts to 1.6% of the total isotropic scattered intensity. This

*See figure 2.2.

term may therefore be neglected in the liquids investigated here.

Hence simplifying equation (2.20)

$$\langle \Delta \epsilon^2 \rangle = \left(\frac{\partial \epsilon}{\partial \rho} \right)_T^2 \left[\left(\frac{\partial \rho}{\partial S} \right)_P^2 \langle \Delta S^2 \rangle + \left(\frac{\partial \rho}{\partial P} \right)_S^2 \langle \Delta P^2 \rangle \right] \dots \dots \dots (2.20b)$$

and substituting from equations (2.15) and (2.16)

$$\langle \Delta \epsilon^2 \rangle = \left(\frac{\partial \epsilon}{\partial \rho} \right)_T^2 k_{T_0} \rho_0^2 \left[\alpha_{VP}^2 + \beta_S / V_0 \right] \dots \dots \dots (2.21)$$

where α_V is coefficient of thermal expansion. Also from eq. (2.19)

$$\langle \Delta \epsilon^2 \rangle = k_{T_0} \rho_0^2 \left(\frac{\partial \epsilon}{\partial \rho} \right)_T^2 \beta_T / V_0 \dots \dots \dots (2.22)$$

These equations show several important features. Firstly, the total scattering is directly proportional to β_T , whereas that part scattered from pressure fluctuations is proportional to β_S , with the same constant of proportionality. Secondly this implies that, if pressure and entropy fluctuations may be separated experimentally, the ratio of intensity in the two modes may be used to give

$$I_p / I_{tot} = \beta_S / \beta_T = C_P / C_V = 1/\gamma \dots \dots \dots (2.23)$$

where I_{tot} is total intensity, and I_p is that due to pressure fluctuations. The ratio I_p / I_s , (where I_s is intensity due to entropy fluctuations) is known as the Landau-Placzek ratio, and is equal to $\gamma-1$.

Let us now consider the spectrum to be measured. First it should be noted that since quasi-elastic scattering is being considered, $|\underline{k}'|$ and $|\underline{k}|$, where \underline{k}' , \underline{k} are wave-vectors of scattered and incident light respectively, are nearly equal, and equation (1.11) is applicable. This may be rewritten

$$|q| / (2n \sin \theta / 2) = |\underline{k}| \dots \dots \dots (2.24)$$

where $\hbar k$ is momentum associated with light-wave,

$\hbar q$ is momentum associated with scattering fluctuation,

n is mean refractive index of medium,

θ is scattering angle.

So by fixing the scattering angle by the geometry of the apparatus, and using monochromatic light, $|q|$ is fixed for all fluctuations causing scattering at that angle.* The value of $|q|$ may be changed by varying θ . By spectrally analysing the light at a given θ , the Fourier transform of the time-variation of the scattering fluctuations may be obtained.

a). The pressure fluctuations.

As has already been mentioned, the adiabatic pressure fluctuations are propagating, and may be thought of as Debye sound-waves permeating the liquid in all directions. The wavelength of the sound-wave causing scattering is fixed by equation (2.24) or (1.11)

$$\lambda_s = \lambda_0 / (2n \sin \theta / 2) \quad \dots \dots \dots (2.25)$$

where λ_s is wavelength of sound, and λ_0 that of light.

Regarding the light and sound from the point of view of their wave-properties, the light is scattered from successive periodic variations in the dielectric constant, the sound-wave acting like a diffraction grating. The scattered light only interferes constructively when the path-difference from successive maxima is a whole number of wavelengths,

* * * * *

*This assumes that no external changes are made to the liquid which affect the mean value of the refractive index.

and equation (2.25) is just the Bragg relation. The light frequency is Doppler-shifted by an amount determined by the velocity of the sound-wave, given by

$$\Delta\omega/\omega_0 = \pm 2 (v_s / c) n \sin\theta/2 \quad \dots\dots\dots (2.26)$$

where ω_0 is frequency of incident light wave,

$\Delta\omega$ is frequency shift,

c is velocity of light,

v_s is velocity of sound.

The \pm refers to the possibility of waves in either direction. From a quantum point of view, the energy change in the light is just such as to create or annihilate one phonon, the total number of phonons being so great and their distribution in this region of q sufficiently uniform that a negligible difference is made to the phonon population, and the probabilities of creation and annihilation are equal.

Therefore one would expect to see an intensity peak on either side of the central frequency in the scattering spectrum. The shape of the peak depends on the time-dependence of the correlation-function for pressure. If the sound-wave were a perfect sine-wave of infinite duration each component of the doublet would be a δ -function, which is the Fourier transform of a single frequency. If the sound wave decays, its time-limitation implies a finite spread in its frequency, and if it decays exponentially, the δ -functions become Lorentzians with width determined by the phonon lifetime. The symmetrical doublet is known as the Brillouin doublet, so that if the intensity in each peak is I_B ,

$$I_p = 2I_B \quad \dots\dots\dots (2.27)$$

The dissipation of the energy of the sound-wave as a result of viscosity and thermal conductivity are considered in Landau and Lifshitz, "Fluid Mechanics", § 77. (ref 19). They consider reversible adiabatic processes, so that the original division into pressure and entropy fluctuations is not contradicted. Their calculation of the absorption coefficient α_s , where the intensity of the sound-wave decreases with distance x as $\exp(-2\alpha_s x)$ gives the result

$$\alpha_s = \frac{\omega_s^2}{2\rho v_s^3} \left[\left(\frac{4}{3}\eta + \zeta \right) + K \left(\frac{1}{c_v} - \frac{1}{c_p} \right) \right] \dots\dots\dots (2.28)$$

where η is shear viscosity

ζ is volume or bulk viscosity

K is thermal conductivity.

and the subscript 's' refers to properties of the sound-wave.

Although the temperature fluctuations have a negligible direct effect on the dielectric constant, there is a temperature change associated with the sound-wave which provides an additional means of decay through the thermal conductivity. However, for the liquids to be considered here, this term is negligible compared with the viscosity term in (2.28). The phonon "lifetime" associated with α_s will be given by

$$1 / (\alpha_s v_s) = \tau_s \dots\dots\dots (2.29)$$

and $\tau_s = 1 / \Gamma_B \dots\dots\dots (2.30)$

where Γ_B is the Brillouin semi-halfwidth in rad/sec.

This calculation has been performed for low-frequency values of the viscosity coefficients and specific heats. The absorption of energy from the sound-wave by these mechanisms implies a mean time, τ , for

the energy transfer, and this implies a dispersion region characterizing each mechanism as the frequency passes through the region of $1/\tau$. The dispersion equation for the sound velocity may be written

$$\omega_s^2 / q^2 = v_{s,0}^2 - \sum_i v_{s,i}^2 \left(\frac{j\omega_s \tau_i}{1 - j\omega_s \tau_i} \right) \quad \dots\dots\dots (2.31)$$

where $v_{s,0}$ is velocity of sound at low frequency

the subscript 'i' refers to one mechanism for decay, and

$$v_{s,i}^2 = B_i / \rho \quad \dots\dots\dots (2.32)$$

where B_i is the appropriate modulus for mechanism i. See, for example, ref (5), section 13.2, p 164. The following table is also taken from this reference. In it, the values of $v_{s,i}^2$ and τ_i for different mechanisms are given.

TABLE 2.2

Effect	$v_{s,i}^2$	τ_i
Shear viscosity η	$(4/3)G/\rho$	η/G
Volume viscosity ζ	B/ρ	ζ/B
Thermal conduction (K)	$(C_p - C_v) / (C_v \rho \beta_T)$	$\rho C_v / (K q^2)$

where G is rigidity modulus and B bulk modulus.

For the liquids investigated here, the τ are of order 10^{-11} - 10^{-12} s for the viscosity effects, and 10^{-6} s for thermal conduction. The relaxing volume viscosity takes account of structural relaxation, but there may in addition be relaxation due to exchange of energy with internal molecular degrees of freedom. This may be expressed in terms of a relaxing or frequency-dependent specific heat.

b) The entropy fluctuations.

The entropy fluctuations are non-propagating, and give rise to a narrow line at the incident frequency in the scattered light spectrum. The width of the line is inversely proportional to the decay time characterizing thermal diffusion at constant pressure, τ_T .

$$\tau_T = \rho C_p / (\kappa q^2) \dots\dots\dots (2.33)$$

τ_T is generally of order 10^{-6} s, and hence the line is less than 10^6 Hz in width, which cannot be resolved in this work. It can be measured using special techniques, for example, (7).

Of the effects listed in the introduction to this chapter, a, c, and d, if present, also cause scattering at the incident frequency, and so also does any extraneous scattering, due to a few dust particles or stray reflections. Hence this line, even if it can be resolved, may be difficult to interpret.

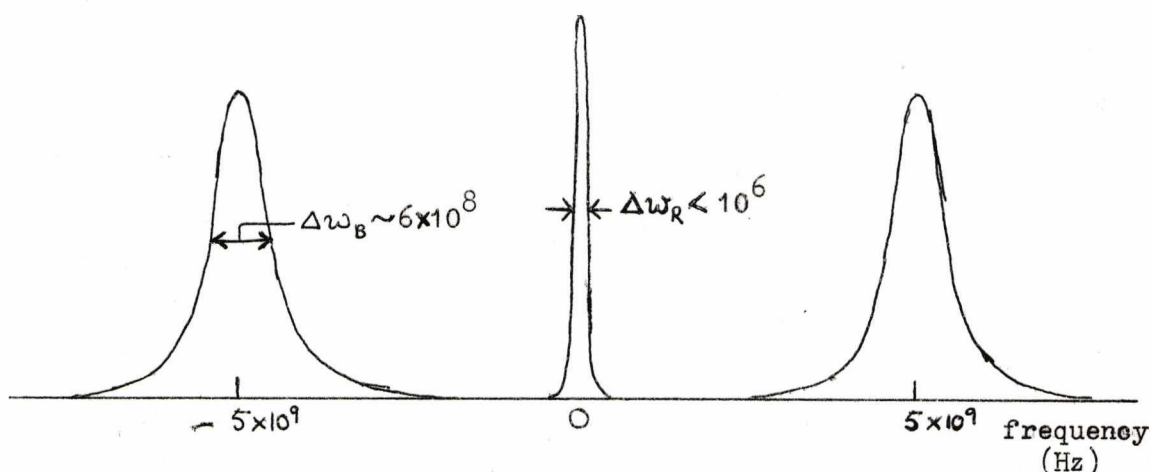


Fig. 2.2 Expected isotropic spectrum (without instrumental broadening), giving typical values for Brillouin splitting at $\theta = 90^\circ$, and Brillouin and Rayleigh linewidths, in Hz.

The ideas so far discussed lead to the main features of the observed isotropic spectrum, but to account for its shape with more accuracy, it is necessary to consider the behaviour of the liquid more theoretically. Several authors have published papers quite recently on this subject (16,20,22,23,35,63) the most important theoretical treatises being (16,20,35). Their basic assumptions, general method and main results will be presented here.

They begin with the linearized hydrodynamic equations of irreversible thermodynamics.

$$\frac{\partial \rho}{\partial t} + \rho_0 \nabla \cdot \underline{u} = 0 \quad \dots\dots\dots (2.34)$$

$$\frac{\partial \underline{u}}{\partial t} = -\frac{v_{s,0}^2}{\rho_0 \gamma} \nabla \rho - \frac{v_{s,0}^2 \alpha_v}{\gamma} \nabla T + \frac{\eta_L}{\rho_0} \nabla (\nabla \cdot \underline{u}) \quad \dots (2.35)$$

$$\frac{\partial T}{\partial t} = \frac{(\gamma-1)}{\rho_0 \alpha_v} \frac{\partial \rho}{\partial t} + \frac{\kappa}{\rho_0 c_v} \nabla^2 T \quad \dots\dots\dots (2.36)$$

where \underline{u} is particle velocity

$\eta_L = (4/3)\eta_0 + \zeta_0$ is low frequency longitudinal viscosity

T, ρ are departures from the mean temperature and density, T_0, ρ_0

ζ_0 is volume viscosity, which may be used also as a general loss term representing any loss mechanism other than shear viscosity.

(see below).

Equation (2.34) is the continuity equation, (2.35) the longitudinal part of the Navier-Stokes equation, and (2.36) the energy transfer equation.

An initial value of the density fluctuation, $\rho(\underline{q}, 0)$, is assumed, and its value at later times, $\rho(\underline{q}, t)$ is calculated using the above equations. The density-density correlation function as a function of

wave-number and time may then be evaluated by summing over all initial states of the system. The Fourier transform with respect to time of this function is the generalized structure factor $S(q, \omega)$, which may be written (omitting the vector notation for q since the medium is isotropic)

$$S(q, \omega) = \sigma(q, \omega) \langle \rho(q) \cdot \rho(-q) \rangle = \langle \rho(q, \omega) \rho(-q) \rangle \quad \dots\dots (2.37)$$

where the term $\langle \rho(q) \rho(-q) \rangle$ gives the scattered intensity at wave-number q , and the factor $\sigma(q, \omega)$ gives the shape of the spectrum.

The spectral density $\sigma(q, \omega)$ is a complicated expression; however it may be separated into two parts if the assumption is made that

$$k / c_v \ll \eta_L \quad \dots\dots\dots (2.38)$$

This assumption is reasonable except in the case of liquid metals.

The result is

$$\sigma(q, \omega) = \left(1 - \frac{1}{\gamma}\right) \frac{2kq^2 / (\rho_0 c_p)}{[kq^2 / (\rho_0 c_p)]^2 + \omega^2} + (2V_{s,0}^2 q^2 / \gamma) \frac{2\Gamma}{(2\omega\Gamma)^2 + (\omega^2 - \omega_0^2)^2} \quad \dots\dots\dots (2.39)$$

where $\Gamma = \eta_L q^2 / 2\rho_0 \quad \dots\dots\dots (2.40)$

$\omega_0 = V_{s,0} \cdot q \quad \dots\dots\dots (2.41)$

The first term represents the central Rayleigh line, and the second the Brillouin doublet. Since

$$\langle \rho(q) \rho(-q) \rangle = \rho_0^2 kT_0 \beta_T / v_q \quad \dots\dots\dots (2.42)$$

where v_q is volume of fluctuation (c.f. eq. 2.17), the adiabatic part of the structure factor may be written, using equations (2.37), (2.42),

$$S_s(q, \omega) = \frac{[2(\rho_0^2/v_q)kT_0\eta_L]}{(\omega\eta_L)^2 + (\rho_0\omega^2/q^2 - M_0)^2} \dots\dots\dots (2.43)$$

where $M_0 = \rho_0 v_{s,0}^2$ is adiabatic bulk modulus.

The second term in eq. (2.39) may be separated into partial fractions, and the result is not the simple sum of two Lorentzians. We obtain

$$\sigma_s(q, \omega) = \frac{1}{8} \left[\frac{\Gamma}{\Gamma^2 + (\omega - \omega')^2} + \frac{\Gamma}{\Gamma^2 + (\omega + \omega')^2} - \frac{\Gamma}{\omega' \Gamma^2 + (\omega - \omega')^2} + \frac{\Gamma}{\omega' \Gamma^2 + (\omega + \omega')^2} \right] \dots (2.44)$$

$$\text{where } \omega' = \omega_0 \left[1 - \frac{1}{4}(\omega_0\eta_L/M_0)^2 \right]^{\frac{1}{2}} \dots\dots\dots (2.45)$$

The first two terms are Lorentzians centred at $\pm\omega'$, and of semi-halfwidth Γ . The second two terms are antisymmetric functions centred on $\pm\omega'$, of total area zero. Their effect on the spectrum is shown in figure 2.3. They shift the Brillouin peaks closer to the centre, so that the peak frequency becomes

$$\omega'' = \omega_0 \left[1 - \frac{1}{4}(\omega_0\eta_L/M_0)^2 \right]^{\frac{1}{2}} \dots\dots\dots (2.46)$$

and they redistribute the Brillouin intensity so that some of it is included in the Rayleigh line. It is generally assumed that the peak value gives ω_0 . A calculation of the correction factor using results presented here for chlorobenzene, gives a shift of 0.4%, which may be neglected in comparison with the experimental error of 1-2% of these Brillouin shift measurements. However it would clearly not be negligible in more accurate work. The effect of these terms on the measurement of Γ is insignificant (ref. (50)), provided that it is measured as shown in fig. 2.3. The extent to which the redistribution of Brillouin intensity affects the measured

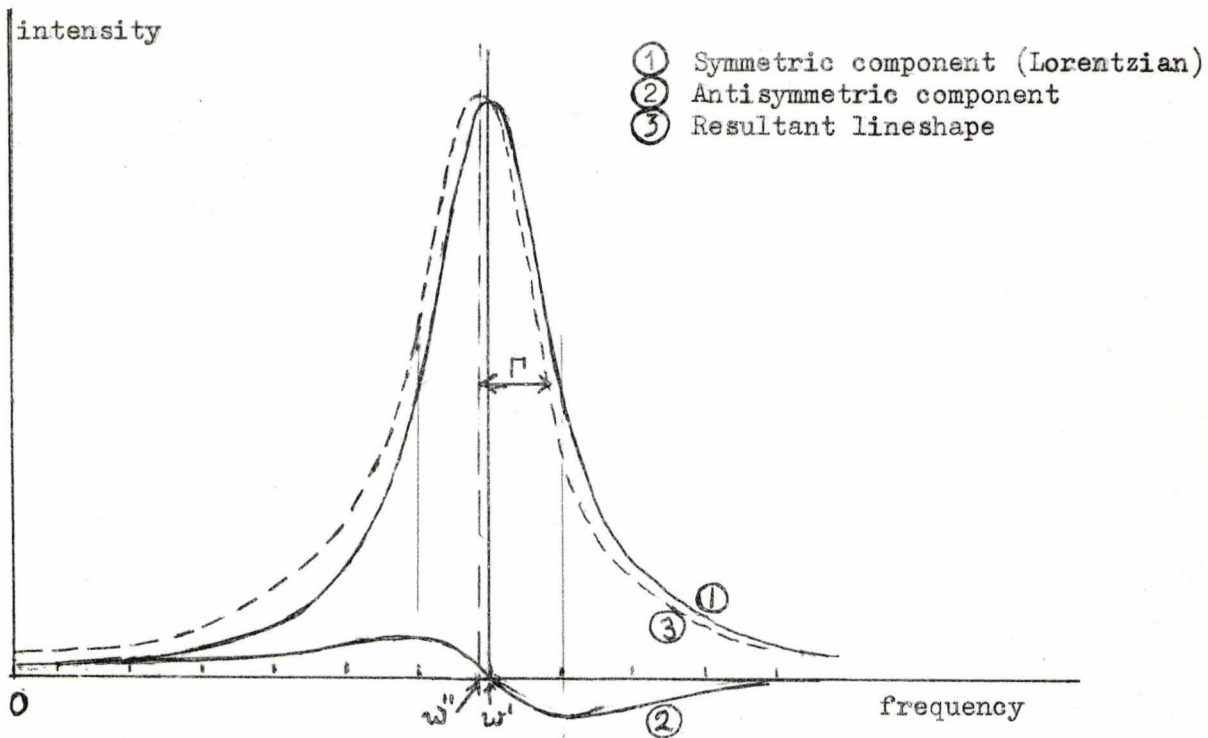


Figure 2.3. Effect of absorption on Brillouin line.

* * * * *

Landau-Placzek ratio depends on the instrumental resolution.

Further insight may be gained into these terms by considering the correlation function causing them. The Lorentzian terms are the Fourier transform of a correlation function

$$F_1(q,t) = F(q) e^{-\Gamma|t|} \cos \omega't \quad \dots\dots\dots (2.47)$$

Due to the presence of the term in Γ , this function does not satisfy the requirement that its time derivative should be zero at zero time. This may be achieved by adding a term in $\sin \omega't$

$$F_2(q,t) = F(q) \left(\frac{\Gamma}{\omega'} \right) e^{-\Gamma|t|} \sin \omega't \quad \dots\dots\dots (2.48)$$

This term vanishes if Γ is zero, and is in fact the out-of-phase component

of the density-density correlation function corresponding to energy dissipation.

The calculation of the spectrum is still incorrect, insofar as the frequency-dependence of the "constants" in eq. (2.34)-(2.36) has been ignored. This may be rectified by the addition of a term

$$\frac{1}{\rho_0} \int_0^t dt' \eta(t-t') \cdot \nabla [\nabla \cdot \underline{u}(t')] \quad \dots\dots\dots (2.49)$$

to the right-hand side of eq. (2.35). This accounts for a frequency-dependent shear or bulk viscosity. The after-effect function $\eta(t)$ describes the visco-elastic force at a time t after the application of stress. A relaxing internal specific heat may also be included in this term if the time-scale of energy transport is long compared with the thermal relaxation time. (See (26)). The parameters C_v, α_v may then be assigned their static values in eq. (2.36).

The frequency-dependent viscosity is given by

$$\eta(\omega) = \int_0^\infty dt \eta(t) \cos \omega t \quad \dots\dots\dots (2.50)$$

and the relaxing part of the longitudinal modulus by

$$M_r = \omega L_r(\omega) = \int_0^\infty dt \eta(t) \sin \omega t \quad \dots\dots\dots (2.51)$$

A single relaxation time or a distribution of relaxation times may be included via $\eta(t)$. (16). The value of M_r is given by

$$M_r = \rho_0 [v_{s,\infty}^2 - v_{s,0}^2] \quad \dots\dots\dots (2.52)$$

where $v_{s,\infty}$ is infinite-frequency sound-velocity. In the case of the relaxation of an internal specific heat, (ref. 11)

$$M_r = \rho_0 v_{s,0}^2 \frac{(C_p - C_v)C_i}{(C_v - C_i)C_p} \dots\dots\dots (2.53)$$

where C_i is internal molar specific heat. For relaxing shear and compressional moduli (cf table 2.2)

$$M_r = K_r + (4/3)G_\infty \dots\dots\dots (2.54)$$

where K_r is relaxing part of compressional modulus, and G_∞ infinite-frequency shear modulus.

Hence the spectral density $\sigma(q, \omega)$ (2.39) is modified to

$$\sigma(q, \omega) = \left(1 - \frac{1}{\gamma}\right) \frac{2Kq^2/\rho_0 C_p}{[Kq^2/(\rho_0 C_p)]^2 + \omega^2} + \frac{2M_0 (\eta(\omega) + \eta_L)}{\gamma [w(\eta(\omega) + \eta_L)]^2 + (\rho_0 \omega^2/q^2 - M_0 - w\zeta(\omega))^2} \dots\dots\dots (2.55)$$

The assigning of static values to α_v , C_v , γ , leaves the Rayleigh line unchanged, but the Brillouin doublet shows several new features.

a). The splitting reflects the dispersion in the sound velocity and is now given by $q[(M_0 + w\zeta(\omega))/\rho_0]^{1/2}$.

b). The Brillouin linewidth is now $(\eta(\omega) + \eta_L)q^2/2\rho_0$, so that

$$\alpha_s = \Gamma_B/v_s = q^2(\eta(\omega) + \eta_L)/(2\rho_0 v_s) \dots\dots\dots (2.56)$$

c). The numerator contains a frequency-dependent term which gives a peak at the incident frequency, which may approximately be separated out as another line. In fact there will be two extra lines, one with width corresponding to the relaxation time for volume viscosity, and another with width corresponding to that for shear viscosity, if these

times are different. The existence of these peaks was pointed out by Mountain (20), the theory extended by Montrose et al (16) and Bhatia and Tong (35), and the prediction verified experimentally by Mountain himself, and by Gornall et al (22) and (23). The Mountain line is a general phenomenon to be expected in connection with all dispersion mechanisms. If it is due to viscosity effects, the width of the line should be correspondingly temperature-dependent, but if it is due to thermal effects, the width should be approximately independent of temperature.

d). The apparent Landau-Placzek ratio is now frequency-dependent, because some of the Brillouin intensity is redistributed into the region of the Rayleigh line (ref.(21)), although the total intensity due to adiabatic pressure fluctuations remains unchanged.

If the entire volume and shear viscosity relaxes with a single relaxation time τ_{dis} , the widths of Brillouin and Mountain lines become

$$2\Gamma_B = (v_{s,\infty}^2 - v_{s,0}^2) \frac{q^2 \tau_{dis}}{1 + \omega_0^2 \tau_{dis}^2} \dots\dots\dots (2.57)$$

$$= \frac{M_r}{\rho_0} \cdot \frac{q^2 \tau_{dis}}{1 + \omega_0^2 \tau_{dis}^2} \dots\dots\dots (2.57b)$$

$$2\Gamma_M = v_{s,0}^2 \cdot q^2 / (\omega_0^2 \tau_{dis}^2) \dots\dots\dots (2.58)$$

There is an additional small correction to the position of the Brillouin peaks, which is a maximum in the centre of the dispersion region, and largest for a single relaxation time, acting in the same direction as that discussed on p.2.20. An expression for it is given in ref. (16), and these authors show that it is at most 1% for benzene.

In a light-scattering experiment, dispersion regions may be examined

in two possible ways.

a). The scattering angle θ , and hence the wave-number, may be changed. Generally, values of θ of 5° and 175° limit the range practically attainable. This varies the frequency, through the term $\sin\theta/2$ in eq. (2.24), through about a decade.

b). The temperature may be changed, thus varying the τ , while keeping θ constant. This technique is particularly useful if the results may be written in terms of reduced functions that depend on the temperature, ω and τ only through the product ($\omega\tau$). For example, the velocity of sound obeys the relation, for a single relaxation mechanism

$$V_s^2 = V_{s,0}^2 + (V_{s,\infty}^2 - V_{s,0}^2) \frac{\omega^2 \tau_i^2}{1 + \omega^2 \tau_i^2} \quad \dots\dots\dots (2.31b)$$

so that a suitable reduced function is the reduced modulus

$$M' = \frac{V_s^2 - V_{s,0}^2}{V_{s,\infty}^2 - V_{s,0}^2} = \frac{\omega^2 \tau_{dis}^2}{1 + \omega^2 \tau_{dis}^2} \quad \dots\dots\dots (2.59)$$

For the absorption, a suitable parameter is (from eq. (2.57)):

$$M'' = \frac{\omega \Gamma_B}{V_{s,\infty}^2 - V_{s,0}^2} = q^2 \frac{\omega \tau_{dis}}{1 + \omega^2 \tau_{dis}^2} \quad \dots\dots\dots (2.60)$$

If τ_{dis} varies with temperature according to the Arrhenius relation

$$\tau_{dis} = \tau_0 \exp(E_a/RT_0) \quad \dots\dots\dots (2.61)$$

where E_a is the activation energy for the process causing dispersion, then the effective range of frequency attained by varying the temperature may be large. The actual range clearly depends on the value of E_a .

iii). The anisotropic spectrum.

The theory of the anisotropic spectrum is in a considerably less well-developed state than that of the isotropic spectrum. This is due to mathematical complexity of dealing with orientation-dependent functions, the fact that many such functions necessary to the theory are not known, and the considerable uncertainty about the causes of different parts of the spectrum. As yet, no authors have succeeded in calculating the entire spectrum from first principles. However, certain theories have been developed, based on assumptions which are obviously very oversimplified, and from these, some features of the spectrum have been predicted which may be verified experimentally. Some of these will be considered here.

There are several possible causes for off-diagonal elements in the dielectric constant tensor. One of these is the shear deformation produced in atoms or molecules by translational or rotational motion with respect to their neighbours. This should arise even for atoms where the induced polarizability of an individual atom is scalar. Part of this deformation may correspond to shear waves. If the induced polarizability of an individual molecule is itself a tensor, as will be the case for non-spherical molecules, several additional effects will occur. It is possible for the average polarizability in a small volume of liquid to differ from the mean, due to the statistical fluctuations in orientation of the molecules. Such a fluctuation will decay due to the reorientation of the molecules. If the molecules have a permanent dipole-moment, or interact together by other strong non-central forces such as hydrogen-bonding, it is possible that rotation may be hindered, which is equivalent

to saying that the local field surrounding a given molecule is markedly non-spherical. In this case the apparent induced polarizability of a molecule will differ from the value obtained assuming that it is surrounded by a homogeneous medium of uniform dielectric constant.

In fact any interaction which distorts the molecule, causes it to rotate or vibrate orientationally, or applies a non-spherical electric field to it, will be mirrored in the induced polarizability and hence the scattered-light spectrum. Either the value of the induced polarizability, or the time-decay of fluctuations in it, may be affected. Each type of fluctuation may decay with a different time, and thus the spectrum may be characterised by several different widths, and hence of complex shape. Even propagating shear waves, unlike compressional waves, do not generally give rise to distinct peaks which may be readily separated from the rest of the spectrum. The waves, which propagate only at high frequencies (ref. 5, p. 168), are of lower velocity than compressional waves, and heavily damped, so that the peaks are close together and very broad. If the instrumental resolution is too low to resolve them they approximate to a Lorentzian. If each contribution to the spectrum gives rise to a Lorentzian of characteristic width, the result will be the sum of a number of Lorentzians. The spectrum observed experimentally may extend up to about 100 cm^{-1} or $3 \times 10^{12} \text{ Hz}$, or have a central peak as narrow as 0.3 cm^{-1} (10^{10} Hz), or both. A typical anisotropic spectrum is shown in Fig. 2.4, together with the inverse lineshape, which is a common way of presenting the experimentally observed spectrum. The spectrum is considerably sharper than a single Lorentzian, and the wings fall off initially more slowly with frequency, but then more rapidly, as

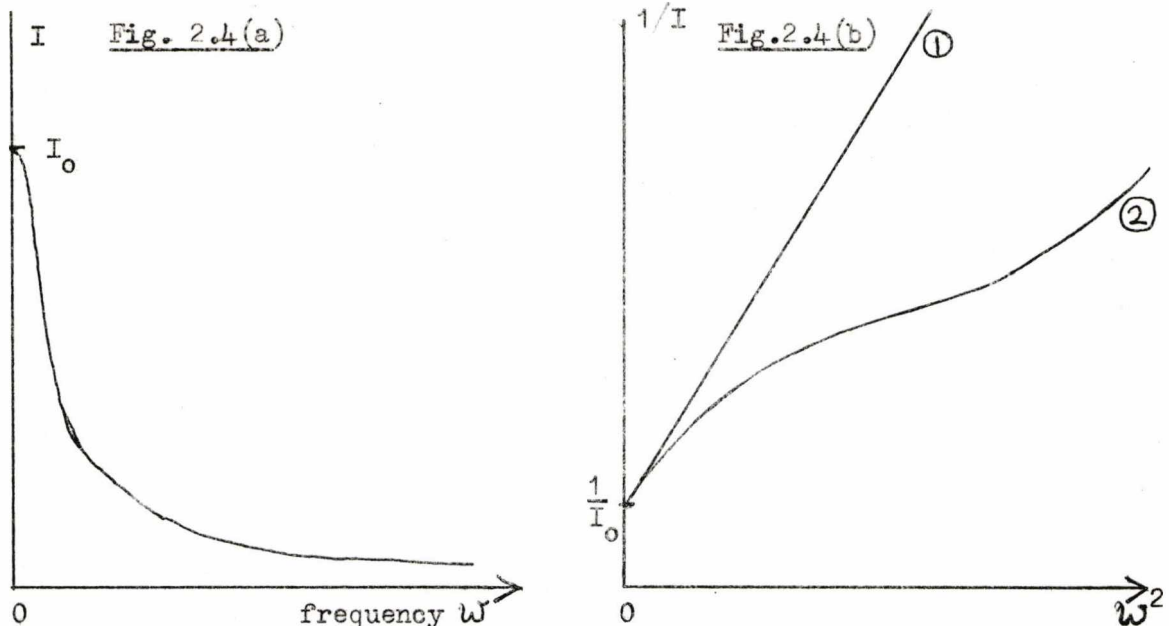


Fig. 2.4. (a) Intensity I of typical anisotropic spectrum for a liquid of complex molecules. (plotted against frequency)
 (b) Reciprocal intensity $1/I$ (plotted against $(\text{frequency})^2$), for
 ① single Lorentzian of height I_0 ,
 ② anisotropic spectrum as in (a).

* * * * *

indicated by the upward curvature of the inverse curve at high frequencies.

A variety of techniques may be needed to study the whole spectrum, and the Fabry-Perot interferometer, used in this work, is only applicable for examining the very central region of the spectrum, in liquids exhibiting a narrow central peak. Only the longest relaxation time may be measured accurately, although sometimes a width for a second broader Lorentzian may be estimated.

The theories may be divided into two main groups; those which start by considering the polarizability tensor of an individual molecule and its time-dependence, and those which approach from a macroscopic viewpoint by considering fluctuations in the shear stress and deformation. A certain amount of confusion has arisen in the inclusion of the results of both

approaches in the interpretation of the spectrum. The auto-correlation function of the polarizability of an individual molecule is not taken into account by the second approach, but the first approach may include terms due to fluctuations in stress or deformation if it takes into account terms describing the correlation of the orientation of one molecule with that of another.

The assumptions, method and results of the two approaches will be considered in turn, first noting several assumptions which all the theories have in common. They all assume the pure shear dielectric constant tensor to be symmetric, so that eq. (2.6) becomes

$$\epsilon_{ik} = \frac{1}{3}\bar{\epsilon} + s_{ik} \quad \dots\dots\dots (2.62)$$

This always leads to a depolarization ratio $\rho_{v,anis}$ of $\frac{3}{4}$, as has already been shown. They all neglect the dependence of the polarizability on the incident field-strength, and in most cases they neglect its dependence on the local density. Theories which start by considering individual molecules, also include the assumption that the phase difference between light scattered from neighbouring molecules may be neglected, since the correlation range for fluctuations is generally short compared with the wavelength of light, and the time-scale for molecular motion very long compared with its frequency. This last assumption is invalid in the case of scattering from shear waves.

The microscopic approach, considering the behaviour of individual molecules, will be dealt with first. Aspects of this problem have been considered by Pinnow et al (27), Starunov (32), Pecora and Steele (28), Kielich (36,38), and Ben-Reuven (61), among others. The more detailed

theories (28,36) provide a general mathematical framework, but because of mathematical complexity and lack of knowledge of necessary orientational functions, do not make many experimentally verifiable predictions.

The molecular polarizability $\underline{\alpha}$, may be written in diagonal form in the principal molecular axes

$$\underline{\alpha} = \begin{pmatrix} \alpha_{11} & 0 & 0 \\ 0 & \alpha_{22} & 0 \\ 0 & 0 & \alpha_{33} \end{pmatrix} \dots\dots\dots (2.63)$$

It is assumed that $\alpha_{11} > \alpha_{22} > \alpha_{33}$. The induced dipole moment is given by

$$\underline{\mu} = \underline{\alpha} \cdot \underline{E} \dots\dots\dots (2.64)$$

\underline{E} is the applied field, assumed to include the effect of the local field through a scalar factor only; i.e. it is parallel to the direction of polarization of the incident light. The magnitude of $|\underline{\alpha}|$ will be given by

$$\alpha = \alpha_{11} n_1^2 + \alpha_{22} n_2^2 + \alpha_{33} n_3^2 \dots\dots\dots (2.65)$$

where $\underline{n}_1, \underline{n}_2, \underline{n}_3$ are unit vectors in the molecular axes.

The induced dipole moment in the laboratory axes may then be calculated. Let the molecular orientation be described by angular co-ordinates (θ, ϕ, ψ) , and the incident light be polarized in the z-direction. θ is polar and ϕ azimuthal angle. The z-component of $\underline{\mu}$ is given by

$$\mu_z = E \left[\alpha_0 + \alpha_1 \left(\cos^2 \theta - \frac{1}{3} \right) + \alpha_2 \sin^2 \theta \cos 2\psi \right] \dots\dots\dots (2.66)$$

$$\left. \begin{aligned} \text{where } \alpha_0 &= (\alpha_{11} + \alpha_{22} + \alpha_{33})/3 \\ \alpha_1 &= \alpha_{11} - (\alpha_{22} + \alpha_{33})/2 \\ \alpha_2 &= (\alpha_{22} - \alpha_{33})/2 \end{aligned} \right\} \dots\dots\dots (2.67)$$

The first term corresponds to the average polarizability, and the values of α_1, α_2 are measures of the molecular anisotropy, the second two terms in (2.66) being second-order Legendre polynomials in the co-ordinate angles. The x- and y-components contain only terms in α_1, α_2 and second-order Legendre polynomials. Hence the term $E\alpha_0$ gives rise to the isotropic spectrum, and the other terms, which are orientation-dependent, vanish for optically isotropic molecules.

The calculation of the total scattering intensity then requires summation of the light scattered from each molecule over all N molecules in the illuminated region. The electric field in the z-direction at a point \underline{R} due to the nth molecule at \underline{r}_n is given by

$$E_z(n) = \mu_z(n) \exp[j \underline{q} \cdot (\underline{R} - \underline{r}_n)] \dots\dots\dots (2.68)$$

so that the total electric field is

$$E_z = \sum_{n=1}^N E_z(n) \propto \sum_{n=1}^N \mu_z(n) \exp[j \underline{q} \cdot (\underline{R} - \underline{r}_n)] \dots\dots (2.69)$$

The spectrum of the scattered light is then proportional to the Fourier time transform of the self-correlation function of the electric field, which is the ensemble-averaged product of two such sums as (2.69).

$$\langle E_z(t) E_z(0) \rangle = \sum_{n=1}^N \sum_{m=1}^N \mu_z(n) \mu_z(m) \exp[j \underline{q} \cdot (\underline{r}_n(t) - \underline{r}_m(0))] \dots\dots\dots (2.70)$$

The resultant expression for the spectrum is complex, and has been simplified by different authors in different ways, to illustrate different features. Pecora and Steele (28) do not attempt to consider the time dependence, but calculate the total scattering intensity. Their result for light scattered at 90° , polarized at ϕ_0 to the vertical (0-z) is:

$$\lim_{q \rightarrow 0} I(\phi_0, 90^\circ) = \left(\frac{E_0^2}{4\pi R \epsilon} \right)^2 \left\{ \cos^2 \phi_0 F_{\text{iso}} + (3 + \cos^2 \phi_0) F_{\text{aniso}} \right\} \dots (2.71)$$

$$\begin{aligned} \text{where } F_{\text{iso}} &= \rho_0 \alpha_0^2 \left\{ [1] + \rho_0 \int (g(r) - 1) 4\pi r^2 dr \right\} \dots \dots \dots (2.72) \\ &= \rho_0^2 k T_0 \beta_T \alpha_0^2 \quad \text{from (1.6)} \end{aligned}$$

which is clearly the isotropic spectrum.

$$F_{\text{aniso}} = \frac{1}{15} \rho_0 \left\{ \left[\left(\frac{1}{3} \alpha_1 \right)^2 + \alpha_2^2 \right] + \frac{1}{5} \rho_0 \int T(\alpha, \theta, \dots) \right\} \dots \dots (2.73)$$

where $T(\alpha, \theta, \dots)$ means terms in α_1, α_2 which contain products and squared terms of second-order Legendre polynomials, describing intermolecular correlations in orientation. These orientation-dependent distribution functions are not known. The factors contributing to them have been considered in some detail by Kielich (36,38). He considers the effects of anisotropic dispersive forces, dipole-dipole and dipole-induced-dipole interactions, and quadrupole interactions, assuming that these may be treated as small corrections to a central potential. He develops a useful framework, but is still prevented by lack of adequate models, from evaluating results for the liquid state which are comparable with experiment. Hence these terms cannot be evaluated further.

Both F_{iso} and F_{aniso} may be divided into two terms. One refers to the individual molecules, and comes from terms with $n=m$ in the product (2.70). These terms will be known as the self-scattering terms, and are shown in square brackets in equations (2.72) and (2.73). The other two terms, containing the pair distribution function as a function of distance and orientation, will be known as the correlation terms. They correspond to terms with $n \neq m$ in the product (2.70)

Pinnow et al (27) simplify the product (2.70) by making several

assumptions. They assume that the orientation of a molecule is independent of its position, so that angle-dependent terms and those in \underline{g} may be summed separately. They assume that the local field surrounding a molecule is spherical and there is no preferential orientation, which means that a number of terms vanish, and they further assume that there is no correlation between the orientation of different molecules, so that all the terms with $n \neq m$ vanish. Hence they have ignored the correlation terms in eq. (2.73).

It is still necessary to use a model for molecular reorientation to calculate the spectrum for the remaining self-scattering term. If the molecules rotate by simple diffusion, reorientation time τ_0 , then the spectrum will be Lorentzian with width given by

$$\tau_1 = \tau_0 / [1(1 + 1)] \dots\dots\dots (2.74)$$

where l is the order of the Legendre component of (1.10) being measured. Hence the time appropriate for light-scattering, τ_{1s} , will be

$$\tau_{1s} = \tau_0 / 6 \dots\dots\dots (2.75)$$

which will be related to the time measured by dielectric relaxation, τ_D , by the relation

$$\tau_{1s} = \tau_D / 3 \dots\dots\dots (2.76)$$

However, if the molecules rotate by large-angle jumps, the times for all Legendre components are nearly the same, and hence

$$\tau_{1s} \approx \tau_D \dots\dots\dots (2.77)$$

These considerations have been discussed in more detail in ref. (13). A measurement of the ratio $\tau_{I=1}/\tau_{I=2}$ may be indicative of the type of rotation taking place in the liquid, if it is influenced by no other factors.

If the temperature dependence of the spectrum is being studied, it is apparent on examining eq. (2.73), that the total anisotropic intensity, if correlation terms are ignored, is proportional to the density. Hence it should be nearly independent of temperature. The simplest derivation of the temperature-dependence of τ_{1s} is that based on the assumption that a potential barrier of height E_a must be crossed for reorientation to occur. The result is an Arrhenius temperature-dependence

$$\tau_{1s} \propto \exp[E_a/RT_0] \dots\dots\dots (2.78)$$

A comparison of the value of E_a with values obtained from other types of measurement may give an indication of the molecular processes involved in relaxation of the induced polarizability. (Non-Arrhenius behaviour may indicate additional complexity in the reorientation mechanism.) In the calculation of relaxation times from models for reorientation, the assumption has been made that the permanent and induced dipole moments have the same molecular axes, or experience the same molecular motions. In fact, in the liquids considered here, the moment of inertia, permanent dipole moment, and principal direction of induced polarizability, are all in different directions in some cases. For very non-spherical molecules, it is unlikely that all directions of rotation will be equally probable. Hence it is possible that this assumption will be invalid. A comparison of the value of E_a with values obtained by other methods may establish this fact.

Pinnow et al (27) have performed measurements on a number of liquids which tend to justify their neglect of the correlation terms, since the total scattering in each case is approximately independent of temperature. However, the exact temperature-dependence of the other terms is by no means obvious.

Starunov (32) considered a model for molecular reorientation which takes into account both rotation and orientational vibration, and showed that the spectral shape of a simple Lorentzian is modified if inertial effects are present. If rotational diffusion is considered, the intensities I_v , I_h , (defined on p. 2.7) for incident light polarized in the z-direction, are given by

$$I_v = (4/3)I_h = \frac{4}{45\pi} \frac{\tau_{1=2}}{\left(1 - \frac{I}{4kT_0}\omega^2\right)^2 + \omega^2\tau_{1=2}^2} \dots\dots\dots(2.79)$$

where I is moment of inertia of molecules. If the molecules are vibrating elastically in the field of their neighbours, then

$$I_v = (4/3)I_h = \frac{4}{45\pi} \frac{6kT_0}{\mu} \frac{(\eta/\mu)}{\left(1 - (I/\mu)\omega^2\right)^2 + \omega^2(\eta/\mu)^2} \dots\dots(2.80)$$

where η is internal friction, and μ is shear modulus.

The spectrum will be the sum of these modified Lorentzians. The relaxation time (η/μ) characteristic of vibration will be much shorter than that for rotation, so that the vibrational curve will correspond to the far wings of the anisotropic spectrum, and the rotational curve will be closer to the centre. The inertial terms tend to cut off the wings of the Lorentzians, so that the reciprocal intensity curve (fig. 2.4b) curves upwards. Zaitsev and Starunov (33) performed measurements on the wings of the anisotropic line (using a monochromator) which tend

to verify these predictions, although their resolution was not high enough to measure the central part of the line. They performed measurements on the linear molecules chloroform and carbon disulphide, and on the non-linear molecule acetic acid. For this last, they separated regions corresponding to the two moments of inertia. This illustrates the increasing complexity of the spectrum as more complex molecules are used.

There are two main theories which deal with the scattered-light spectrum from the point of view of fluctuations in shear stress and deformation. These are the theories of Leontovich (29) and Rytov (30). The work of Rytov includes the results of Leontovich. Recently some experimental results have been published (31), (54), which verify Rytov's work, and the question has arisen of incorporating his results into the "single-particle" framework already outlined.

His basic approach is similar to that employed in calculating the isotropic spectrum, except that he uses the general equations of elasticity instead of those of hydrodynamics. He does this so that the frequency-dependence of the parameters characterizing the medium may be included from the outset. He assumes the medium to be isotropic, and characterizes it by two elastic moduli, shear and compressional, and the scalar coefficients of thermal expansion and conductivity, as well as the heat capacity. Assuming small fluctuations, he uses the linearized equations

$$j\omega\rho v_i = \partial\sigma_{ik} / \partial x_k \quad \dots\dots\dots (2.81)$$

$$v_i = j\omega s_i \quad \dots\dots\dots (2.82)$$

$$\sigma_{ik} = 2\tilde{\mu}u'_{ik} + \bar{K}(u - c\theta)\delta_{ik} \quad \dots\dots\dots (2.83)$$

$$u_{ik} = \frac{1}{2}(\partial s_i / \partial x_k + \partial s_k / \partial x_i) \quad \dots\dots\dots (2.84)$$

$$u \equiv u_{ii} = \text{div } \underline{s}, \quad u'_{ii} = u_{ii} - \frac{u}{3} \delta_{ik} \quad \dots\dots\dots (2.85)$$

$$j\omega \rho_0 \underline{s} = \kappa \nabla^2 \theta \quad \dots\dots\dots (2.86)$$

$$\rho_0 T_0 \underline{s} = C/3 \sigma_{ii} + D \theta \quad \dots\dots\dots (2.87)$$

where \tilde{K} is complex bulk modulus

$\tilde{\mu}$ is complex shear modulus

\underline{s} is displacement of particles

\underline{v} is velocity of particles

u_{ik} is deformation tensor, u'_{ik} is pure shear deformation tensor

σ_{ik} is stress tensor

S is entropy per unit mass

θ is change in temperature, T/T_0

K is thermal conductivity

C, D are constants, which in the absence of dispersion are given by

$$\left. \begin{aligned} C &= \alpha T_0 \\ D &= \rho_0 T_0 C_p \end{aligned} \right\} \quad \dots\dots\dots (2.88)$$

These equations may be used to calculate the components for given ω and q , of the auto and cross correlation functions of the parameters flow velocity, temperature, tensor stress and tensor deformation. The relation of these parameters to the dielectric constant then gives the spectrum.

Rytov assumes that the dielectric constant is given by

$$\epsilon_{ik}(\omega, q) = \tilde{X}(j\omega) u'_{ik}(\omega, q) + \tilde{Y}(j\omega) u(\omega, q) \delta_{ik} + \tilde{Z}(j\omega) \theta(\omega, q) \delta_{ik} \quad \dots\dots\dots (2.89)$$

and so evaluates the isotropic and anisotropic spectrum for horizontally

and vertically polarized incident light. The direction of polarization of the incident light will from now on be indicated by a superscript x or z . The spectra of I_h^x , I_v^x and I_v^z contain terms in $|X|^2$ only. The spectrum of I_v^z also contains terms in $|Y|^2$, $|Z|^2$, and cross-terms between X, Y, Z . These give the isotropic spectrum, and Rytov draws attention to the components of this spectrum, including the continuous background dependent on the dispersion.

The equations for the spectra of I_h^x , I_v^x , and I_h^z are given below.

$$I_h^x = \frac{\textcircled{H}}{8\pi j \omega} \left\{ \frac{1}{\tilde{\mu}^*} \left(1 + \frac{d_1 \tilde{\mu} q^2}{\Delta} \right) - \text{complex conjugate} \right\} \dots\dots (2.90)$$

$$I_v^x = I_h^z = \frac{\textcircled{H}}{16\pi j \omega} \left\{ \frac{1}{\tilde{\mu}^*} \left(1 + \frac{\rho_0 \omega^2}{|A_4|^2} \right) - \text{complex conjugate} \right\} \dots\dots (2.91)$$

$$\text{where } \textcircled{H} = kT_0 \dots\dots\dots (2.92)$$

$$d_1 = D + kT_0 q^2 / j\omega - c^2 \tilde{\kappa} \dots\dots\dots (2.93)$$

$$A_4 = (\rho_0 \omega^2 - \tilde{\mu} q^2) \dots\dots\dots (2.94)$$

$$\Delta = D \left[\rho_0 \omega^2 - \left(\tilde{\kappa} + \frac{4}{3} \tilde{\mu} \right) q^2 \right] - c^2 \tilde{\kappa} \left(\rho_0 \omega^2 - \frac{4}{3} \tilde{\mu} q^2 \right) \dots\dots\dots (2.95)$$

Rytov simplifies equations (2.90) and (2.91) by means of the following assumptions;

a) The coefficient X is proportional to the complex shear modulus

$$X(j\omega) = B \tilde{\mu}(j\omega) = (A/\mu_\omega) \cdot \mu(j\omega) \dots\dots\dots (2.96)$$

b) The coefficient Y is dispersionless and therefore given by

$$Y = -\rho_0 (\partial \epsilon / \partial \rho)_{T_0} \dots\dots\dots (2.97)$$

c) The shear modulus obeys the simplest dispersion law, relaxing with the single relaxation time τ_μ ,

$$\tilde{\mu} = \mu + j\omega\eta = \mu \left[\frac{j\omega\tau_\mu}{1 + j\omega\tau_\mu} \right] \dots\dots\dots (2.98)$$

Equations (2.90) and (2.91) then become

$$I_{\text{h}}^{\text{x}} = \frac{\textcircled{H} A^2 \tau_{\mu}}{16 \pi \mu_{\infty}} \left\{ \frac{3(\omega^2 - \omega_{\text{L}}^2)^2}{(\omega^2 - \omega_{\text{L}}^2)^2 + \omega^2 \tau_{\mu}^2 (\omega^2 - \omega_{\text{s}}^2)^2} + \frac{1}{1 + \omega^2 \tau_{\mu}^2} \right\} \dots (2.90b)$$

$$I_{\text{v}}^{\text{x}} = I_{\text{h}}^{\text{z}} = \frac{\textcircled{H} A^2 \tau_{\mu}}{8 \pi \mu_{\infty}} \left\{ \frac{\omega^2}{\omega^2 + \tau_{\mu}^2 (\omega^2 - \omega_{\text{T}}^2)^2} + \frac{1}{1 + \omega^2 \tau_{\mu}^2} \right\} \dots (2.91b)$$

$$\text{where } \omega_{\text{T}}^2 = \mu_{\infty} q^2 / \rho_0$$

$$\omega_{\text{L}}^2 = K_0 q^2 / \rho_0$$

$$\omega_{\text{s}}^2 = \omega_{\text{L}}^2 + \frac{4}{3} \omega_{\text{T}}^2$$

The shape of these curves is shown in figure(2.5). In each of the equations (2.90b), (2.91b), the non-Lorentzian first term is derived from the factors inside the bracket in equations (2.90) and (2.91). The second simple Lorentzian centred at the incident frequency is derived from the factor $|X|^2$. Hence the dependence of the two curves in each equation on the same relaxation time is derived from assumption a). The first term in eq.(2.90b) contains factors relating to compression, as may be seen from the moduli involved, and gives rise to a very sharp "Brillouin" doublet with peaks at the frequency $\omega = \pm \omega_{\text{s}}$, width governed by the parameter $\omega_{\text{T}}^2 / \omega_{\text{L}}^2$. The first term in eq. (2.91b) gives peaks due to the scattering of light from transverse shear waves. The difference between the spectra is due to the directional properties of shear and compressional waves. (See figure 2.6). If the shear waves are travelling in the 1' direction, the displacement can only occur in the 2'-3 plane, and there is no associated variation in density. (See, for example, ref. 5). Hence the shear stress contains terms in u'_{31} , and u'_{21} . The terms in u'_{31} may be transformed by rotation through 45° about the 3-axis into terms in u'_{31} and u'_{32} . These terms give rise to scattered light of polarization

Figure 2.5a (equation (2.91b))

- ① Single Lorentzian term
- ② Shear wave term
- ③ Sum: ① + ②

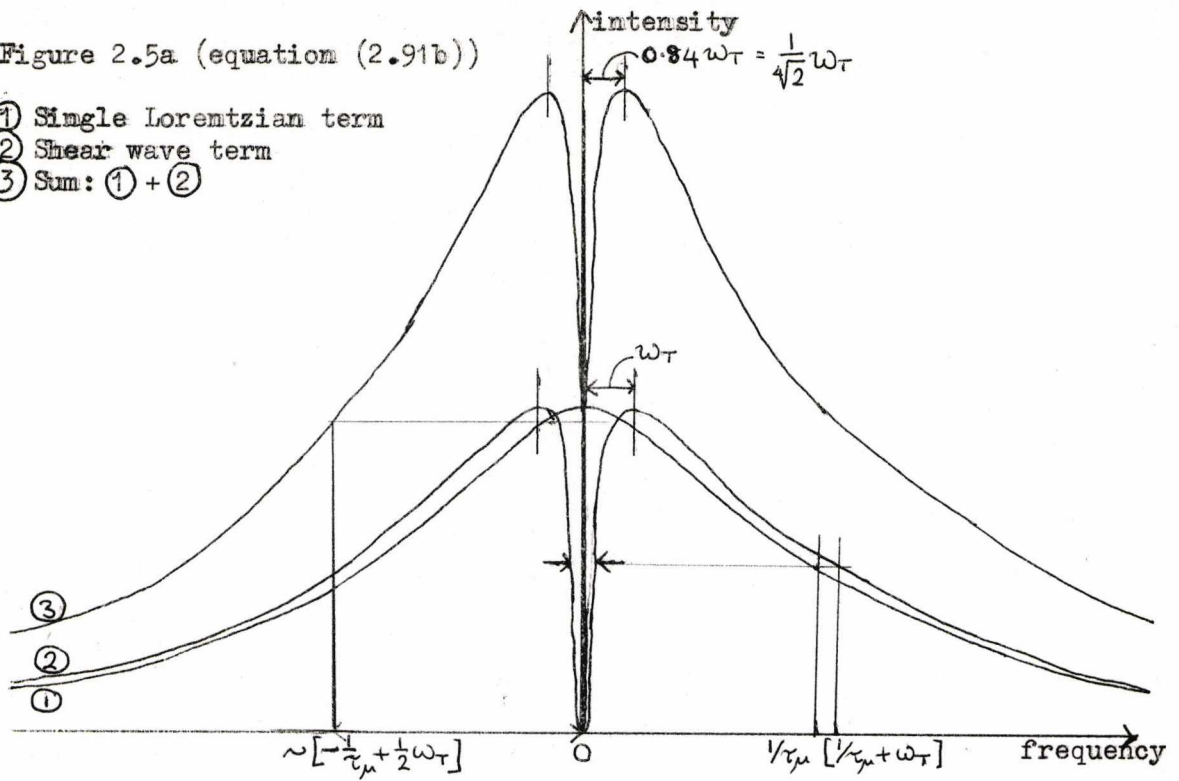


Figure 2.5b (equation (2.90b))

- ① Single Lorentzian term
- ② Sum of ① + shear term

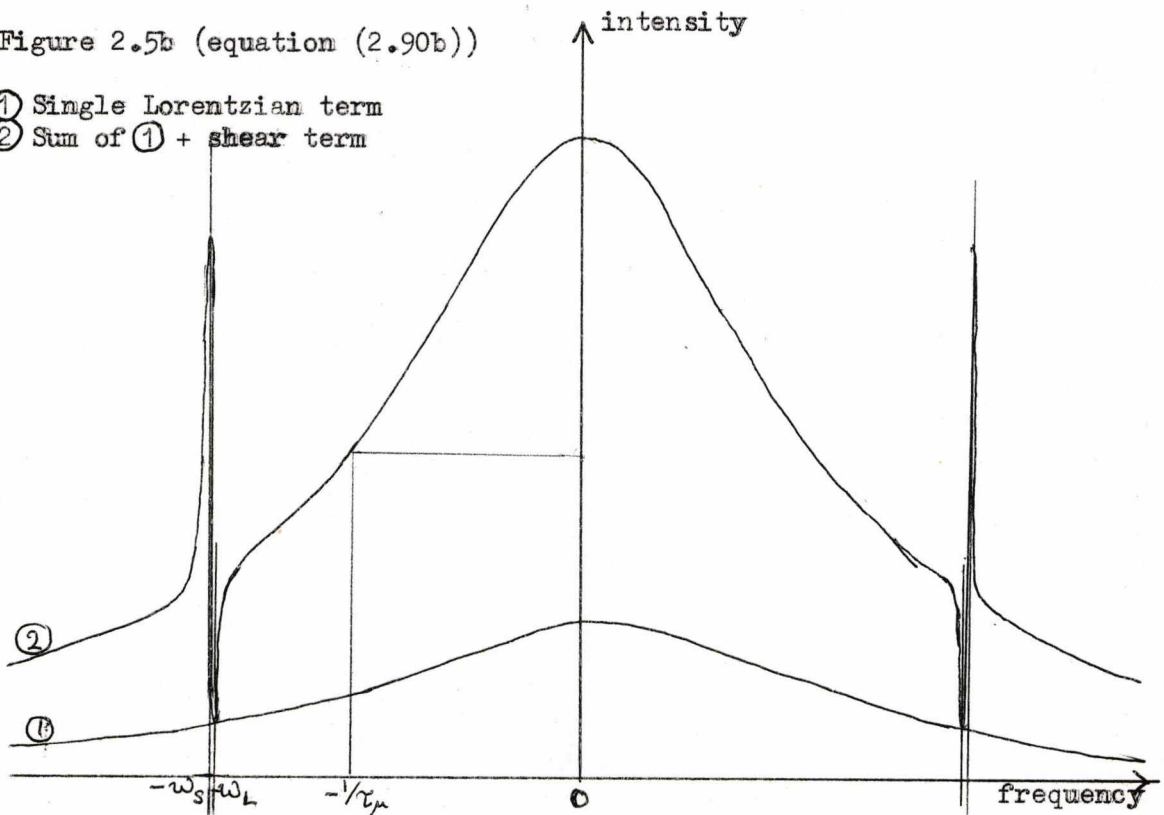
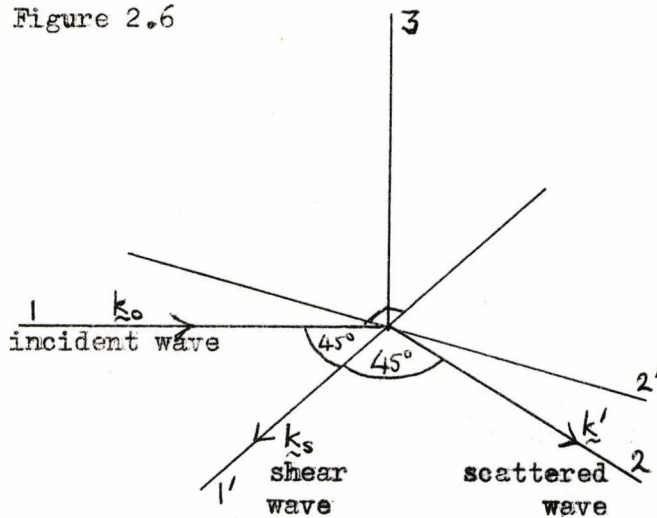


Figure 2.6



I_h^z and I_v^x , using eq. (2.89).
 However, the component of stress appropriate to I_h^x is u'_{12} , which on transformation by rotation through 45° about the 3-axis becomes $\frac{1}{2}u'_{1'1'} - \frac{1}{2}u'_{2'2'}$. These terms are related not to shear waves, but to compressional waves; hence the appearance

of components at the Brillouin frequency in the spectrum I_h^x . (The peaks due to shear waves are only completely absent for 90° scattering). The total intensity in all three components is the same.

If ω_T is negligible in equations (2.90b) and (2.91b), the first term in each simplifies to a single Lorentzian with width governed by γ_μ , so that the equations become

$$I_h^x = I_v^x = I_h^z = \frac{(\hbar) A^2 \gamma_\mu}{4 \pi \mu_\infty} \left\{ \frac{1}{1 + \omega^2 \gamma_\mu^2} \right\} \dots \dots \dots (2.99)$$

and the total intensity of each is then given by

$$I = \frac{(\hbar) A^2}{4 \mu_\infty} = \frac{(\hbar)}{4} \mu_\infty \left| \frac{\chi}{\mu} \right|^2 \dots \dots \dots (2.100)$$

The value of μ_∞ is related to the shear viscosity by the equation

$$\mu_\infty = \gamma_\mu \eta \dots \dots \dots (2.101)$$

from eq. (2.98), so that the temperature-dependence of the intensity is governed by these factors. If the ratio $\left| \frac{\chi}{\mu} \right|$ remains constant, and the relaxation time has an Arrhenius temperature-dependence (eq. 2.78), and we assume that the viscosity has the same exponential temperature-dependence as γ_μ ,

$$\eta \propto T_0 \exp(E_a/RT_0) \dots\dots\dots (2.102)$$

$$\tau_\mu \propto \exp(E_a/RT_0) \dots\dots\dots (2.103)$$

then the total intensity varies with temperature as

$$I \propto T_0^2 \exp(2E_a/RT_0) \dots\dots\dots (2.104)$$

Hence, unless E_a is very small, the intensity should decrease with temperature, possibly rapidly, if E_a is large compared with RT_0 .

The deviations from Lorentzian lineshape shown in fig. (2.5) disappear if $\omega_T \tau_\mu$ is much less than unity. They may be clearly resolved if the instrumental linewidth, $2\Gamma_p$, is of order

$$2\Gamma_p = 2\sqrt{2} \omega_T^2 \tau_\mu \dots\dots\dots (2.105)$$

and they may not be resolved if the instrumental linewidth is of order

$$2\Gamma_p = (1.7)\omega_T \dots\dots\dots (2.106)$$

(see fig. 2.5). The true resolution limit lies between these values. An estimate of the expected shear-wave splitting in any liquid may be obtained from the relation

$$\omega_T = \sqrt{\frac{K}{\rho_0}} = \sqrt{\frac{K}{\rho_0} \frac{\eta_0}{((4/3)\eta + \zeta)}} = \omega_L \sqrt{\frac{\eta_0}{((4/3)\eta + \zeta)}} \dots\dots\dots (2.107)$$

where η_0 is low-frequency shear viscosity, and the bulk viscosity and frequency of sound-waves may be obtained from the isotropic spectrum. This relation is based on the assumption that bulk and shear viscosity decay with the same relaxation time. The value obtained will be an upper limit, since a low-frequency bulk viscosity should really be used, and

part of this may have relaxed out at frequencies below ω_L . Ultrasonic measurements of the absorption coefficient of sound, if available, will give ω_T to greater accuracy.

The resolution limit imposed by the relations (2.105) and (2.106) is near to the limit of the Fabry-Perot technique, using a multimode laser. The predictions of equations (2.90b) and (2.91b), have, however, been verified, within the experimental error, by Stegemann and Stoicheff (31) and Starunov et al. (37). Stegemann and Stoicheff report the existence of a central dip in the I_h^z and I_v^x polarization components for nitrobenzene, aniline, quinoline and m-nitrotoluene, and also the existence of a weak doublet at the Brillouin frequency in the wings of I_h^x .

Rytov, however, certainly did not expect that the shear waves would be the cause of the central region of the spectrum. He realized that his predictions did not agree with experiment in that the shape of the experimental line is not a simple Lorentzian. The deviations he predicted tend to flatten, rather than sharpen, the basic Lorentzian shape. To allow for this disagreement, he dispensed with the assumption that the constant B ($= X/\tilde{\mu}$) is independent of frequency. (Assumption a, p. 2.39). He replaced it by the assumption that $\tilde{\mu}$ has the same form as before:

$$\tilde{\mu} = j\omega\tau_\mu\mu_\infty / (1 + j\omega\tau_\mu) \quad \dots\dots\dots (2.98)$$

but the value of \tilde{X} is now governed by two relaxation times

$$\tilde{X} = \frac{X_0 + j\omega\tau_\mu X_\infty}{1 + j\omega\tau_\mu} \cdot \frac{j\omega\tau_2}{1 + j\omega\tau_2} \quad \dots\dots\dots (2.108)$$

where X_0 gives rise to a low-frequency dielectric constant, still proportional to the shear deformation, which relaxes with characteristic time τ_2 , which is much greater than τ_μ .

This assumption now makes the spectrum into the sum of two Lorentzians, of which the central one has a width $2/\tau_2$, and the shear waves are responsible for the wings. The same interpretation has been put forward recently by Ben-Reuven (61), attributing the longer time to molecular reorientation, which is the contribution Rytov's theory omits. It would seem unlikely that there are slower processes for the decay of shear fluctuations than molecular reorientation, but the shear waves might well decay more rapidly. Hence it appears that the liquids mentioned, ⁽³¹⁾ if it is true that the central region of the spectrum is due to shear waves, must be rather unusual. Szöke et al (34) postulate the existence of 'clusters' of molecules in nitrobenzene, with orientation strongly correlated over unusually large distances; this may be equivalent to saying that shear-waves persist for long times.

These theories lead to the following interpretation of the spectrum. From a microscopic viewpoint, the far wings are due to molecular vibrations, and the central region to molecular rotation. The shear-stress fluctuation theory of Rytov, which takes into account only the correlation terms omitted in the microscopic theories, predicts another curve, approximately Lorentzian. It seems likely that this curve usually lies in the wings of the molecular rotation curve, but in some liquids it may cause effects which appear in the central region of the spectrum. Measurements on the temperature dependence of total intensity and linewidth may help to clarify the situation in individual liquids.

CHAPTER 3Experimental.

A series of measurements has been undertaken on six benzene derivatives, whose anisotropic spectra are sufficiently narrow for the central part to be resolved using a Fabry-Perot etalon. These liquids were nitrobenzene ($C_6H_5NO_2$), aniline ($C_6H_5NH_2$), chlorobenzene (C_6H_5Cl), bromobenzene (C_6H_5Br), benzonitrile (C_6H_5CN) and benzoyl chloride (C_6H_5COCl).

Both isotropic and anisotropic spectra were examined, by using both directions of polarization of the incident light, and different values of the Fabry-Perot spacer were used to enable different ranges of frequency-change to be studied.

A preliminary series of experiments was performed on the anisotropic spectra at room temperature, using several values of Fabry-Perot spacer to illustrate the effects of the overlap of successive orders. This will be known as experiment I. The isotropic and anisotropic spectra were then recorded over a temperature range from the freezing point of the liquids to $160^\circ C$. or the boiling point, at atmospheric pressure. These measurements were all made at a fixed scattering angle of 90° . This will be known as experiment II.

The experimental arrangement was as illustrated in figure 3.1. The laser beam passed along the axis of the cylindrical scattering cell containing the liquid sample. Light scattered at 90° was collimated by a collecting lens, passed through a series of apertures to eliminate extraneous light, and entered the Fabry-Perot etalon. The Fabry-Perot ring pattern was focussed in the plane of the photomultiplier aperture by a long focal length lens, and centred upon the aperture. The ring-

pattern was scanned either by varying the pressure between the etalon plates, or by varying the plate-separation piezoelectrically (see below). In the case of pressure-scanning, the pressure varied linearly with time, and the light signal, having been amplified by the photomultiplier and d.c amplifier, was recorded on the X-t recorder.

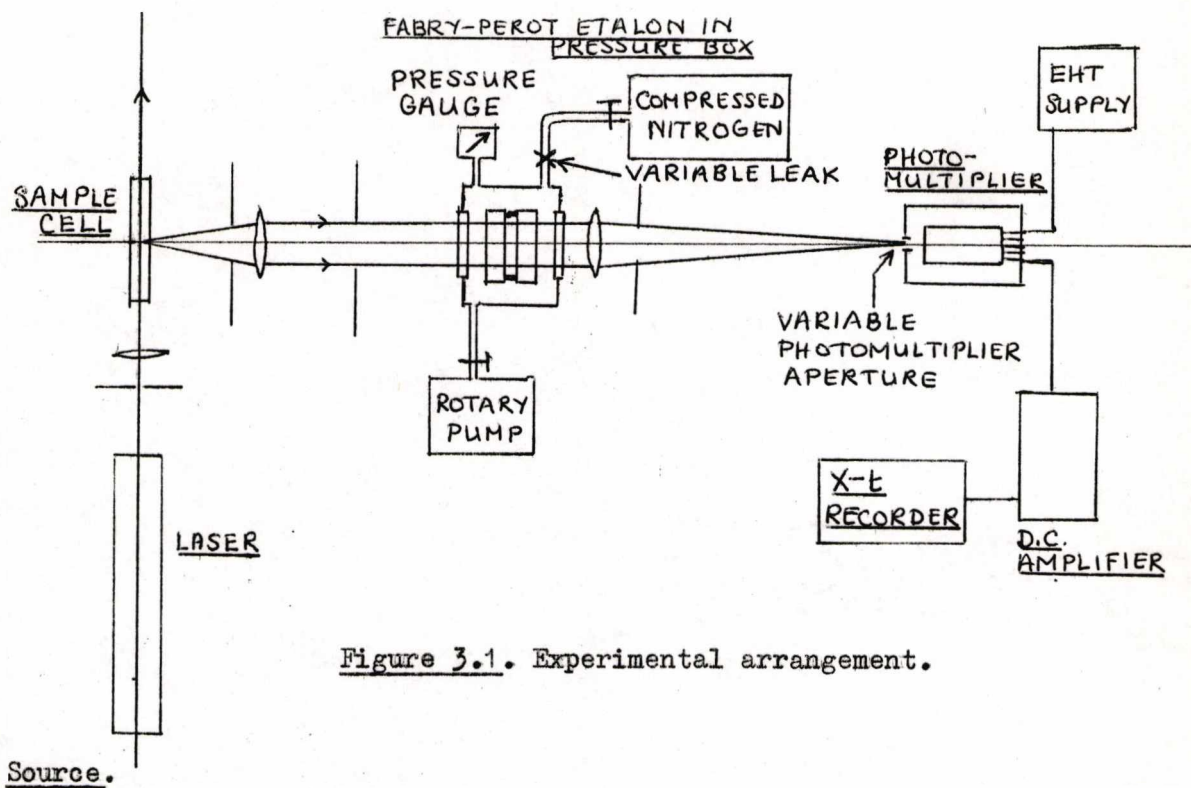


Figure 3.1. Experimental arrangement.

Source.

The light-sources used were He-Ne lasers operating at 6328 \AA . Two lasers were used; a Spectraphysics 124 of power 15-20 mW and linewidth about $7 \times 10^8 \text{ Hz}$, and a Spectraphysics 125, of power 40-90 mW and linewidth about $9 \times 10^8 \text{ Hz}$. These were fitted with a Spectraphysics polarization rotator type 310, which could be adjusted to an accuracy of $10'$, and caused no change either in intensity or position of the laser beam with rotation. The lasers operated in the Tem_{00} mode, meaning that a number of longitudinal modes were present within the Doppler profile, and the line-shape was approximately Gaussian.

Optics.

The choice of optics is governed by the need for the maximum scattered intensity and the best possible resolution consistent with this. The factors to be taken into account are listed below. (See fig. 3.2)

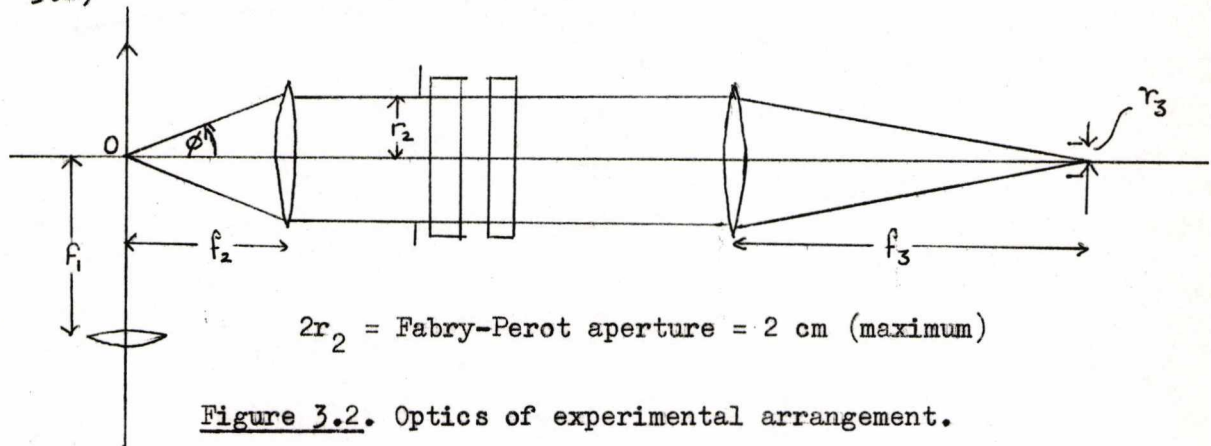


Figure 3.2. Optics of experimental arrangement.

- 1) The laser beam must be focussed so that its diameter at the point of observation O is less than the diameter of the image of the photomultiplier aperture in the object plane. This criterion must be satisfied for the entire length of the beam under observation. A lens of 25 cm focal length was used, and this criterion was satisfied for all measurements except where thermal defocussing occurred. (See appendix B).
- 2) The angle of acceptance of scattered light, ϕ , is maximised by reducing f_2 . In experiment I, a cylindrical lens of focal length 5 cm., aperture 2 cm., was used. For large collection angles, the amount of light due to horizontally polarized incident light, which is accepted by the apparatus*, must be calculated. This contribution was found to be a negligible proportion of the scattered intensity collected. The spread in scattering angle accepted is given by

$$d\theta = r_3/f_3 \quad \dots\dots\dots (3.1)$$

*See figure 2.1. The isotropic light, is being considered.

In experiment II, a spherical lens of focal length 30 cm was used for practical reasons. A spherical lens introduces a larger error due to the spread in scattering angle accepted. This is now given by

$$d\theta = r_2/f_2 + r_3/f_3 \quad \dots\dots\dots (3.2)$$

Using this lens, light scattered between about 89° and 91° is accepted. The Brillouin lineshape is changed slightly due to this spread in θ , but the Brillouin splitting is unchanged, and the linewidth is increased by about 3%, which is within the experimental error of these measurements.

The light-collecting efficiencies of a cylindrical and spherical lens of the same focal length are identical, if an "infinite" line-source is used. The total intensity reaching the photomultiplier is given by

$$i = I \cdot 2\pi x r_2^2 r_3 / (f_2 f_3) \quad \dots\dots\dots (3.3)$$

in each case, where I is scattered intensity per unit length per unit solid angle at 90°

x is fraction of incident light passing through Fabry-Perot.

3) The instrumental resolution is maximised if the factor r_3/f_3 is very small. The size of the ring-pattern is governed by f_3 . The final aperture has no effect on the instrumental linewidth if its diameter is much less than that of the central "finesse-broadened" spot when about to disappear. However, in this work it was found convenient to allow a small amount of aperture-broadening and gain the associated increase in intensity (see eq.(3.3)). The value of f_3 was chosen to be 50 cm, and the photomultiplier aperture was of variable diameter between about 0.8 mm and 1.0 cm, so that at minimum aperture the angle r_3/f_3 was about $3'$, which is negligible in comparison with r_2/f_2 (see eq 3.1, 3.2).

The aperture was kept at its minimum for all these measurements, except when the smallest Fabry-Perot spacer was being used to study very weak and broad lines. The aperture broadening was never more than about 10% of the finesse width.

Interferometer.

For Brillouin spectra, anisotropic spectra measured at low temperatures, and measurements of the relative intensity of the components of the spectra, a pressure-scanning Fabry-Perot was used. The etalon (Hilger and Watts B 297), had plates of diameter 1" (aperture 2 cm), flat to $\lambda/80$, and dielectrically coated for 95% reflectivity and minimum absorption. (Silvered or aluminized plates were found to reduce the intensity of the Fabry-Perot peaks by 70-80% due to absorption) A range of spacers was used (values of free spectral ranges shown in brackets).

- 1) 1.42 mm (3.52 cm^{-1})
- 2) 3.00 mm (1.67 cm^{-1})
- 3) 4.94 mm (1.01 cm^{-1})
- 4) 9.98 mm (0.501 cm^{-1})

The three largest spacers were of polished silica, and the smallest was of invar, machined in this department and polished by Optical Surfaces, Ltd. Using the silica spacers, the Fabry-Perot remained in adjustment for days at a time inside the evacuated pressure box, but with the invar spacer it remained set-up for at most three experimental runs, and usually required adjustment before every spectrum was taken, and measurement of the finesse before and afterwards. Other invar spacers showed similar behaviour, and it appears to be too springy a material to be

ideal for this application.

The pressure-box was of the shape and design shown in the diagram (figure 3.3) and incorporated the following features.

- a) The etalon was adjustable inside the box so that its optic axis could be tilted vertically or horizontally. It could then be clamped in position.
- b) The box itself could be rotated about a vertical axis so that stray images could be thrown off to one side of the optic axis of the system.
- c) The box had to withstand a pressure of at least one atmosphere, and be so designed that pressure could equalise rapidly in all parts of it.
- d) The end-plates were of polished borosilicate glass, flat to $\lambda/10$, and $\frac{1}{4}$ " thick. They were sealed in place by rubber O-rings.

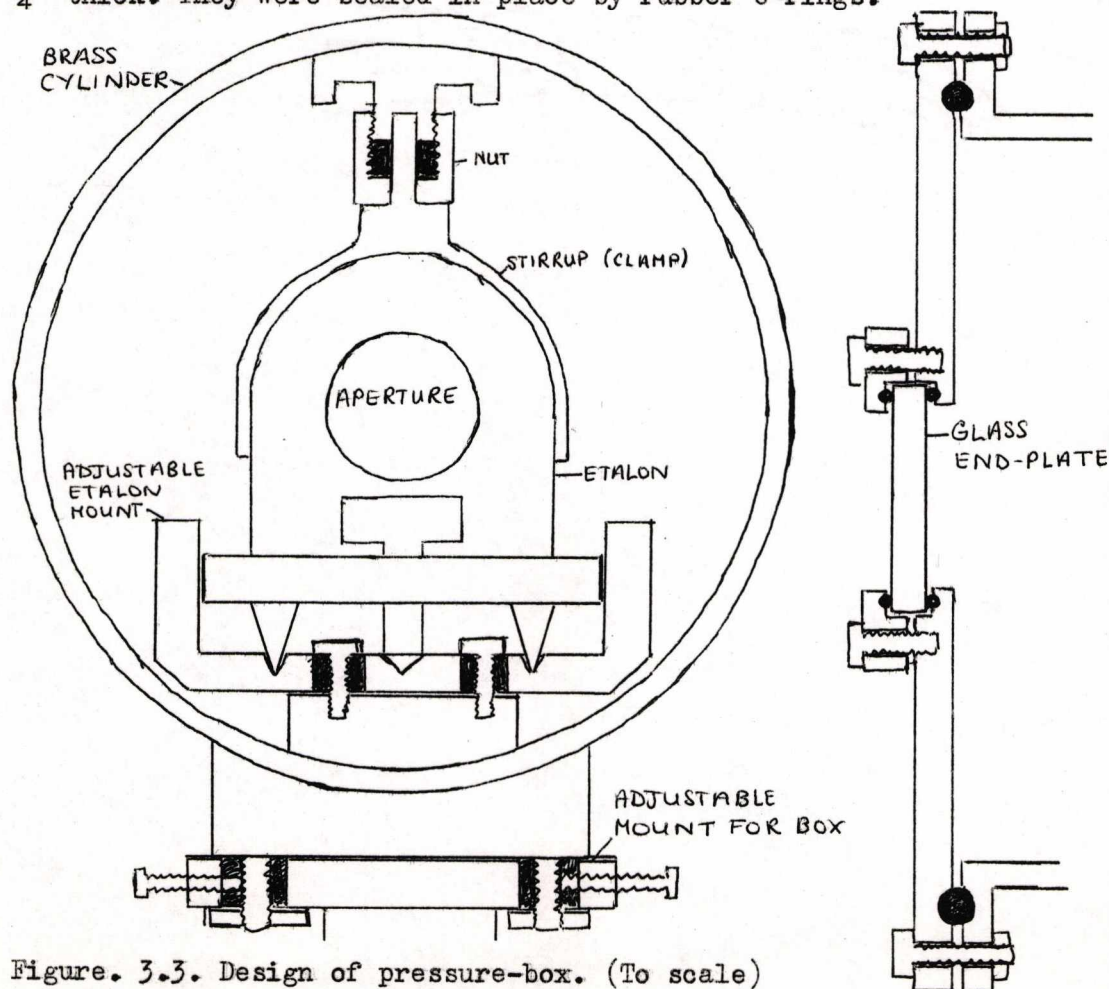


Figure. 3.3. Design of pressure-box. (To scale)

In scanning, the box was evacuated, and nitrogen from a compressed nitrogen cylinder allowed to leak slowly into it through an Edwards valve type OSID (variable leak-rate). For the smallest spacer, a pressure change between the Fabry-Perot plates of one atmosphere corresponded to a spectral range of just over one order. A pressure of 60-70 p.s.i. above atmospheric pressure was needed on the high pressure side of the leak to keep the gas flow linear with time to better than 1% throughout this range. The linearity was measured by observing the spacing of successive orders using a 1.5 cm spacer over the entire range. The flow was found to be linear up to about 4 p.s.i. above atmospheric pressure, once the flow had become steady after the leak was opened, for several settings of the leak-rate. For the larger spacers lower pressures could be used. The spectra were scanned quite slowly to ensure that pressure had equalised everywhere in the box, response times were negligible, and random noise could be smoothed. A typical time of scan was 10-20 minutes.

Using the 9.98 mm spacer, a typical finesse* was 15 for the Spectraphysics 125 at high power and 20 for the Spectraphysics 124. (Finesse-widths 1×10^9 Hz, 0.75×10^9 Hz). The finesse shapes were very nearly Gaussian, indicating that in this region of resolution, the finesse is limited by the Doppler-broadening of the source, and the flatness and reflectivity of the Fabry-Perot plates have little effect. Using the 1.42 mm spacer, a finesse of 30-40 could be obtained ($3.5-2.6 \times 10^9$ Hz), even higher values being possible if only the central region of the plates was used. Hence the finesse was limited intrinsically by the flatness and reflectivity of the plates, but it fell off very rapidly with slight

*Defined as ratio of interorder spacing to instrumental width.

errors in alignment or distortion of the plates due to pressure on the setting screws. A value of 25-35 was practicable, and the lineshape was a convolution of a Gaussian and a Lorentzian.

Detection apparatus.

Before entering the photomultiplier, the light passed through a dielectric multilayer filter (Grubb Parsons), coated for 58% transmission at 6328 \AA , bandwidth 130 \AA . This cut out extraneous scattering far from the frequency region under investigation, and did not affect the region surrounding the incident wavelength.

The photomultiplier used in this work was an EMI 9558A (trialkali photocathode for high sensitivity in the red region of the spectrum). When operating at 1350 V, the tube had a d.c. noise level of 0.4 mA . The signal level was at worst twice as great as this, and usually greater by a factor of 15-20. Hence it was unnecessary to cool the photomultiplier.

The output from the photomultiplier was fed into a Claude Lyons MV -07C DC Micro-Volt Ammeter, which recorded a full-scale deflection for currents of $10 \mu\text{A} - 1000 \mu\text{A}$, and whose output could be taken to the Servoscribe pen-recorder type RE 511.

Piezo-electric scanning Fabry-Perot.

For high temperature measurements on the anisotropic spectrum, where the linewidth was very broad, it was necessary to use a Fabry-Perot whose spacer could be reduced to values lower than 1.5 mm, to give increased free spectral range. The pressure-scanning technique is limited by the size of the smallest fixed spacer that can be made. Hence these measurements were taken using a piezo-electric scanning Fabry-Perot*, whose plate separation could be reduced to 0.1 mm. This instrument will

*Built and used for these results by B. Simic-Glavaski.

be described elsewhere (64). The aperture was considerably smaller than in the pressure-scanning Fabry-Perot, meaning that the signal:noise ratio was lower, and errors, due to uncertainty in the position of the zero-level for the spectra, were introduced. A finesse of about 30 could be obtained, and since the broadening in this resolution region is entirely due to flatness, reflectivity and alignment of the plates, the lineshape was accurately Lorentzian. The value of the spacer was variable, and could be measured to 1% by photographing the ring-pattern.

The Scattering Cells.

These were made to order by Tintometer Ltd., and were of size and shape shown in fig.(3.4a). Cells of spherical and conical shape were also considered. A cell using a conical lens is shown for comparison, (fig 3.4b). The cylindrical shape was selected for the following reasons:

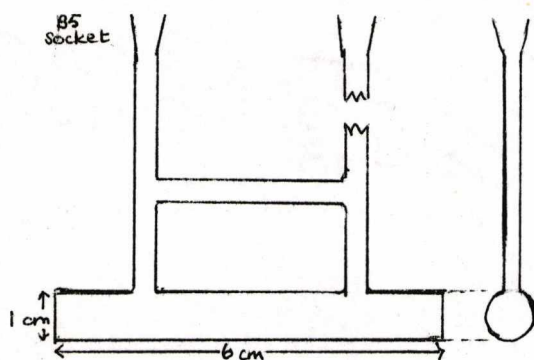


Fig. 3.4a. Cylindrical cell.

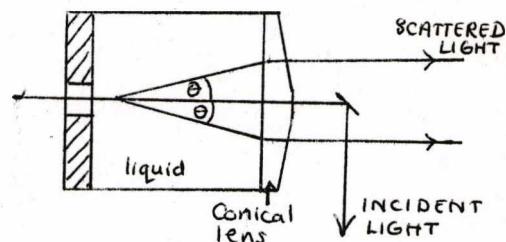


Fig. 3.4b. Illustrating the use of conical optics.

- 1) The cylindrical cell has the same symmetry as the beam, and light scattered at an azimuthal angle ϕ is refracted in the same way from all parts of the beam.
- 2) If a cylindrical lens may be used, the light-collection is much more efficient than may be obtained using a spherical lens for the same resolution.

3). The conical optics, although very efficient in light-collection, is extremely difficult to adjust, and also loses all the polarization information (see fig. 3.4b). Conical components are also virtually unobtainable.

The cells were made of polished borosilicate glass, and the pipes were fitted with Quickfit and Quartz standard B5 sockets and cones.

Temperature Baths.

Two temperature baths were used, covering the ranges 20-160°C., and -50 - +40°C. The high-temperature bath is shown in figure(3.5).

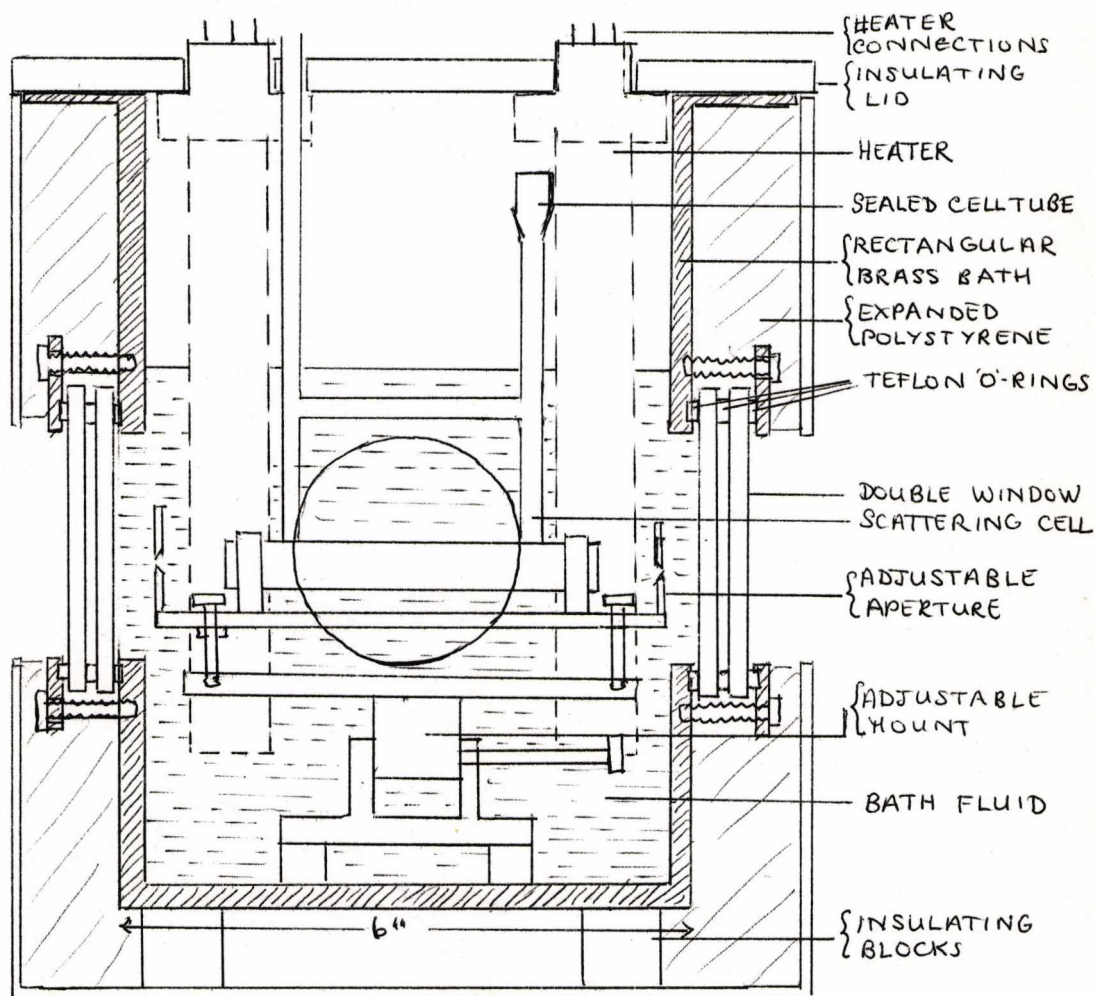


Figure. 3.5. High temperature bath. Some important features.

The high temperature bath incorporated the following features.

- 1). The bath fluid was silicone oil of viscosity 10 cs from Hopkins and Williams. This served to transmit and stabilize the temperature, and also to reduce reflection at the glass surfaces by approximately matching the refractive index of the glass.
- 2). The bath was stirred by bubbling laboratory compressed air through it from under the cell.
- 3). The scattering cell was mounted firmly on the base, and surrounded by black formica apertures and plates, to eliminate stray reflections, and prevent bubbles from passing through either incident or scattered beams.
- 4). The four 65 Watt heaters were sheathed in copper and mounted on tufnel handles. They were wired in parallel, and two or four of them could be used as desired. The temperature probe (see below) was attached to one of the heaters for immediate response to any temperature change.
- 5). The double glass windows were sealed with teflon O-rings.
- 6). The bath was mounted on laboratory adjustable tables so that the height and tilt could be adjusted from outside. The cell could be rotated and tilted independently.
- 7). The temperature was measured using mercury in glass thermometers, one calibrated to 0.1°C in the range $0-100^{\circ}\text{C}$., and the other to 0.5°C in the range $0-200^{\circ}\text{C}$..

The temperature was controlled using the Fisher Proportional Temperature Control type 15-177-50, and probe 15-177-56. Provided that the bath was stirred vigorously, the temperature was controlled to better than 0.1°C throughout the 10-20 minutes needed to record a spectrum.

Measurements of the temperature in different regions of the bath showed no variation. At temperatures below about 50°C , the control was not so good, and the controller tended to operate in an "on-off" manner, since the losses were insufficient for proper control. The temperature would remain constant to about 0.3°C , which is sufficient to cause no measurable variation in any of the spectra.

The low temperature bath consisted of a 6" diameter pyrex dewar, silvered except for a band all round it through which incident and scattered light could pass. The use of the dewar eliminated the problem of frosting on the windows. The small amount of condensation that did occur could be dried by blowing on hot air. The bath was stirred as before, and mounted on adjustable tables. Otherwise it differed from the high temperature bath in the following respects;

- 1). The bath fluid was acetone, which could be used from $+40^{\circ}\text{C}$ down to the lowest temperatures required.
- 2). The scattering cell was mounted on the lid on adjustable mounts, surrounded by the same plates and apertures as before.
- 3). The bath was cooled by a copper cooling coil through which liquid nitrogen could be passed. It also contained a single 65 Watt heater, with a thermistor temperature probe for use at low temperatures attached to it, which could be used with the Fisher Temperature Control.
- 4). The temperature was measured using a copper-constantan thermocouple, which had been calibrated using the more accurate of the mercury in glass thermometers.

The liquid nitrogen was passed through the cooling coil by boiling liquid nitrogen in a 25 litre dewar with a 50 W heater, the heating

probe also acting as a pipe, with a hole well below the liquid surface, thus forcing liquid nitrogen through the coil. The heater was connected to a variac, so that the rate of cooling could be varied. The cooling effect was offset by the heater in the bath, which was connected to the Fisher Proportional temperature control. Hence temperature control could also be obtained at low temperatures.

The two baths could thus be used in overlapping temperature ranges if desired. It was found possible to eliminate all scattering at the incident wavelength due to stray reflections, by correct tilting of glass surfaces and positioning of the apertures. It was found necessary in both cases to correct measurements of the Brillouin splitting for the slight deviation of the beams due to traversing several air-glass surfaces, since the Brillouin splitting is proportional to $\sin\theta/2$, where θ is the scattering angle.

In both cases, one entry tube to the scattering cell passed through the lid of the bath, and could be connected through a sintered disc filter to a large volume of air to keep the pressure atmospheric, or to a pump. Alternatively it could be sealed. It was found impossible to prevent a small quantity of dust from entering the cell during a long series of readings if the tubes were not sealed.

Preparation of samples.

The samples used were from freshly opened bottles of Analar grade reagents from British Drug Houses, where available. Otherwise they were distilled before use. Aniline in particular needed to be distilled over zinc dust in a moisture-free atmosphere to reduce the nitrobenzene impurity content. It then needed filtering to remove the zinc dust, and

this was done with all vessels surrounded by ice, since aniline is very photo-active and sensitive to moisture, but both these effects are greatly slowed down at low temperatures. Distillation of benzoyl chloride was not undertaken.

The samples were then prepared in the following way. The glass cells were cleaned with chromic acid and then distilled water. Sartorius filters* of about 0.1μ pore size were used, and a Sartorius MD 50 filter holder, which enabled 50 ml of liquid to be forced through filter under pressure of nitrogen from a gas cylinder. The cells and tubes were first rinsed with filtered acetone until the entire system was practically dust-free, and they were then washed out several times with different filtered samples of the liquid to be used, until a pure, dust-free sample was obtained. Occasionally a few particles of dust remained, but these generally settled out after an hour or two. Liquids which could not be completely freed from dust in this way were those which form chemical bonds with the dust particles, and include aniline. Samples of aniline could not be passed through the system more than once without increasing the nitrobenzene content. Benzoyl chloride reacted with any moisture present to form a white precipitate of benzoic acid, attacked the filters slowly, and reacted with nitrogen to form coloured impurities. Hence it was found necessary to filter a liquid which has no reaction with benzoyl chloride to remove all traces of acetone (which contains water) from the system, before introducing the sample, and then use an optimum nitrogen pressure or compressed argon. to perform the filtration. It was thus extremely difficult to obtain a pure dust-free sample of this liquid.

*Agents V.A.Howe.

Filters for use with chemically active liquids arrive packed in 0.4% formaldehyde solution. Before use, they needed to be soaked first in distilled water, then in acetone, and finally in a small amount of the liquid to be filtered. If they were used without soaking in acetone, the water molecules remained bound together in the pores, and some liquids could not be forced through the filters.

Changes in the samples observed during the temperature runs.

1) Photoactivity.

The photosensitivity of the liquids increases at high temperatures, and hence the concentration of absorbing and colouring impurities increased as the temperature was raised. Chlorobenzene, nitrobenzene and bromobenzene showed this effect least, but it was extremely marked in benzonitrile, aniline and benzoyl chloride. Benzonitrile reached a high impurity level, but this was sufficiently low to allow a repeat run to be performed at room temperature when the system had cooled down. No change was observed in the parameters to be measured.

2) Thermal defocussing.

If the absorption of the laser light by the liquid is sufficiently high, local heating effects may change the refractive index and 'defocus' the laser beam. This can spread the beam so that its image in the photomultiplier plane has a diameter greater than that of the photomultiplier aperture, with resultant loss in the intensity accepted. This last effect was only serious in benzoyl chloride, but thermal defocussing was also observed in nitrobenzene and aniline. The effect increased with increasing impurity content of the samples. A separate study was undertaken on this effect. (See Appendix B)

3) Precipitation of impurities at low temperatures.

This effect was observed in chlorobenzene and bromobenzene, the two liquids with the lowest melting points, at temperatures below about 5°C . As the system cooled below this temperature, scattering at the incident wavelength began to increase, until the scattering was so strong that the entire beam intensity was scattered within the cell. This could be much reduced by cooling the samples to below the freezing point until the liquid froze, and then pumping off dissolved gases as the sample was warmed through the melting point. In this way, the spectra could be improved so that values of the Brillouin splitting and linewidth could be obtained below 0°C . However, the effect could not be eliminated entirely, and it was not possible to record the anisotropic spectra. It seems likely that the excess scattering is caused by solid impurities such as ice, precipitating out of solution. It was found that a pressure change of one atmosphere made no difference to the Brillouin spectra.

Measurement of finesse.

It is very difficult to obtain accurate values of the instrumental width using direct laser light, since a laser is effectively a point-source. Unless the laser light is exactly parallel to the optic axis when it passes through the Fabry-Perot, and the beam occupies the whole Fabry-Perot aperture, only light from a small central region of the Fabry-Perot will reach the photomultiplier aperture. The value of the finesse thus measured may be much higher than the true value.

There are two possible ways of measuring the finesse, both of which have been used in this work, according to experimental convenience.

1) A cell containing a suspension of large scattering particles, such as pvc spheres, in water, may be placed in the position of the scattering cell, and the scattered light spectrum recorded.

2). The laser beam may be made to diverge until its diameter is large, when it strikes a ground glass screen. The image on the screen now becomes an extended source for the Fabry-Perot.

Information obtained from these measurements.

1) The isotropic spectrum.

The Brillouin splitting could be measured to an accuracy of 1-2%. The broadening of the Brillouin lines could be clearly observed, but could be measured only with limited accuracy (at best 10%). The temperature dependence of the intensity of the Brillouin lines is known (eq. (2.22)), so that even in the event of impurity absorption or thermal defocussing, the intensity of the Brillouin lines could be used to find that of other components measured at the same time. In measuring both broadening and intensity, it was important to allow for the effect of convolution of the Lorentzian Brillouin line with the Gaussian instrumental lineshape. After allowing for the antisymmetric components centred at the Brillouin frequency, (eq (2.44)), the spectra could be examined for the presence of a Mountain line. The accuracy of measurement of the intensity of the Rayleigh line was limited by extraneous scattering due to dust in some samples, and by uncertainty as to the amount of "Brillouin" intensity which had been redistributed into the region of the incident frequency. (See chapter 2). An estimate of the Landau-Placzek ratio could be obtained.

2) The anisotropic spectrum.

The lineshape and width of the anisotropic spectra could be obtained in the frequency region $0 - 20 \text{ cm}^{-1}$ ($6 \times 10^{11} \text{ Hz}$); that is, the peak could be resolved if the linewidth was less than half the limiting free spectral range of the Fabry-Perot. Beyond this region overlap effects meant that certain interpretation of the results was impossible, but estimates could be obtained by computational analysis. Total scattering intensities could also be obtained in most cases, either directly or by comparison with the Brillouin intensity. Computational analysis of the curves made it possible to estimate the proportion of the total intensity contained in the central Lorentzian in some cases.

From both isotropic and anisotropic spectra, the total depolarization ratio and its variation with temperature could be obtained.

CHAPTER 4.Experimental Results and Discussion.

Section 1. Experiment I. Study of anisotropic spectra at room temperature using several Fabry-Perot spacers. (Published in ref. (43)).

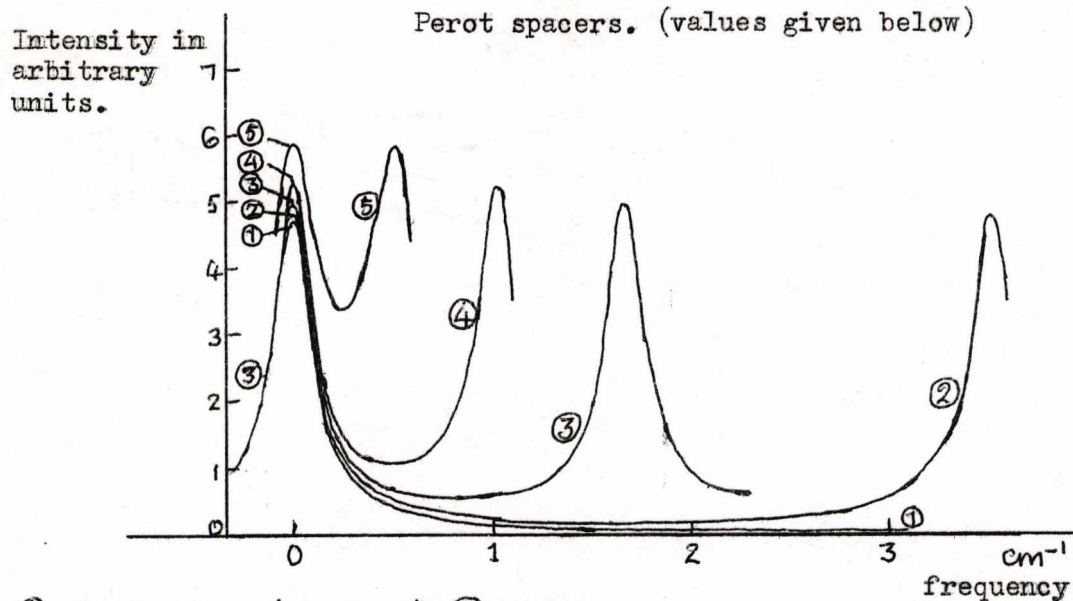
The experimental arrangement was as shown in fig. 3.1. The samples were illuminated with horizontally polarized light, and the total intensity scattered at 90° (including both directions of polarization) was collected. The temperature was $23 \pm 2^\circ\text{C}$.

Results for two of the liquids, nitrobenzene and benzoyl chloride, using several Fabry-Perot spacers, are presented in figures (4.1) and (4.2) in such a way as to make clear the effects of overlap of successive orders. The curve (1) in each case is a basic curve which reproduces the experimental curves when contributions due to successive orders are summed. The intensities have been normalised to agree with the basic curve at all points. For each liquid, the total intensity under each curve is approximately the same.

The results were first analysed by computer to test whether they could be fitted by a single Lorentzian, and whether overlapped spectra using different spacers gave a consistent width for the same liquid. This procedure was found to be completely inadequate. Those spectra which approximated best to a single Lorentzian (such as nitrobenzene) gave widely differing widths for different spacers, and those with an intense 'background' to the central Lorentzian (such as benzoyl chloride and aniline), gave no meaningful results at all.

It was clear that a single Lorentzian was an inadequate representation of the spectra. The departure from Lorentzian lineshape for benzoyl

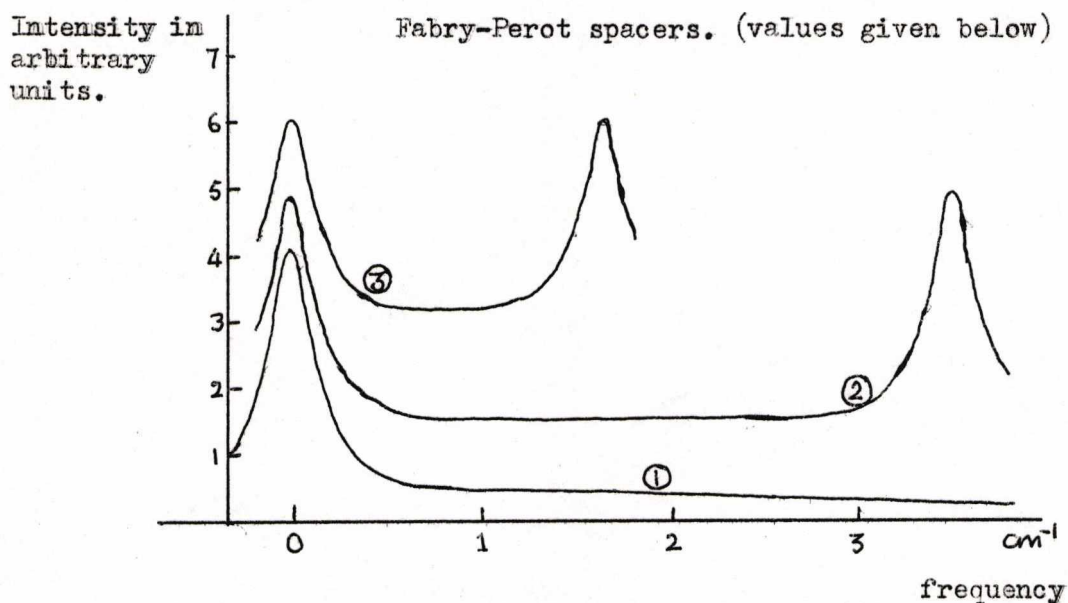
Figure 4.1. Anisotropic spectrum of nitrobenzene using different Fabry-Perot spacers. (values given below)



①. Basic curve (see text). ②. 1.42 mm spacer.

③. 3.00 mm spacer. ④. 4.94 mm spacer. ⑤. 9.98 mm spacer.

Figure 4.2. Anisotropic spectrum of benzoyl chloride using different Fabry-Perot spacers. (values given below)



①. Basic curve. (see text). ②. 1.42 mm spacer.

③. 3.00 mm spacer.

chloride is so marked as to be plainly discernable by eye in fig. (4.2).

In order to test how far the true spectrum could be obtained from the overlapped curves, without making any assumption as to the mathematical form of the lineshape, the experimental curves were first deconvoluted from the finesse curve (assumed Lorentzian) by numerical computation, (See Appendix A). The deconvoluted curves were then plotted as shown in figs. (4.1) and (4.2). The basic curve was estimated by finding a smooth curve, which, when overlapped for the different spacers, reproduced the deconvoluted results. In this way the effects of overlap could be allowed for. It is clear that an adequate correction must be made for the overlap, and that authors who have taken the zero-level as the minimum of the intensity curve, have obtained incorrect results for the linewidth. However, for such curves as the benzoyl chloride spectra, which have a very strong, flat 'background', the behaviour of the true spectrum cannot be estimated uniquely, since a very broad but rather weak, or an intense but steeply decreasing background, can be overlapped to give identical results. Approximate limits only may be found for the behaviour of the spectra beyond the central region. The central peak of the spectrum can be measured unambiguously, but for the study of the wings, the overlap must be minimised by the use of a sufficiently small spacer, or a monochromator must be used.

The accurate designation of the zero-level is very important in estimating such basic curves accurately, since the wings may be very broad, and large numbers of small terms contribute to the overlap. This means that photographic detection is inadequate. For the results presented here, the zero-level was taken as the noise level of the photomultiplier.

Several of the theories predict that the spectrum may be described by the sum of more than one Lorentzian. See pp 2.36, 2.45. Rouch et al (44) presented results for benzene which may be described by the sum of two Lorentzians. The basic curves obtained here are presented in the form $[I(0) - I(\omega)]/I(\omega)$ against ω^2 in units of $\Delta\omega^2$, where $\Delta\omega$ is the measured semi-halfwidth of the curve $I(\omega)$. (Figure 4.3). This presentation would give a straight line through the origin for a single Lorentzian of semi-halfwidth $\Delta\omega$. The departure from Lorentzian lineshape of all the curves is evident.

For two superposed Lorentzians, the spectrum may be described by three parameters, the ratio of the peak amplitudes R , and the two semi-halfwidths, $1/\tau_1$, $1/\tau_2$.

$$I(\omega) \propto \frac{R}{1 + \omega^2 \tau_1^2} + \frac{1}{1 + \omega^2 \tau_2^2} \quad \dots\dots\dots (4.1)$$

If the inverse curve is plotted in the form $[I(0) - I(\omega)]/I(\omega)$, the limiting gradients at low and high frequency, and the intercept of the high-frequency gradient with the $[I(0) - I(\omega)]/I(\omega)$ axis, give the values of the three parameters. The relations connecting them are: -

slope for small ω is

$$\frac{R\tau_1^2}{1 + R} \left(1 + \frac{\tau_2^2}{R\tau_1^2} \right) \longrightarrow \frac{R\tau_1^2}{1 + R} \quad \dots\dots\dots (4.2)$$

slope for large ω is

$$(1 + R)\tau_2^2 \left(1 + R \frac{\tau_2^2}{\tau_1^2} \right)^{-1} \longrightarrow (1 + R)\tau_2^2 \quad \dots\dots\dots (4.3)$$

and the intercept is

$$R(1 - \tau_2^2/\tau_1^2)^2 (1 + R\tau_2^2/\tau_1^2)^{-2} \longrightarrow R \quad \dots\dots\dots (4.4)$$

where $\tau_1 > \tau_2$, and the limiting values are for $\tau_1 \gg \tau_2$.

The three parameters R, τ_1, τ_2 were calculated from the curves shown in fig. 4.3, using these relations. As originally published, no correction was made for the effect of the non-Lorentzian instrumental shape (see p. 3.8, line 3). The results presented here have been corrected using the results of Leidecker and LaMacchia (39). The widths of the broader Lorentzians were unaffected by this correction, but the values of τ_1 were made smaller by an amount of 2-10%. The corrected values are presented in Table 4.1, where they are compared with values of τ from other types of measurement. The values of τ_1 were close to those obtained by measuring the semihalfwidth of the basic curve. The values of τ_2 are of doubtful accuracy, but the ratio of the intensities in the two Lorentzians, I_1/I_2 , is more accurate, since an error made in

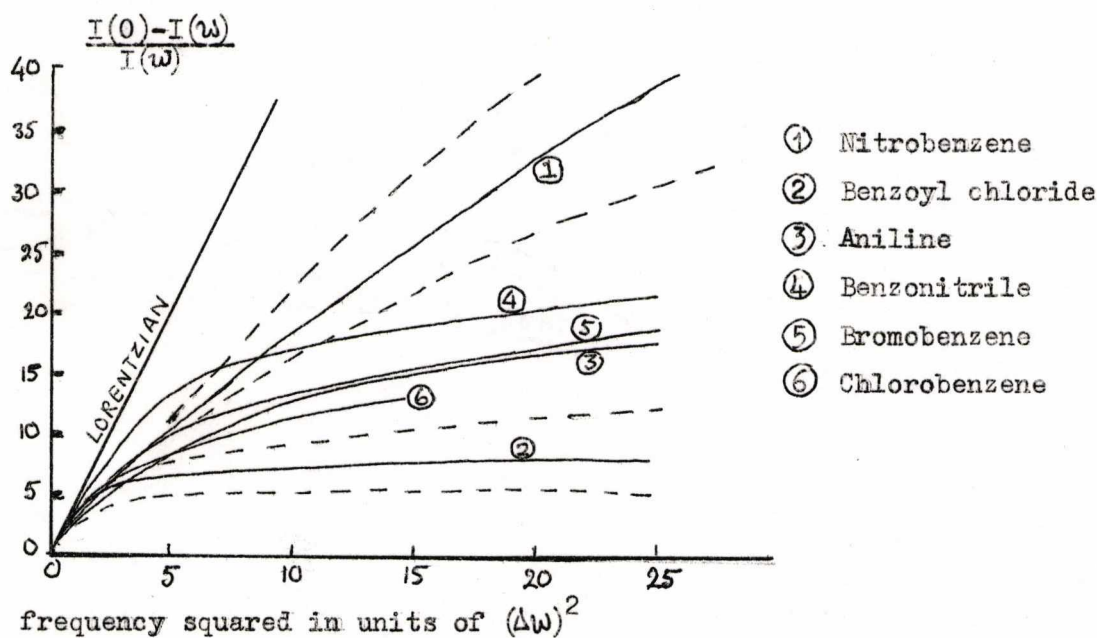


Figure 4.3. Comparison of inverse lineshapes of the six liquids. The behaviour of a single Lorentzian is included for comparison. Limiting values are given for curves ① and ②.

estimating the height of the second Lorentzian will be compensated by one in the width, so that the area is in agreement with that of the experimental curve. The value of I_1/I_2 is difficult to obtain by other methods, and in this case the overlap effect, which amplifies the weak wings, may be turned to advantage.

Table 4.1

Liquid at $23 \pm 2^\circ\text{C}$	$\Delta\omega$ cm^{-1}	Correlation times in units of 10^{-11} sec.							
		τ_{1s}	τ_d	τ_Q	$\tau_D/3$	τ_{11s}	τ_{21s}	I_1/I_2	R
$\text{C}_6\text{H}_5\text{NO}_2$	0.24	4.4	-	$>0.3^{(46)}$	$1.6^{(8)}$	3.8	0.36	3.5	37
$\text{C}_6\text{H}_5\text{COCl}$	0.36	2.9	-	-	-	3.2	0.14	0.29	6.7
$\text{C}_6\text{H}_5\text{NH}_2$	0.47	2.3	-	-	$0.6^{(45)}$	2.0	0.14	1.0	14.6
$\text{C}_6\text{H}_5\text{CN}$	0.52	2.0	-	$1.0^{(34)}$	-	1.9	0.15	1.3	17
$\text{C}_6\text{H}_5\text{Br}$	0.97	1.1	$0.5^{(47)}$	$\sim 0.5^{(48)}$	$0.6^{(8)}$	1.1	0.11	1.2	11.7
$\text{C}_6\text{H}_5\text{Cl}$	1.29	0.82	$0.4^{(50)}$	$0.3^{(50)}$	$0.4^{(8)}$	0.9	0.077	0.8	9.3
C_6H_6	-	-	$0.14^{(49)}$	$\sim 0.14^{(48)}$	-	$0.16^{(44)}$	$0.051^{(44)}$	$1.0^{(44)}$	$32^{(44)}$

In this table, τ_{1s} refers to the correlation time calculated from the semi-halfwidth $\Delta\omega$, measured directly from the basic curve $I(\omega)$. τ_d refers to nuclear magnetic resonance dipole relaxation, and τ_Q to nuclear quadrupole resonance. τ_D refers to dielectric relaxation measurements. The times τ_{11s} and τ_{21s} are determined from the relations (4.2)-(4.4), for each inverse curve.

It should be noted that if R is very much greater than unity, the gradient at low frequency, given by equation (4.2), depends on τ_{11s} only. If this condition is not satisfied, the spectrum must be known accurately over a frequency range wide enough to give all three parameters, if this

method of deriving them from the experimental results is to be used. The slope of the inverse curve at high frequencies always depends on at least two parameters. It is erroneous to suppose, as Rouch et al (44) have done, that any part of the curve may be described by one parameter only. Their results for benzene have been recalculated using relations (4.2)-(4.4), and are included in Table(4.1).

The discussion on pp. (2.33)-(2.34) gives the relations between the correlation times for different Legendre components of the orientational correlation function, for the rotational models of simple diffusion and jump diffusion. These are:

for simple diffusion;

$$\tau_{1=2} = \tau_{1=1}/3 \quad \dots\dots\dots(2.76b)$$

and for jump diffusion;

$$\tau_{1=2} \approx \tau_{1=1} \quad \dots\dots\dots(2.77b)$$

We only have correlation time values from all the techniques for two liquids, bromobenzene and chlorobenzene. For both these, the values of $\tau_D/3$ and τ_d, τ_Q are in close agreement, suggesting that the molecules rotate by simple diffusion. However, the light-scattering results are in agreement with the other methods only in the case of benzene, where τ_{1ls} is about 15% higher than τ_d, τ_Q . In the case of the other liquids, τ_{1ls} is larger than τ_d, τ_Q , or $\tau_D/3$ by a factor of about two or three. The ratios of τ_{1ls} to values from other methods are given in Table(4.2). The discrepancy is observed in chlorobenzene and bromobenzene, where correlation times for the different Legendre components are known from experimental techniques in which the motion of single molecules is measured, so that the appropriate model for reorientation has been established. Hence

the discrepancy is not, in these cases, related to the Legendre component that is being measured, but rather to the difference between the parameters measured by the different techniques. The light-scattering technique does not measure the motion of single molecules directly, but rather the decay of the induced polarizability summed over a large number of molecules.

Table 4.2.

Liquid	Ratio of times	Dipole moment esu/cm $\times 10^{-18}$	Molecular weight	Average molecular volume at $23 \pm 2^\circ\text{C}$.
$\text{C}_6\text{H}_5\text{NO}_2$	$\tau_{11s}/(\tau_D/3)=2.4$	3.98	123	170 (\AA) ³
$\text{C}_6\text{H}_5\text{COCl}$		3.67*	140.5	194 (\AA) ³
$\text{C}_6\text{H}_5\text{NH}_2$	$\tau_{11s}/(\tau_D/3)=3.3$	1.53	93	154 (\AA) ³
$\text{C}_6\text{H}_5\text{CN}$	$\tau_{11s}/\tau_Q = 1.9$	4.39	103	171 (\AA) ³
$\text{C}_6\text{H}_5\text{Br}$	$\tau_{11s}/\tau_d = 2.2$	1.54	156.9	175 (\AA) ³
$\text{C}_6\text{H}_5\text{Cl}$	$\tau_{11s}/\tau_d = 2.3$	1.58	112.5	170 (\AA) ³
C_6H_6	$\tau_{11s}/\tau_d = 1.14$		78	147 (\AA) ³

*Value obtained by summing bond dipole moments.

Values of dipole moment obtained from ref. (56).

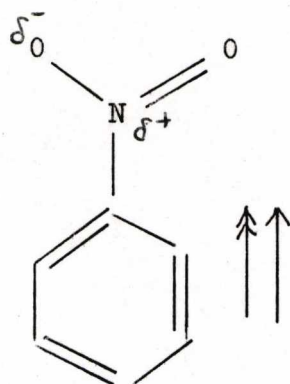
Values of the permanent dipole moment, molecular weight, and average molecular volume at room temperature, are also given in Table(4.2). The molecular shapes are shown in fig. (4.4). The discrepancy between τ_{11s} and correlation times from other methods is greatest for those molecules which are most anisotropic. Benzene is the least anisotropic molecule, and does not have a permanent dipole moment, so that the local field surrounding a molecule is more likely to be spherical on average than for the

other liquids. This is the situation in which the terms describing intermolecular correlation in orientation are negligible in the calculation of the anisotropic spectrum. Hence the theory of Pinnow et al. (27) is applicable, and the width of the spectrum is governed by self-correlation in orientation only, as observed here for benzene. However, if the intermolecular correlations in orientation are not negligible, the width as predicted by this simple theory might well be modified, as observed experimentally for liquids other than benzene.

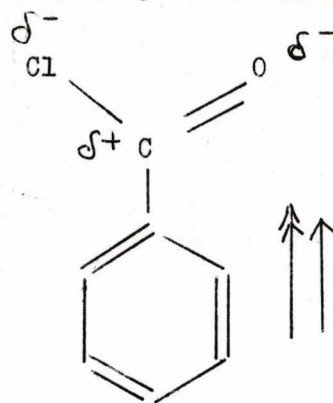
It appears then, from these measurements, that correlation times obtained from the central region of the anisotropic scattered light spectrum, are of the same order as molecular reorientation times, but the central region of the spectrum is not caused by molecular reorientation only. Rather it is caused by a more complex motion involving numbers of molecules.

Figure 4.4. Liquids to be studied; molecular shapes and axes.

Axis of maximum polarizability parallel to major axis for moment of inertia.

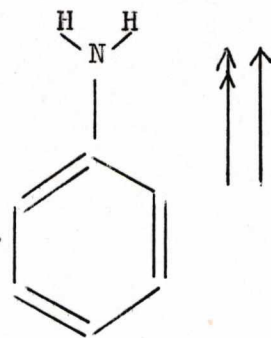


Nitrobenzene

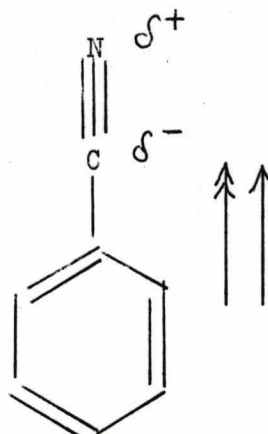


Benzoyl chloride

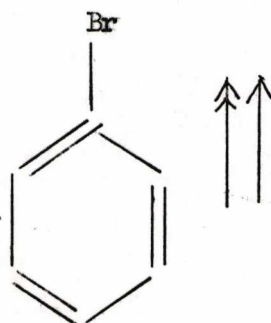
NH₂ group perpendicular to plane of paper.



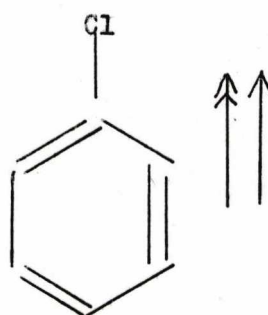
Aniline.



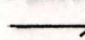

Benzonitrile



Bromobenzene



Chlorobenzene

 major axis for moment of inertia.
 direction of permanent dipole moment

Section 2. Experiment II. Detailed investigation of the scattered light spectra of the six liquids.

The isotropic and anisotropic spectra of the six liquids were studied, and their variation with temperature, in the range from the freezing-point to 160°C or the boiling point. The anisotropic spectra were obtained using either the smallest possible spacer with the pressure-scanning Fabry-Perot, or the piezo-electric Fabry-Perot with spacer adjusted to a suitable value. (64). The isotropic spectra were obtained using the pressure-scanning Fabry-Perot with a 9.98 mm spacer (free spectral range $.501\text{ cm}^{-1}$) and the relative intensity of the anisotropic background was measured at the same time.

When the 9.98 mm spacer was in use, the width of the laser line was about $1/15$ of the free spectral range, and the instrumental lineshape very nearly Gaussian. The Brillouin lines were convolutions of the finesse shape and a Lorentzian. In evaluating the true broadening of the Brillouin lines, and the areas of the components, the lineshapes must be taken into account. Leidecker and LaMacchia (39) give the necessary correction factors, and their results were used in this work. Their results could also be used to correct the linewidths of the anisotropic spectra measured on the pressure-scanning Fabry-Perot. In this case the instrumental width was a convolution of a Gaussian and a Lorentzian. The instrumental lineshapes using the piezo-electric scanning Fabry-Perot were accurately Lorentzian.

The anisotropic spectra were analysed by a slightly different method from that used in experiment I. The assumption was first made that the true curve was composed of two Lorentzians of unknown height and

width, in agreement with the results of the preliminary experiment. The experimental results were fed directly into the computer, where the assumed parameters of the Lorentzians were adjusted until a best fit was found. The results were output either as the heights and widths of the two Lorentzians, or as the height and width of a single Lorentzian, and the intensity of a constant background, if the second Lorentzian could not be resolved. (See Appendix A). The instrumental width could be allowed for afterwards, since the convolution of two Lorentzians gives a Lorentzian of width equal to the sum of the widths of the constituents. The anisotropic spectra obtained on the pressure-scanning Fabry-Perot could be corrected using the result of (39).

The central "dip" predicted by Rytov's theory (30) was not observed for any of these liquids. There are several probable reasons for this. One is that the anisotropic spectrum was observed using horizontally polarized incident light, and collecting both directions of polarization of the scattered light, so that the observed spectrum should have been the sum of the two curves given in Fig.(2.5), tending to obscure the "dip". Secondly the instrumental resolution was inadequate. Equation (2.107) may be used to calculate an upper limit on the expected shear wave splitting. The result for nitrobenzene at room temperature is

$$\omega_T = .07 \times 10^{10} \text{ Hz or } .02 \text{ cm}^{-1}.$$

From this, and using equation (2.106), the instrumental linewidth which is just insufficient to resolve the "dip" may be calculated. The result corresponds to a finesse of 15, using a 9.98mm Fabry-Perot spacer. The values of finesse used in this work were of order 15-20. Stegemann and Stoicheff (31) report a value of ω_T for nitrobenzene of $.046 \times 10^{10}$ Hz, so

the finesse required to see the effect using this spacer is increased yet further. Hence the nitrobenzene "dip" could not have been observed using this equipment. Expected values of the shear splitting for the other liquids (calculated using results given in Table 4.9) are all smaller than for nitrobenzene, with the exception of aniline. The value of shear splitting for this liquid reported by Stegemann and Stoicheff is $\omega_T = .125 \times 10^{10}$ Hz, but the observation of this splitting is still on the limit of the instrumental resolution, and small amounts of dust in samples of this liquid would annul the effect to be observed. The criterion (2.105) corresponds to a finesse value of more than 80 for both liquids.

Measurements of the relative intensities of the different spectral components at each temperature, and the variation of these intensities with temperature, could be made in most cases. The comparison of spectra taken at different temperatures was sometimes unreliable, due to the increase of absorbing impurities at higher temperatures, the thermal defocussing effect (Appendix B), instability of the laser, or slight variation in the position of the laser beam in the cell with temperature. Where there was a large increase in impurities, the Landau-Placzek ratio could not be measured. However, the Brillouin intensity and anisotropic intensity could be measured at each temperature. Since the Brillouin intensity is proportional to known parameters (eq. (2.22)), among them the adiabatic compressibility at hypersonic frequencies, which may be calculated from the sound-velocity results, its variation with temperature is known. Inaccuracies in the scattering intensity recorded may thus be detected and corrected for. The measurements of the intensity of the anisotropic spectra and their variation with temperature have all been

checked in this way. Where the Landau-Placzek ratio could be determined, the total depolarization ratio could also be measured.

The measurements made with the larger spacer consisted of two spectra at each temperature. That obtained with vertically polarized incident light contained the anisotropic spectrum with the isotropic spectrum superimposed upon it. That due to horizontally polarized incident light contained the anisotropic spectrum alone. From the discussion on pp. 2.6-7, the ratio of the intensity of the anisotropic spectrum obtained using horizontally polarized light to that obtained using vertically polarized light is $6/7$, if the anisotropic spectrum is due to that part of the dielectric constant tensor which is a symmetric tensor of zero trace. (This quantity is a measure of the depolarization ratio $\rho_u(\text{anis})$ for the anisotropic spectrum alone.) Assuming a value of $6/7$ for $\rho_u(\text{anis})$, the background level of the isotropic spectrum may be found, and the spectrum scanned for the presence of a Mountain line. This is particularly difficult at low temperatures for liquids which have a narrow central anisotropic component, since even using the larger spacer the anisotropic spectrum is not flat. The assumption $\rho_u(\text{anis}) = 6/7$ gave consistent results for all the liquids except benzoyl chloride. In this case, a reasonable background level could be assumed and $\rho_u(\text{anis})$ measured.

In order to test for the presence of dispersion of the sound velocity, it is necessary to consider the effects of temperature on the non-dispersive parameters in the velocity and absorption equations, so that these variations may be eliminated in looking for the effects of dispersion. One way of eliminating these variations is to work with

reduced parameters which vary with frequency and temperature only through the product $\omega\tau$. Two such reduced functions have been given in equations (2.59) and (2.60). They are

$$M' = \frac{V_s^2 - V_{s,0}^2}{V_{s,\infty}^2 - V_{s,0}^2} = \frac{\omega^2 \tau_{dis}^2}{1 + \omega^2 \tau_{dis}^2} \dots\dots\dots (2.59)$$

$$M'' = \frac{\omega \Gamma_0}{V_{s,\infty}^2 - V_{s,0}^2} = q^2 \frac{\omega \tau_{dis}}{1 + \omega^2 \tau_{dis}^2} \dots\dots\dots (2.60)$$

where M' , M'' are the real and imaginary parts of the reduced modulus.

However, in order to use these functions it is necessary that enough of the dispersion region has been spanned for the value of M_r , or $(V_{s,\infty}^2 - V_{s,0}^2)\rho_0$ to be measured accurately. A relaxation process always implies a broad absorption curve even if there is a single relaxation time, and the absorption curve is broadened yet further if there is a distribution of relaxation times. It may be possible to observe only a small part of the dispersion region. Also the velocity dispersion may well be no more than a few percent. Under these conditions, the reduced functions are unsuitable parameters to use when searching for dispersion effects, and the temperature-dependence of the non-dispersive parameters must be considered.

Let us first consider the variation of the Brillouin linewidth with temperature. This is given (from eq. (2.56) and (2.57b)) by the relation

$$\Gamma_B = \alpha_s V_s = (q^2/2\rho_0) \left[(4/3)\eta_\omega + \zeta_\omega + \frac{M_r \tau_{dis}}{1 + \omega^2 \tau_{dis}^2} \right] \dots\dots\dots (4.5)$$

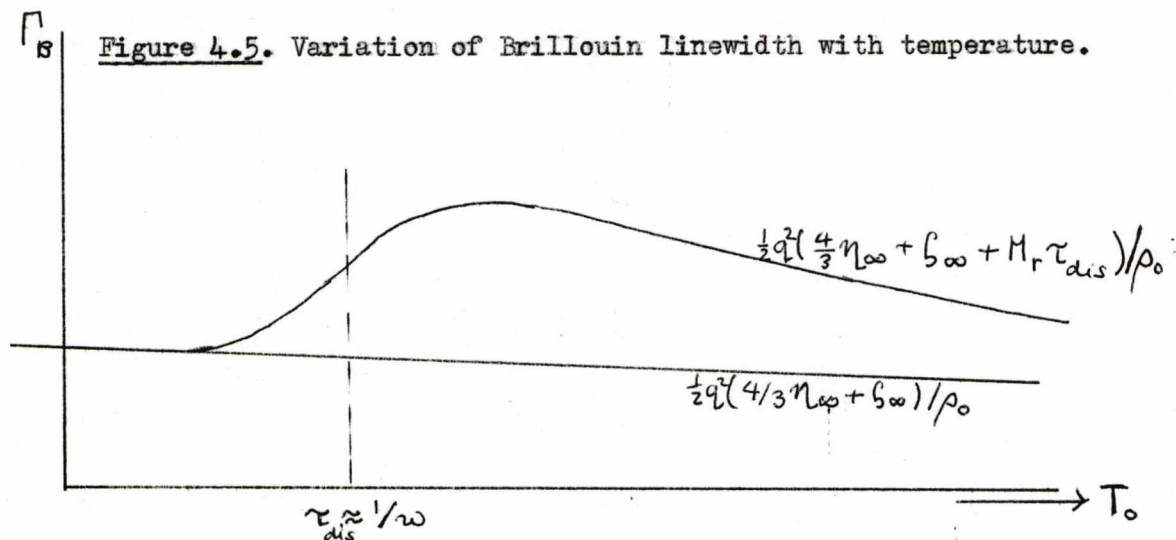
Here M_r is the modulus for a general loss mechanism which may represent a relaxing shear or volume viscosity, or a specific heat. Low frequency thermal losses have been ignored, as these are generally negligible. (cf equation (2.28)). $\eta_\omega, \zeta_\omega$, are high-frequency shear and volume viscosities,

which have been included to allow for more than one dispersion region. They represent that part of the bulk viscosity which relaxes at frequencies above $1/\tau_{dis}$.

The factor q^2 is practically constant with temperature, and ρ_0 decreases by about 10% over the range of temperature considered. The temperature-dependence of the remaining factors may be estimated from low-frequency ultrasonic measurements, where the terms inside the square brackets are given by $[(4/3)\eta_{\infty} + b_{\infty} + M_r\tau_{dis}]$. Even at hypersonic frequencies, the value of this factor is much greater for all the liquids than the static shear viscosity alone, so the first term is unimportant in determining the temperature-dependence. Ultrasonic data for chlorobenzene (41) show that the bulk viscosity given by the sum of these terms decreases by about 10% in 100°C, so that in the absence of dispersion, the Brillouin linewidth for this liquid should remain approximately constant throughout the temperature range. The bulk viscosity for benzene (ref (11), p.412) and bromobenzene ((41), see fig. (4.17)) decrease with temperature slightly more rapidly, so that the Brillouin linewidth should decrease with temperature in the absence of dispersion, but not by more than about 10% over the temperature range used. It is clearly important that the ultrasonic temperature-dependence of the sound absorption is known, for an unambiguous interpretation of the light-scattering results. In this work, variations in the Brillouin linewidth with temperature which are considerably more marked than those described above, have been considered as likely evidence for the existence of a dispersion region.

Clearly the presence of a dispersion region will only be detectable

if the magnitude of the term $M_r \tau_{dis}$ is comparable or greater than the term $4/3 \eta_\infty + \zeta_\infty$. Assuming this to be the case, the approximate temperature dependence of the bulk viscosity in the presence of a dispersion region is shown in figure 4.5.



Let us now consider the temperature-variation of the sound-velocity.

This is given in equation (4.6) (from eq. (2.31)).

$$V_s^2 = V_{s,0}^2 + (V_s^2 - V_{s,0}^2) \left[\frac{\omega^2 \tau_{dis}^2}{1 + \omega^2 \tau_{dis}^2} \right] \quad \dots\dots\dots (4.6)$$

$$= M_0 / \rho_0 + (M_r / \rho_0) \left[\frac{\omega^2 \tau_{dis}^2}{1 + \omega^2 \tau_{dis}^2} \right] \quad \dots\dots\dots (4.6b)$$

A large number of ultrasonic experiments on a wide variety of liquids show that the low-frequency sound velocity decreases approximately linearly with temperature. See, for example, (11), (41), (42). There seems to be no simple explanation for this temperature-dependence. All relaxation effects, except the negligible thermal conductivity losses, give rise to a positive dispersion of the sound velocity, (or $V_{s,\infty}^2$ is greater than $V_{s,0}^2$), and if the liquid shows a linear variation of $V_{s,0}$

with temperature, dispersion will cause a positive departure from linearity at low temperatures. Results showing this behaviour are given in Mason (41), p.317, and also in the work of Pinnow et al on glycerol (50). In the results presented here, the sound velocity has been found to vary linearly with temperature to a high degree of accuracy for several liquids. The results have been compared with ultrasonic values, where available, and if a departure from linearity is accompanied by a marked increase in the width of the Brillouin lines, it appears very likely that a dispersion region is being traversed.

In order to calculate the velocity of sound and modulus of adiabatic compressibility at hypersonic frequencies, using the Brillouin splitting, it is necessary to know values of the density and refractive index over the entire temperature range. Sufficient data was available in the literature only in a few cases. (for refs., see Tables 4.3-4.8) However, it was found that if the density was plotted against temperature for the cases where sufficient data was available, the deviation from a straight line was only 0.4% at the highest temperatures. The graph of refractive index against temperature was linear. Hence it was assumed that these quantities were linear with temperature in all cases, and values for the high temperatures extrapolated from the available data. Ultrasonic results were obtained from Nozdrev (41) and ref. (52).

Results comparable with ~~correlation times from anisotropic spectra~~ of these liquids have been presented in the literature using the techniques of dielectric relaxation, and nuclear magnetic dipole and quadrupole resonance. Comparable times and activation energies may also be obtained using values of the static shear viscosities and the Debye relation (see p 5.6). Times from incoherent neutron scattering are not available.

The six liquids will be considered in turn, and the results presented for each. The isotropic spectra will be discussed at the same time, in some detail. The isotropic spectra and the anisotropic spectra for all the liquids will then be discussed in chapter 5, and conclusions drawn from all the measurements will be compared. The results will be compared with those obtained from other experimental methods, where these are available.

Chlorobenzene.

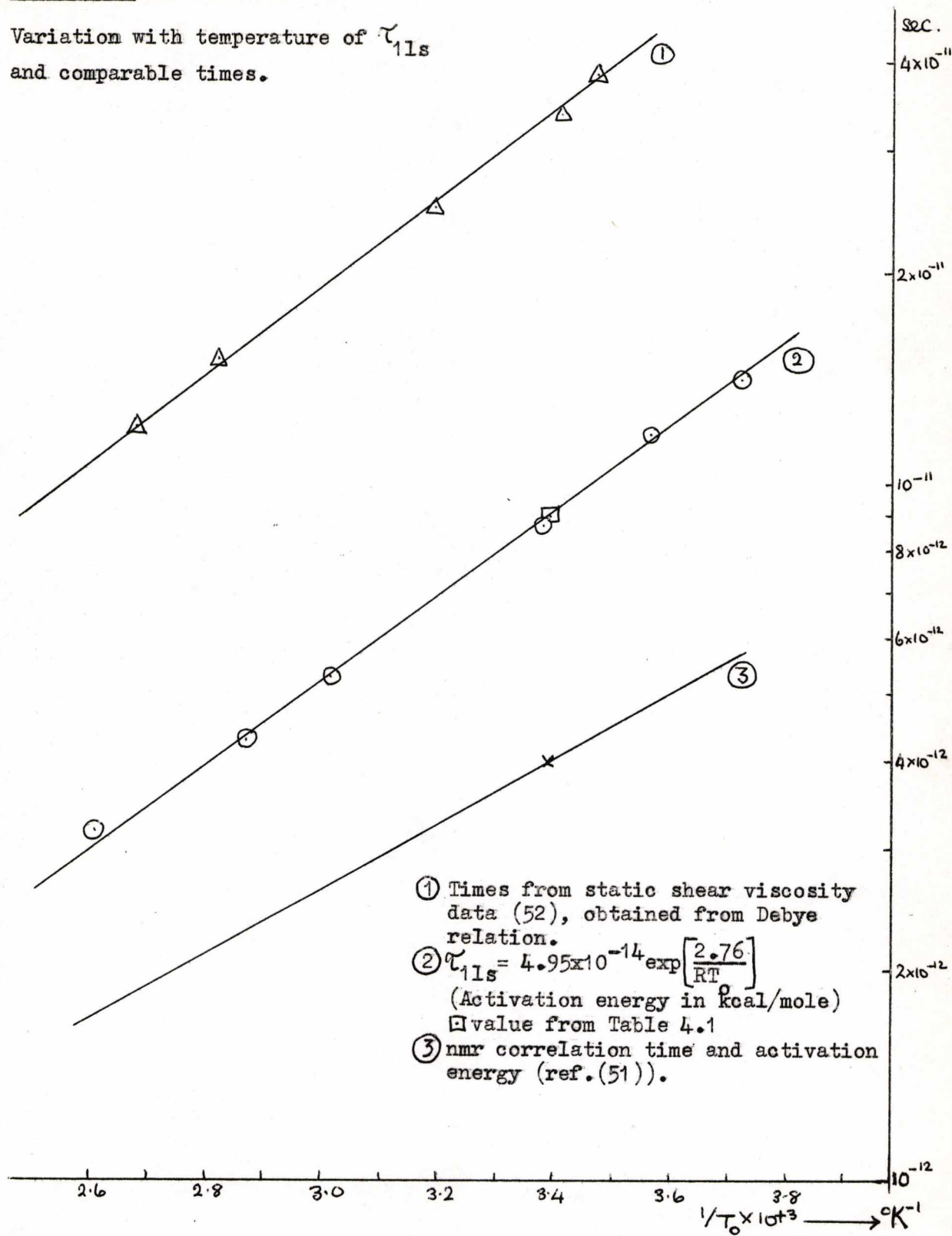
The results for chlorobenzene are presented first, since this liquid shows fewer complexities than some of the other liquids, and there is a certain amount of comparable ultrasonic data.

The temperature dependence of the correlation time deduced from the narrow part of the anisotropic spectrum is given in figure (4.6), and the total intensity of the anisotropic spectrum in figure (4.7). The correlation time follows an Arrhenius temperature dependence, with parameters given in the figure. Times obtained from nuclear magnetic resonance measurements and the Debye viscosity relation (see p. 5.6) are included in figure (4.6) for comparison. The linewidths for the second Lorentzian were too broad to be resolved. The total intensity remains approximately constant throughout the temperature range. The relative intensities of the two Lorentzians were given by the computational analysis of curves obtained using the smaller spacers, and normalised using the values of intensity obtained using the larger spacer. In general, the accuracy of the measurement of relative intensity is least if the curves are very well resolved, so that the high temperature measurements, which were obtained using a very small spacer, are unreliable.

The sound velocity shows a linear variation with temperature, as shown in figure (4.8). The inaccuracy of the low temperature values is due to the precipitation of impurities, as described in chapter 3. The ultrasonic values of the sound velocity, obtained from refs. (41) and (52), show fair agreement, but although they fit the hypersonic line at 40-60°C, the highest temperatures at which ultrasonic measure-

Figure 4.6. Chlorobenzene.

Variation with temperature of τ_{11s}
and comparable times.



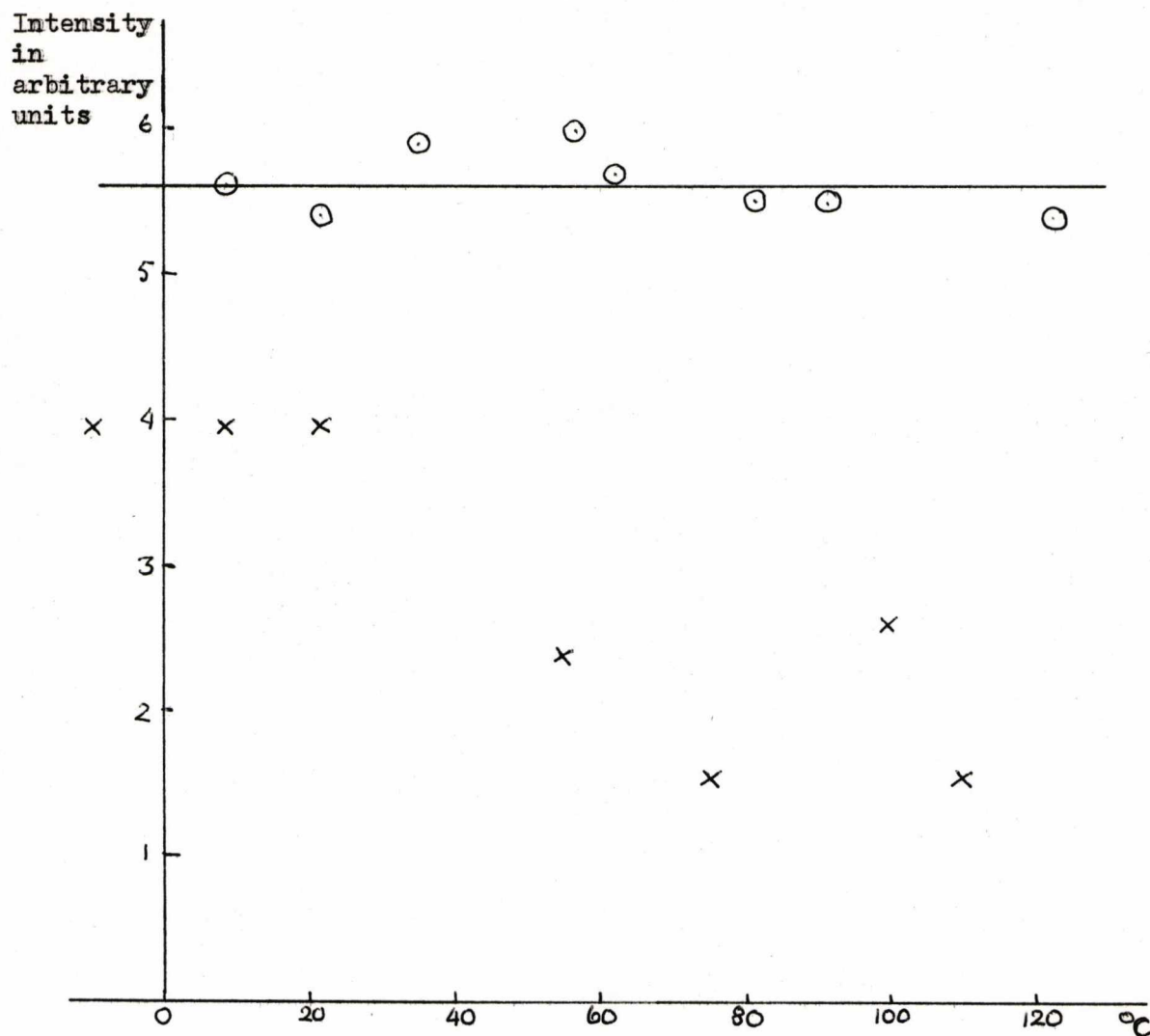


Figure 4.7 Chlorobenzene. Intensity of anisotropic spectrum.

- total intensity values
- × intensity in narrow Lorentzian. (see text)

Figure 4.8. Chlorobenzene. Velocity of hypersound against temperature.
Frequency $\sim 4 \times 10^9$ Hz at 20°C.

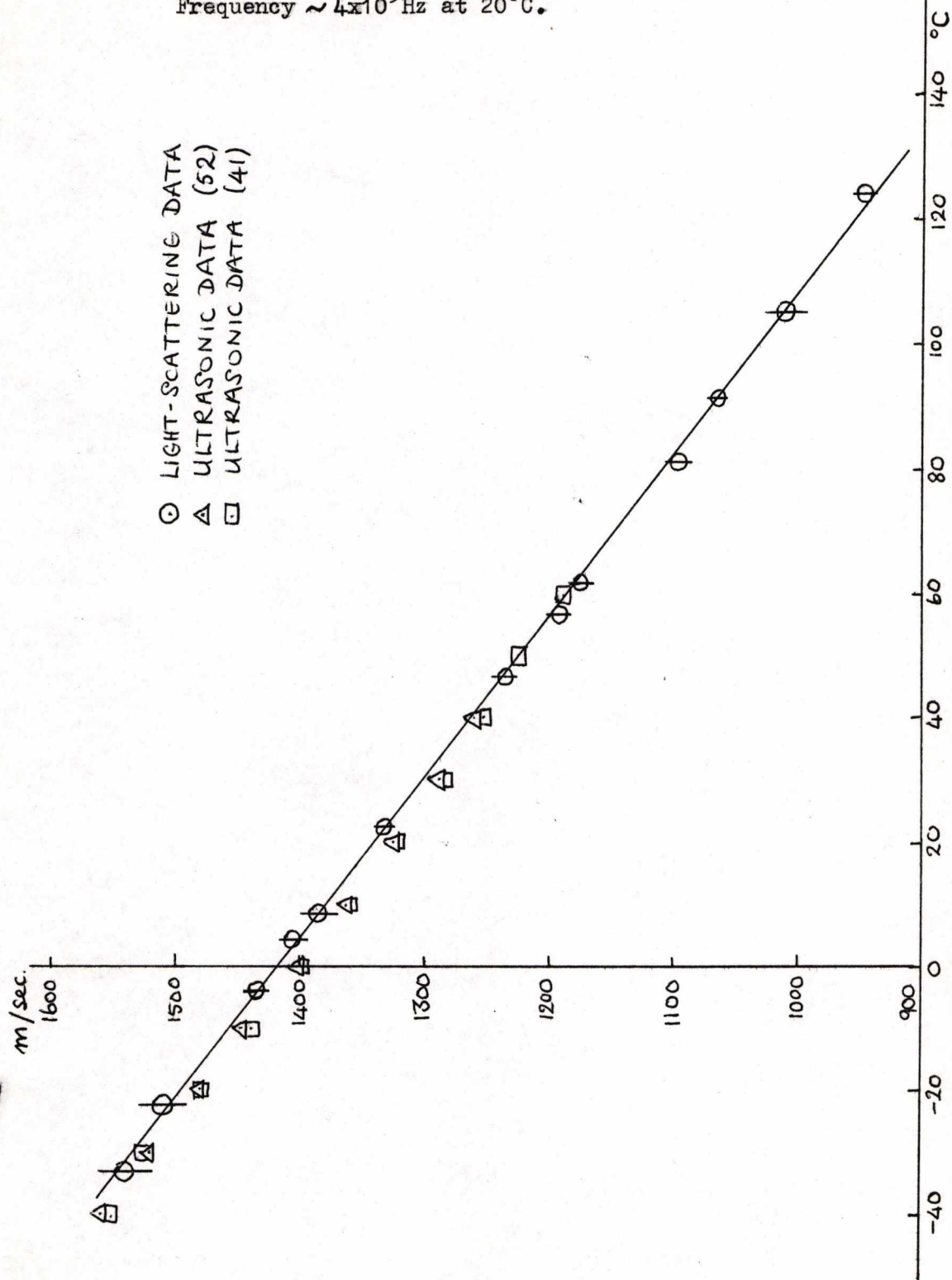


Figure 4.9. Chlorobenzene. Brillouin semi-linewidth.

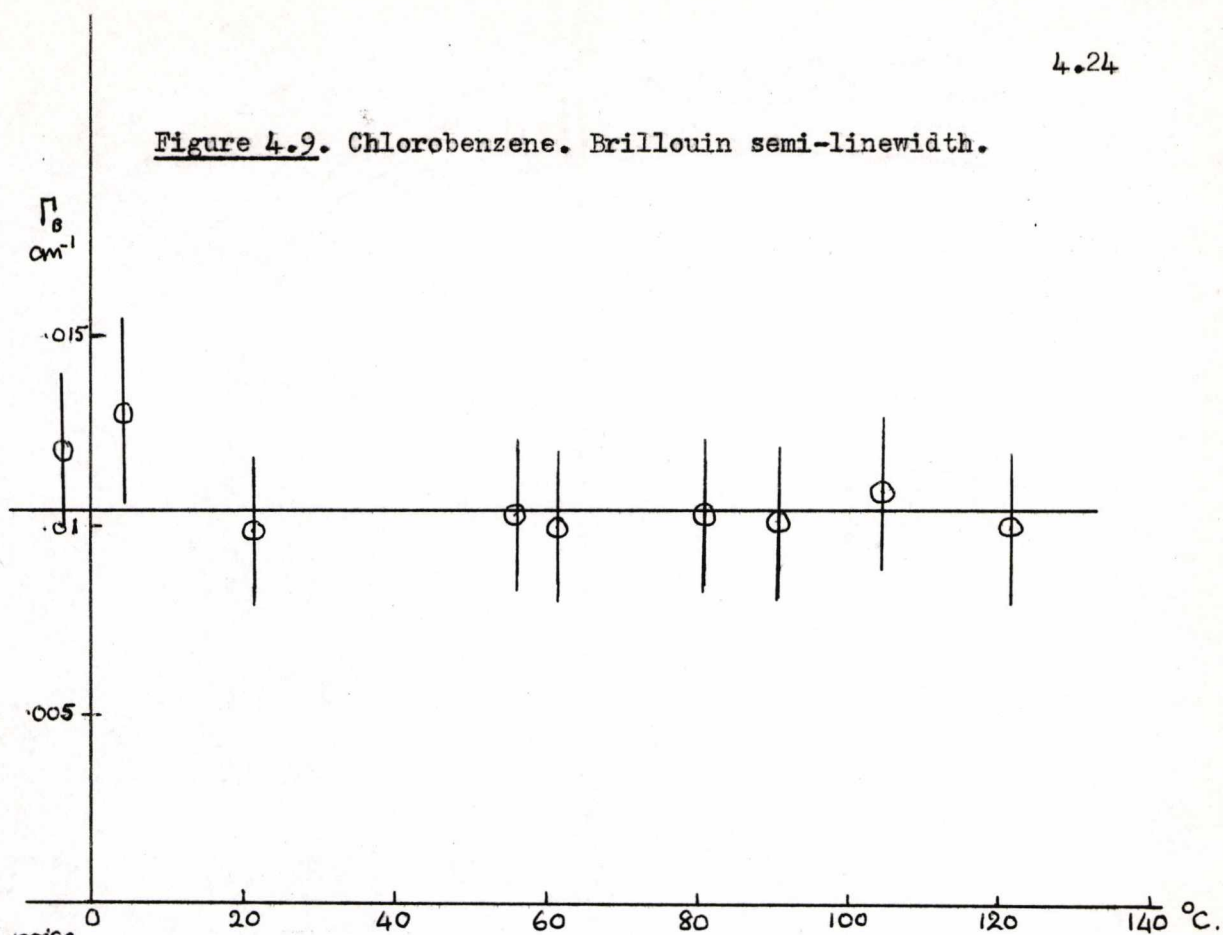
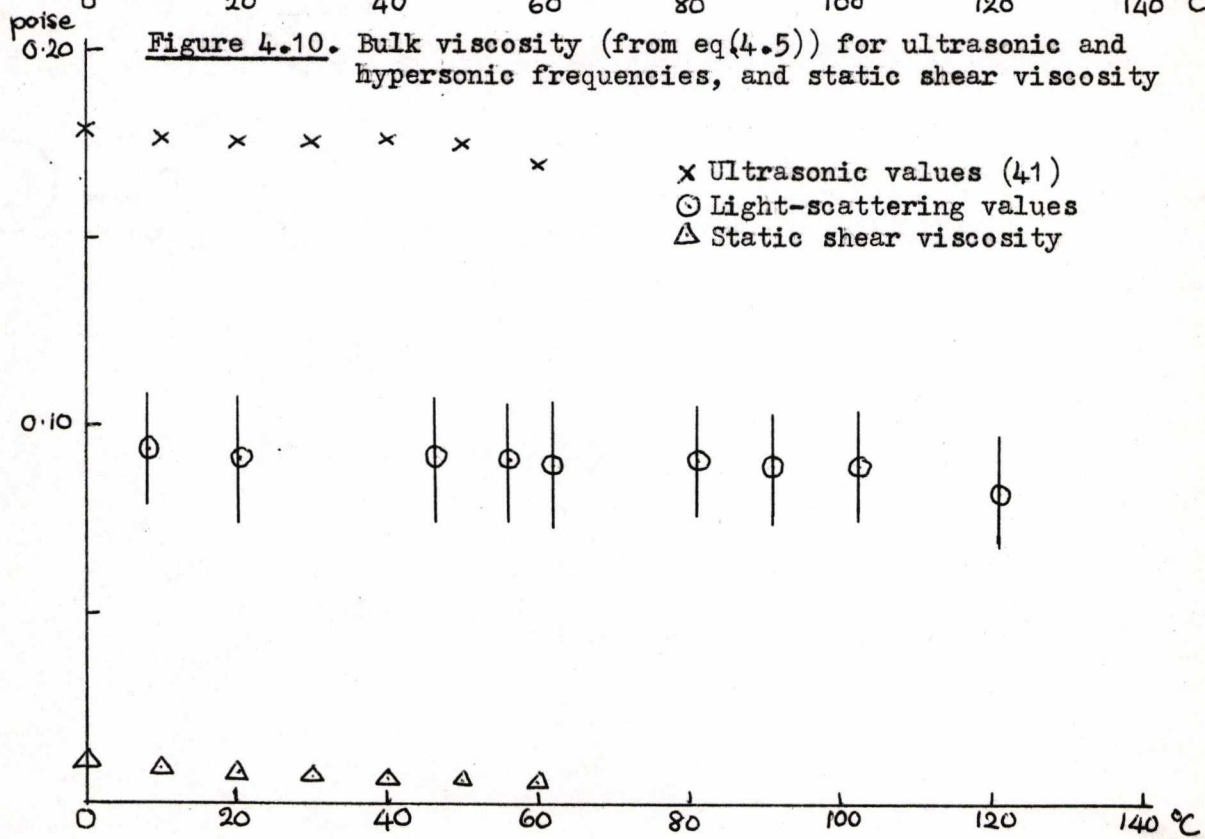


Figure 4.10. Bulk viscosity (from eq(4.5)) for ultrasonic and hypersonic frequencies, and static shear viscosity



ments were performed, they deviate from the line by about 2% at intermediate and low temperatures. This deviation may be interpreted by considering also the temperature-dependence of the Brillouin linewidth, which is shown in figure (4.9). The expected temperature-dependence of the Brillouin linewidth for chlorobenzene has been discussed already on p. 4.16. In the absence of dispersion effects, it should remain constant as the temperature is decreased, then, as the dispersion region is traversed, it should fall below its previous value by an amount $(q^2/2\rho_0)M_T\tau_{dis}$. The expected decrease due to a dispersion of 2% centered at about 20°C (4.5×10^9 Hz, from Table 4.3) may thus be calculated. The result is about 20% of the Brillouin linewidth, and a decrease of this order of magnitude at low temperatures was not observed. In fact the Brillouin linewidth was approximately constant over the entire temperature range, having a value of Γ_B of $.01 \text{ cm}^{-1}$, corresponding to a phonon lifetime of 5.3×10^{-10} sec.

Hence it appears that the apparent agreement of ultrasonic and hypersonic results at 40-60°C. is due to experimental error, and the dispersion region is in fact centred at a frequency between the two frequency regions at which the results were taken.

The ultrasonic results quoted by Nozdrev (41) include the absorption coefficients at different temperatures and the bulk viscosity calculated from them, although he does not give the frequency at which the experiments were performed. The values were obtained using equation (4.5) modified as shown:

$$2\alpha_s = \frac{\omega^2}{v_s \rho_0} \left[\frac{4}{3} \eta + \zeta \right] \dots \dots \dots (4.5b)$$

where the shear and volume viscosities η and ζ now contain the frequency-dependent terms. Values of the bulk viscosity calculated in this way are shown in figure (4.10). Both ultrasonic and light-scattering results are shown, and values of static shear viscosity are given for comparison. The total apparent viscosity has decreased by nearly 50% between the ultrasonic and hypersonic frequency regions. The region of frequency at which the dispersion occurs, assuming that the entire loss in "viscosity" is associated with one dispersion mechanism, may be calculated from the same considerations as before, using the equation

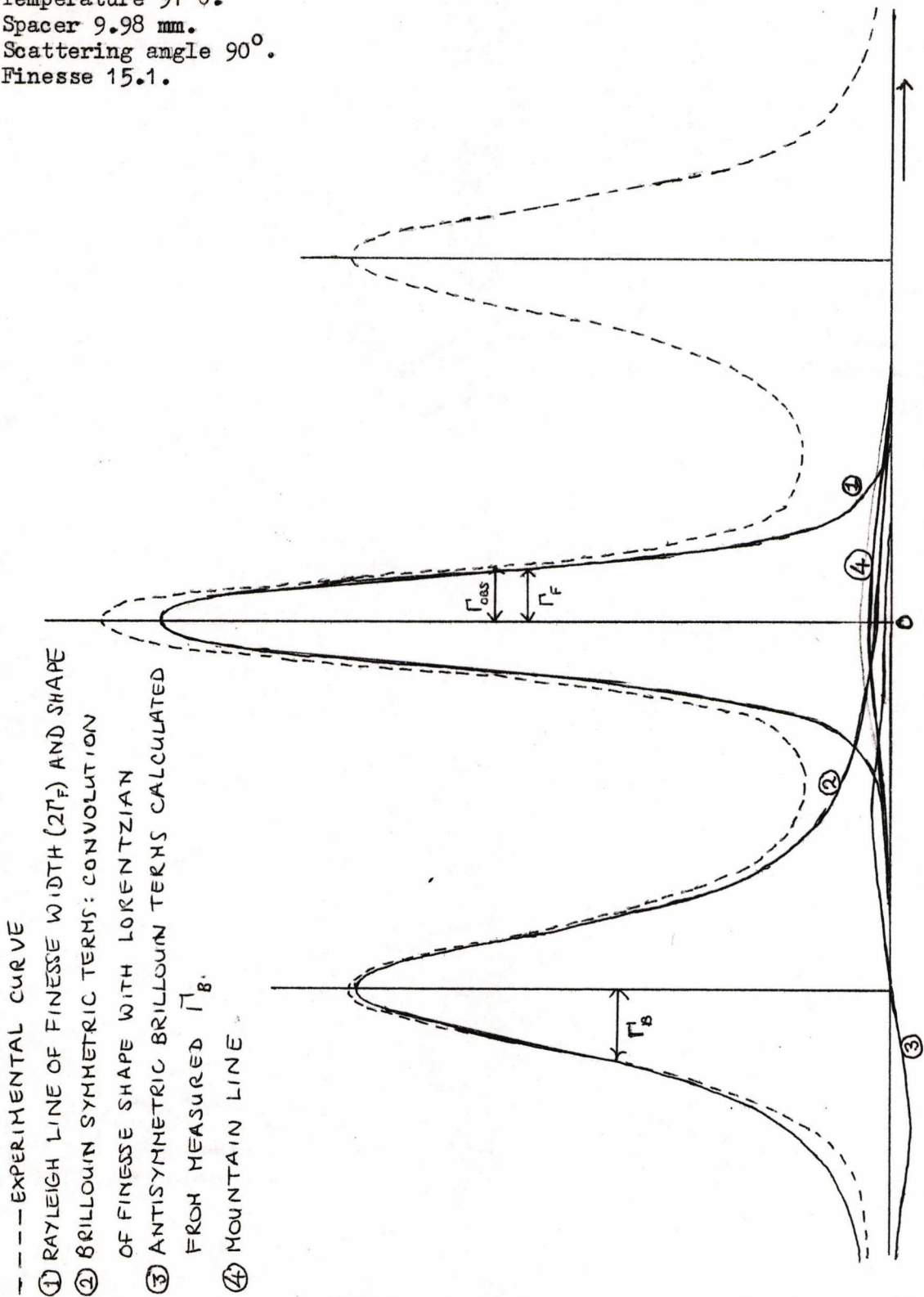
$$\rho_0 \tau_{dis} = \rho_0 (v_{s,\infty}^2 - v_{s,0}^2) \tau_{dis} = \zeta(\omega) \dots\dots\dots (4.7)$$

At room temperature, comparison of the two sets of results gives $\zeta(\omega) = .084$ poise, from which the value of τ_{dis} is 1.4×10^{-10} sec. This corresponds to a frequency of 1.1×10^9 Hz, which is below the frequencies observed in this experiment. (See Table 4.3). The error in estimating these quantities is about 40%, due to the uncertainty in $(v_{s,\infty}^2 - v_{s,0}^2)$. The magnitude of the relaxing bulk viscosity associated with this dispersion is approximately independent of temperature, which means that τ_{dis} varies very little throughout the temperature range. This suggests that the dispersion is caused by a relaxing internal specific heat rather than a structural relaxation.

From equation (2.58), the width of the Mountain line associated with this dispersion will be about 1.1×10^9 Hz, or 0.037 cm^{-1} , at all temperatures.

Throughout the temperature range, the isotropic spectrum for chlorobenzene shows a marked "background" between the Brillouin lines.

Figure 4.11. Isotropic spectrum of chlorobenzene.
 Temperature 91°C .
 Spacer 9.98 mm.
 Scattering angle 90° .
 Finesse 15.1.



A typical curve at 91°C . is shown in Figure 4.11. The Brillouin lines have been corrected for the finesse shape and width using the results of (39). The spectrum must be corrected for the antisymmetric terms centred on the Brillouin frequency, discussed on pp. 2.20-21. The magnitude of the antisymmetric terms may be calculated from the measured Brillouin width, using equation (2.44). This calculation has been performed, assuming that the antisymmetric terms are broadened by the finesse curve in the same way as the Lorentzian components; or that the calculated asymmetry is unaffected by the instrumental broadening. The shape of the instrumental function makes it possible to separate the Rayleigh line. The Mountain line remaining after this analysis has been performed is weak, and difficult to identify or measure unambiguously. The observed spectrum may be accounted for by the presence of the antisymmetric terms and a Mountain line of width given by the predictions above, but the resolution is insufficient for this analysis to be conclusive, in determining the height and width of such a Mountain line. However, the magnitude of the "background" between the Brillouin lines, compared with that seen in other liquids with a similar Brillouin broadening, is additional evidence that a Mountain line is present. Clearly it is of great importance in analysing such spectra, that the antisymmetric terms are taken into account.

The asymmetry of the Brillouin lines has a similar magnitude at all temperatures, since the broadening is constant, but the "background" grows slightly more pronounced at higher temperatures as the Brillouin lines move closer together. It should be noted that the antisymmetric terms and the Mountain line cause the central Rayleigh line to appear

broader than the finesse width.

In view of these considerations, the Landau-Placzek ratio is difficult to measure accurately, but its apparent value is about $0.55^{+.05}$. The effects of the antisymmetric and Mountain components would be to reduce this value by about 10%. The total depolarization ratio may be ascertained more accurately, since its determination only requires an accurate knowledge of the total isotropic intensity. The values of $\rho_u(\text{tot})$ for unpolarized incident light are given in figure 4.12. Its value decreases steadily with temperature. It should be noted that the depolarization ratio obtained from light-scattering does not measure the anisotropy of individual molecules alone, but that of the polarizability tensor summed over a number of molecules. This includes the effects of the anisotropy of the local field surrounding a molecule, the shape of the molecule hindering rotation, and so on. (See Kielich (36) for a detailed consideration of these factors.) The decrease of the depolarization ratio with temperature, indicates that these effects are becoming less important as the molecules move farther apart.

The adiabatic compressibility at hypersonic frequencies may also be calculated from the velocity results. The values will be about 4% lower than those obtained from ultrasonic measurements. These values are given in figure 4.37, together with values for the other five liquids.

Table 4.3 gives the measured values of the Brillouin splitting, and all the other parameters used in calculating the sound velocity, adiabatic compressibility and viscosity.

Figure 4.12. Chlorobenzene: total depolarization ratio.

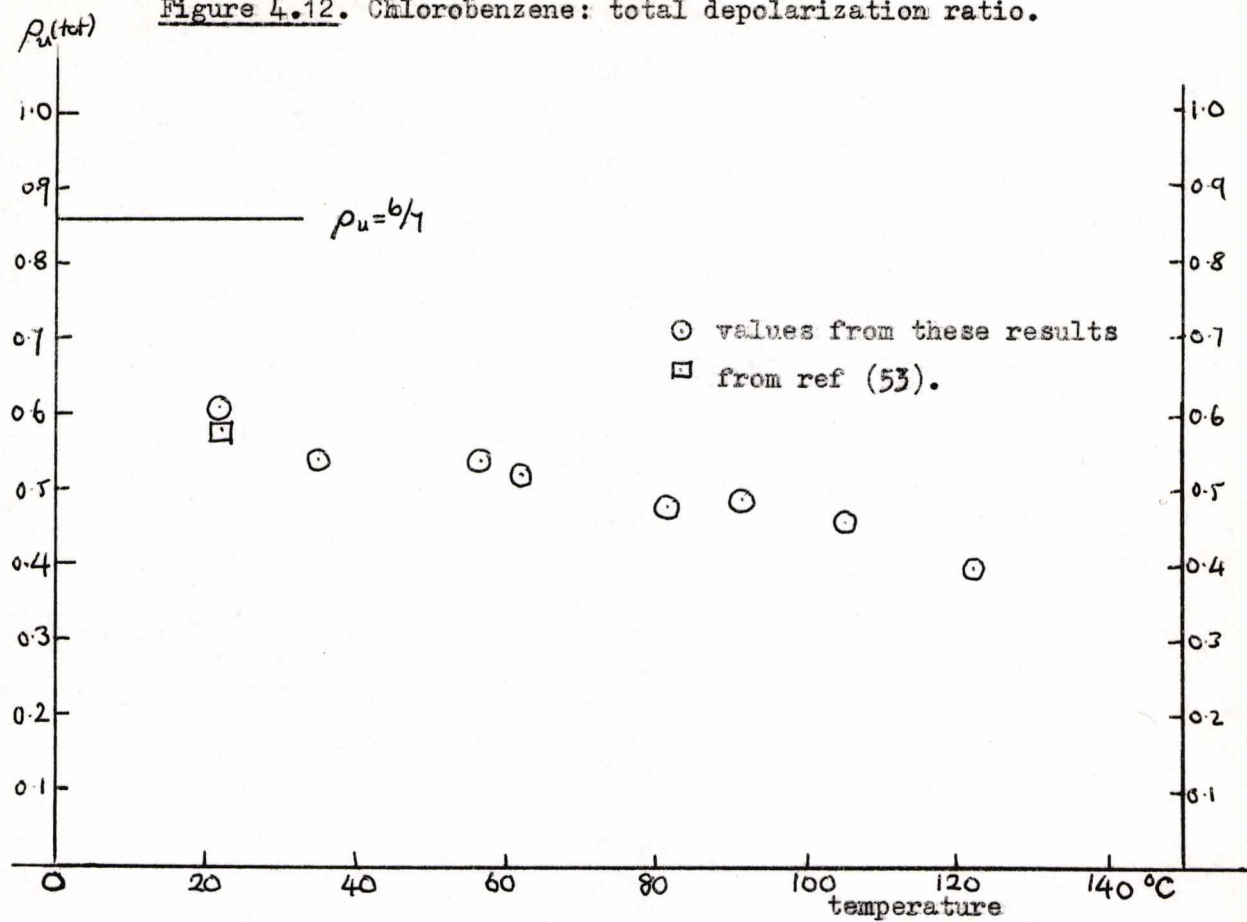


Table 4.3. Chlorobenzene: tabulated results.

Temp. °C.	Brillouin splitting		Refractive	Velocity of	Density
	cm. ⁻¹	Hz($\times 10^9$)	index	hypersound	gm/cc.
				m/sec.	
-33	.177 (2%)	5.33	1.548	1540	1.164
-22.5	.173 (3%)	5.19	1.542	1510	1.152
-4.0	.1636 (1%)	4.91	1.532	1434	1.132
4.5	.1599 (1%)	4.80	1.528	1406	1.123
8.3	.1572 (1%)	4.72	1.525	1384	1.119
21.4	.1507 (1%)	4.52	1.518	1332	1.105
46.4	.1384 (1%)	4.15	1.504	1235	1.077
56.3	.1332 (1%)	4.00	1.499	1192	1.067
61.8	.1310 (1%)	3.93	1.496	1175	1.061
81.2	.1213 (1%)	3.64	1.486	1096	1.040
91.2	.1176 (1%)	3.53	1.480	1066	1.030
105.0	.1109 (2%)	3.33	1.473	1011	1.015
122	.1034 (1%)	3.10	1.464	948	0.997

Values of refractive index and density obtained for entire temperature range from ref. (52).

Bromobenzene.

The results for bromobenzene are presented in figures. 4.13-18 and in Table 4.4. They are similar to those obtained for chlorobenzene in many respects.

The correlation times obtained from narrow and broad parts of the anisotropic spectrum, together with values obtained from nuclear magnetic resonance and from static shear viscosity values, are shown in figure 4.13. The time for the narrow part of the curve, as in the case of chlorobenzene, follows an approximate Arrhenius temperature dependence, with parameters given in the figure.

The measurement of the total intensity of the anisotropic spectrum was made difficult in this liquid by the increase in absorbing impurities as the temperature was increased. Values were corrected as described on p. 4.13. The total intensity obtained was very nearly independent of temperature, if anything showing a slight increase as the temperature was raised.

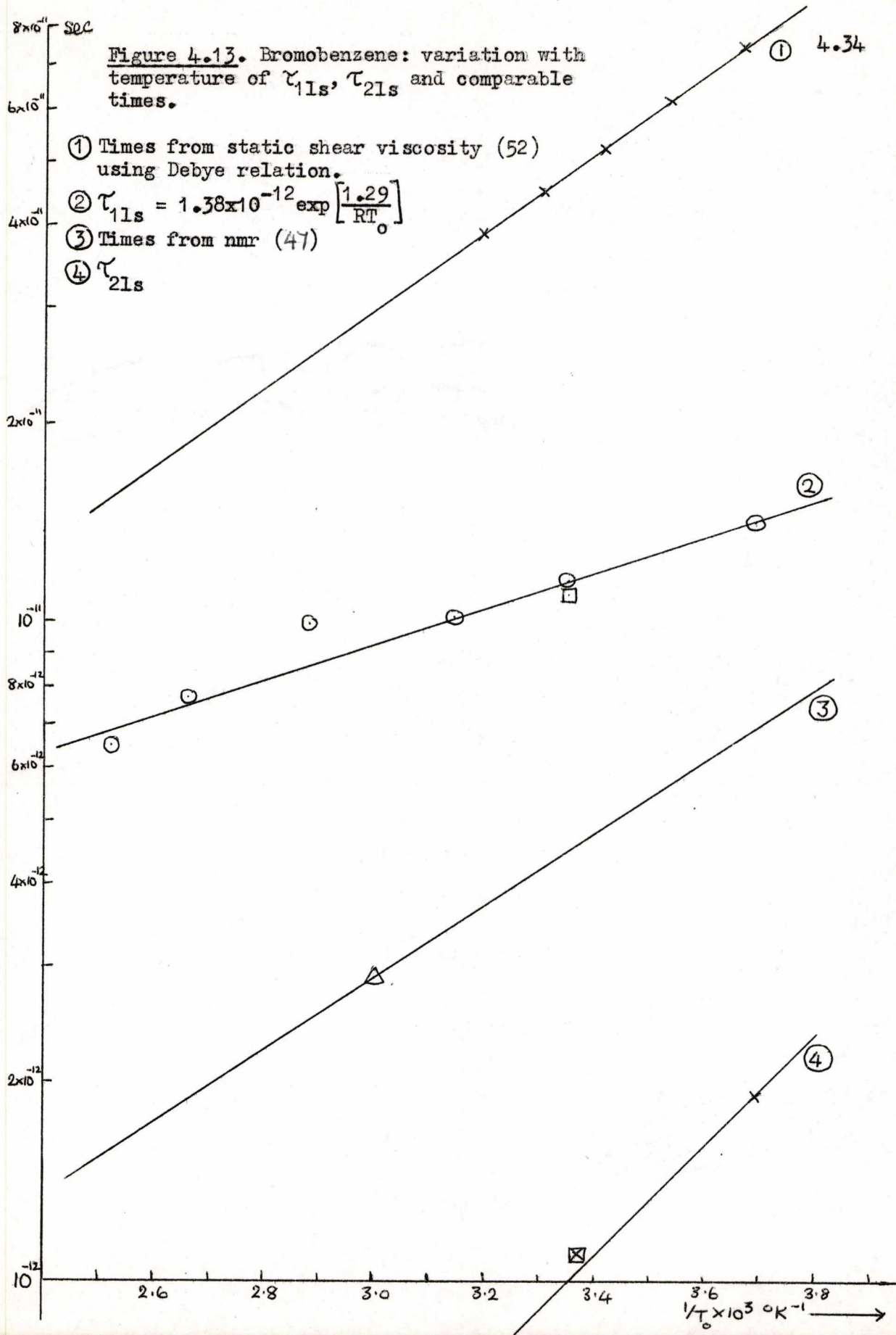
The isotropic spectrum showed a marked "background" between the Brillouin lines, like chlorobenzene, and this was independent of temperature, and of the correct order of magnitude and shape to be accounted for by the antisymmetric terms of equation (2.44).

The sound velocity shows a linear variation with temperature, and very good agreement with two sets of ultrasonic results. (See fig. 4.15) Hence there is no evidence for a dispersion region at or below hypersonic frequencies of greater than 1%. However the values of the "viscosity" obtained using equation (4.5b) (p. 4.25) are once again considerably lower than those determined from ultrasonic results. (See figure 4.17).

This would indicate that a small dispersion of less than 1% has occurred, between the ultrasonic and hypersonic frequency regions. If, in equation (4.7), τ_{dis} is long, the value of M_T could well be very small, compared with $V_{s,0}^2 \rho_0$. This would lead to the presence of a narrow Mountain line, which, by comparison with figure 4.11, would be indistinguishable from the central Rayleigh line. Hence the difference between the "viscosities" is the only way of detecting such a dispersion. Figures 4.16 and 4.17 also show that the decrease of the Brillouin linewidth at low temperatures is not what would be expected in the absence of dispersion. However, the results are not accurate enough to enable any conclusions to be drawn from this.

It would seem reasonable that, if bromobenzene and chlorobenzene exhibit a small dispersion of the sound velocity below hypersonic frequencies, caused by a relaxing internal specific heat, then the other four liquids should do the same, since their molecular structure is so similar. However, there are no ultrasonic absorption measurements which enable the comparison to be made in these cases.

The temperature-dependence of the total depolarization ratio is shown in figure 4.18. As for chlorobenzene, there is a steady decrease of this parameter with temperature. Measured values of the Brillouin splitting, and parameters used in the calculations, are given in Table 4.4. The adiabatic compressibility at hypersonic frequencies, calculated from the sound velocity, is given in figure 4.37.



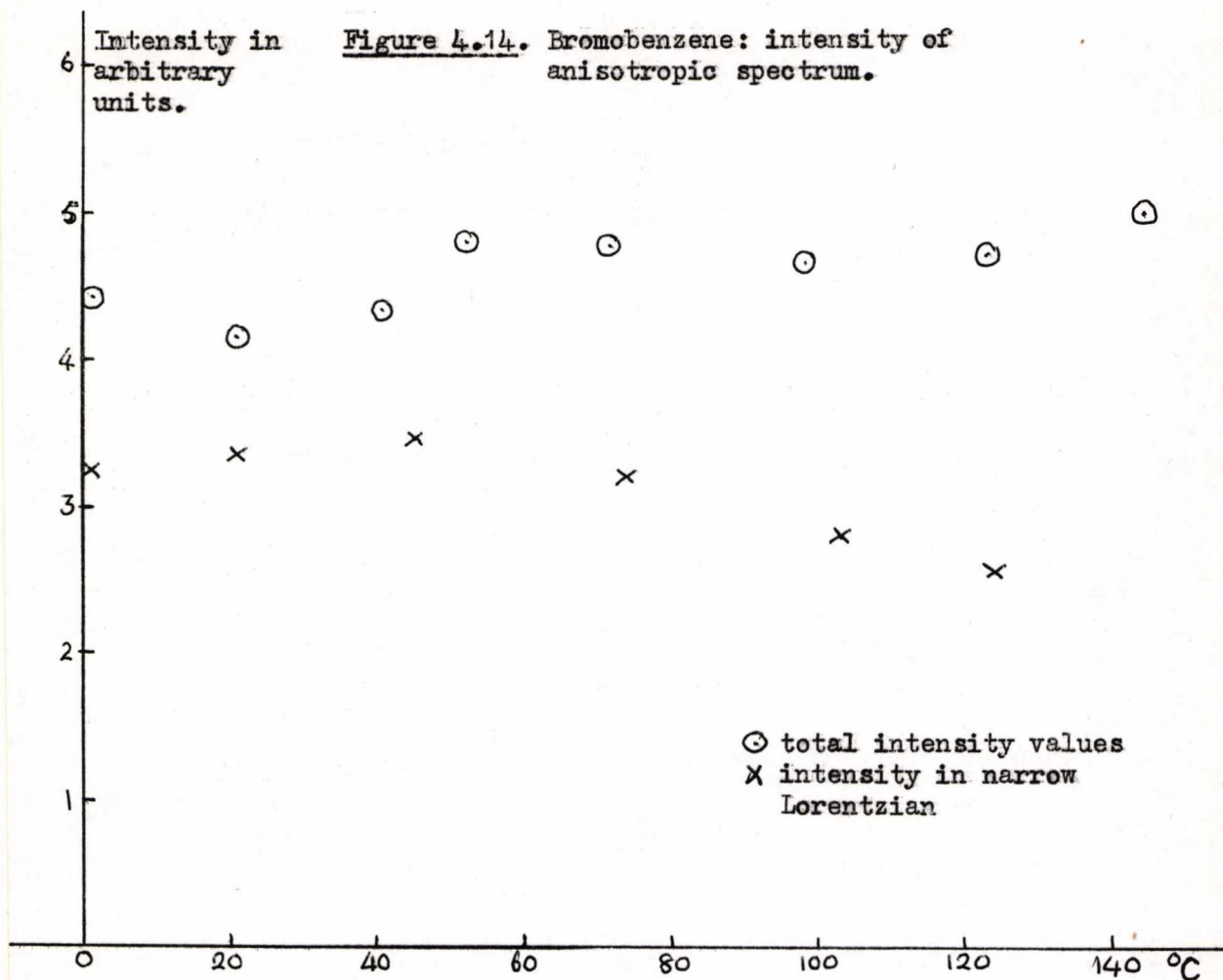


Figure 4.15. Bromobenzene: velocity of hypersound against temperature.
frequency $\sim 4 \times 10^9$ Hz at 20°C .

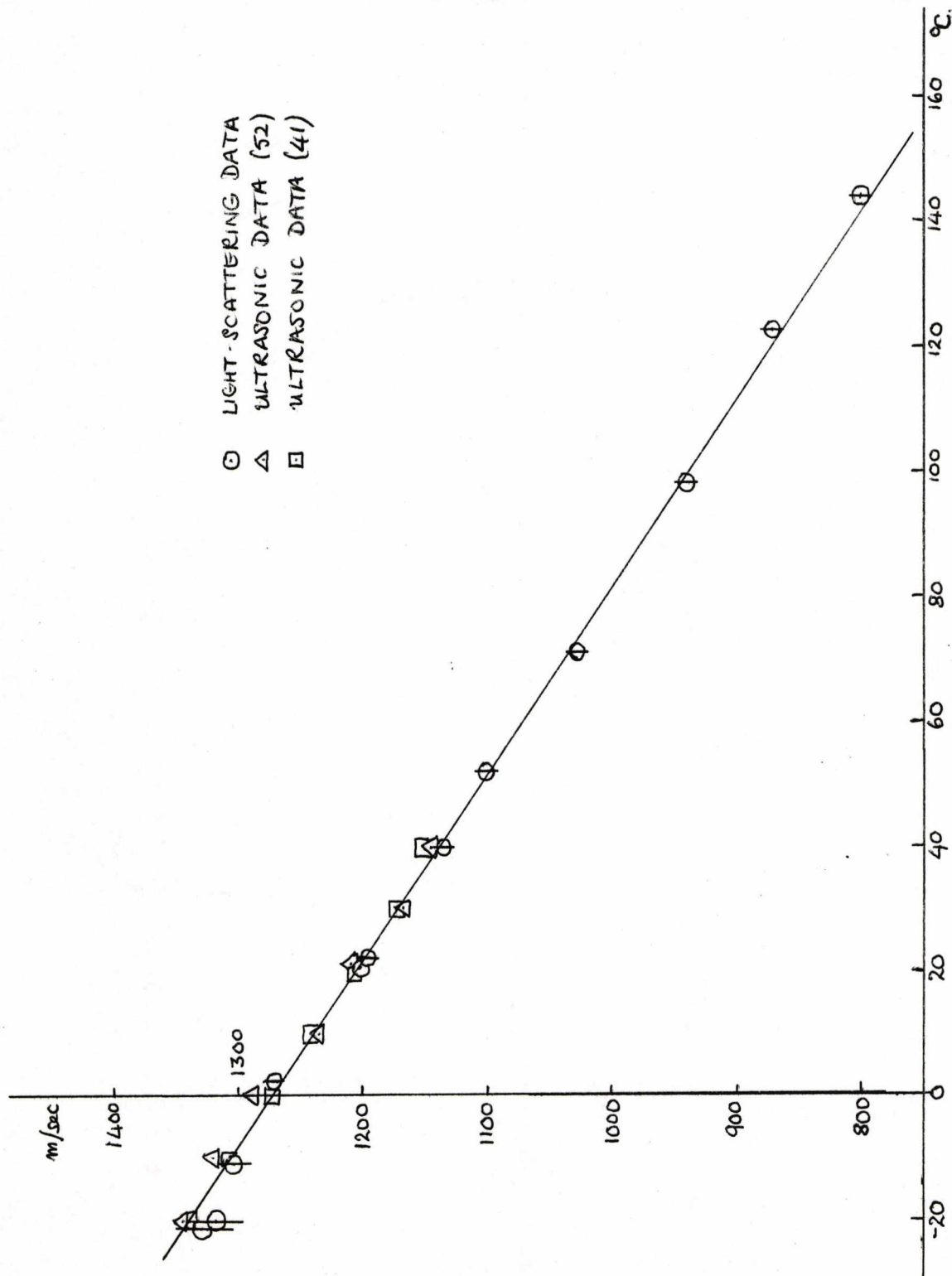


Figure 4.16. Bromobenzene: variation of Brillouin semi-linewidth with temperature

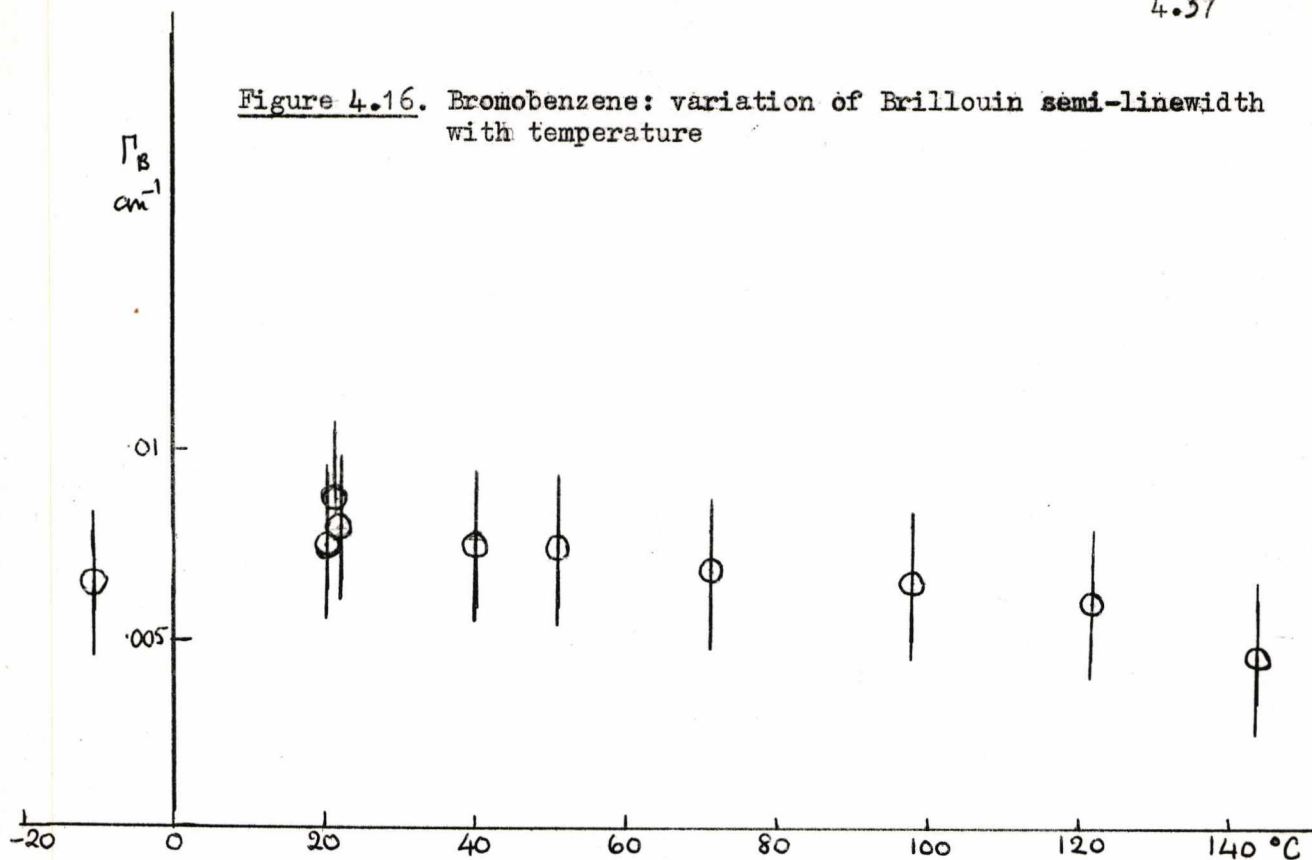


Figure 4.17. Bromobenzene: bulk viscosity (from eq.(4.5)) for ultrasonic and hypersonic frequencies, and static shear viscosity

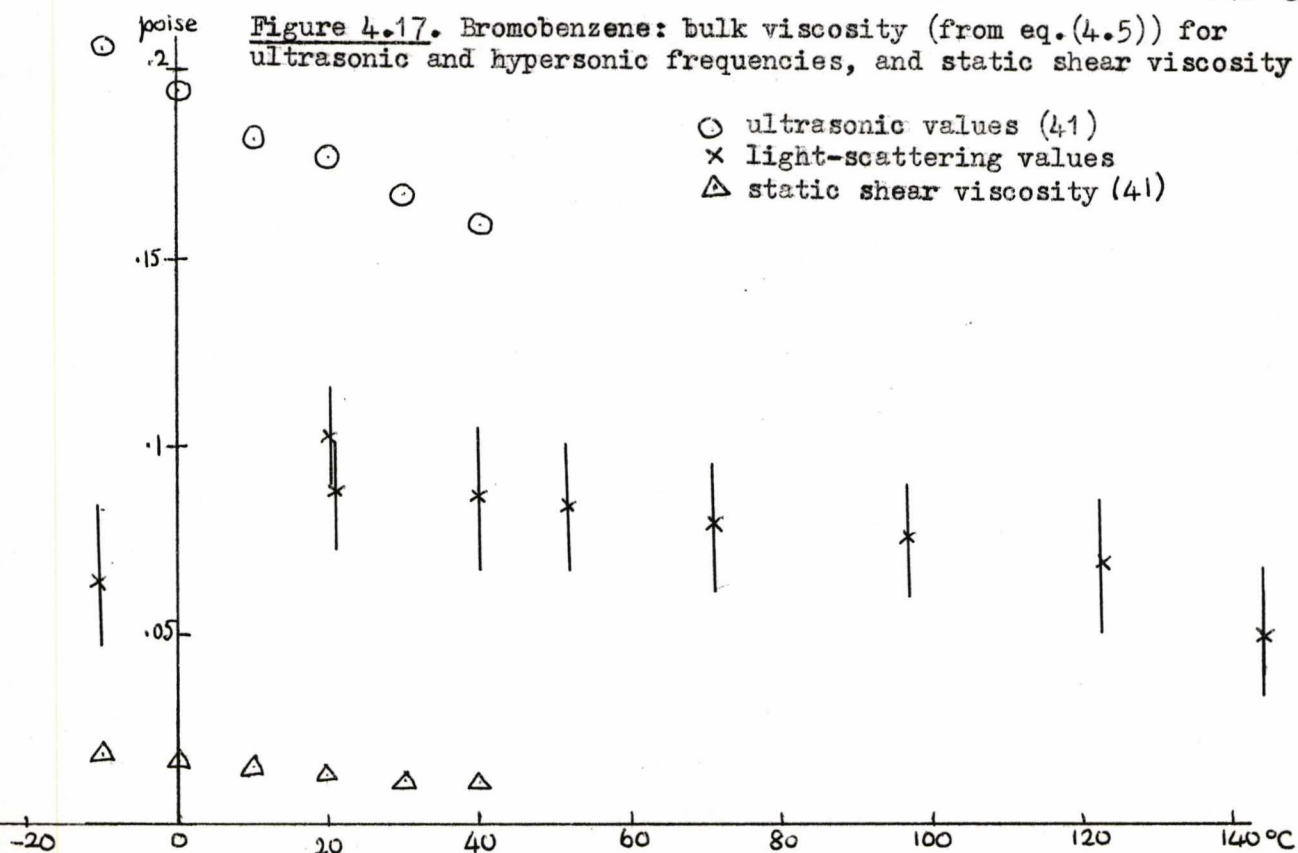


Figure 4.18. Bromobenzene: total depolarization ratio.

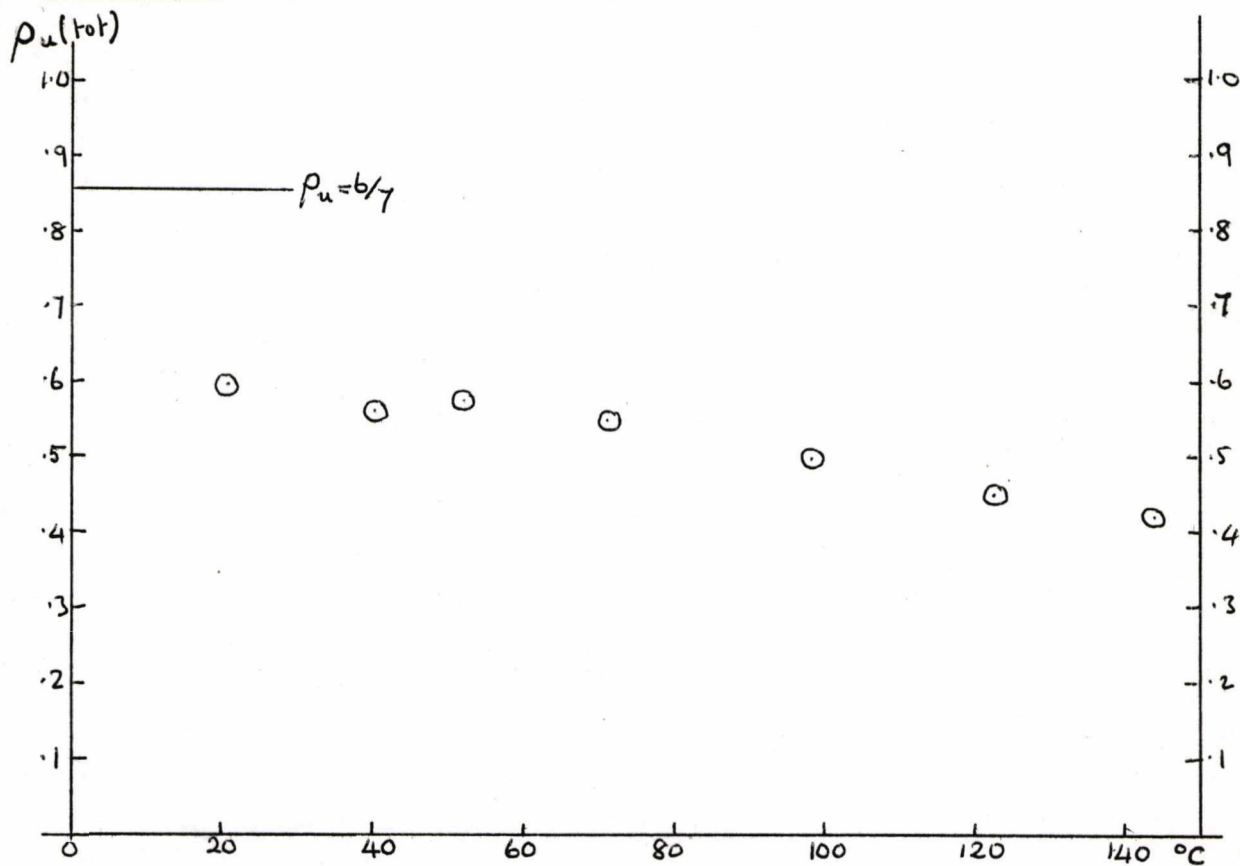


Table 4.4. Bromobenzene: tabulated results.

Temperature °C.	Brillouin splitting cm ⁻¹ .	Brillouin splitting Hz($\times 10^9$)	Refractive index	Velocity of hypersound m/sec	Density gm/cc.
-21	.1559 (1%)	4.67	1.574	1329	1.551
-20	.1547 (1%)	4.64	1.574	1318	1.549
-10.8	.1525 (1%)	4.58	1.570	1304	1.537
2.6	.1481 (2%)	4.45	1.563	1272	1.519
21.8	.1384 (1%)	4.15	1.554	1196	1.494
40.1	.1305 (1%)	3.92	1.545	1134	1.469
51.8	.1264 (1%)	3.79	1.539	1102	1.454
71.3	.1172 (2%)	3.52	1.530	1028	1.427
98.2	.1062 (1%)	3.19	1.517	941	1.392
122.5	.0977 (1%)	2.93	1.505	871	1.360
143.8	.0977 (1%)	2.67	1.495	800	1.331

Values of density from refs. (40) and (52) over entire temperature range. Values of refractive index extrapolated from those given in ref. (40)

Nitrobenzene.

The results for nitrobenzene are presented in figures 4.19-4.2 . The spectrum of light scattered from shear waves has been reported for this liquid, (31), (54), and there has been a certain amount of discussion about nitrobenzene in the literature. An example is ref. (34) where it is suggested that there is strong correlation between the orientations of neighbouring molecules.

As discussed on p. 4.12, the central "dip" predicted by Rytov's theory was not observed in this work. However, the anisotropic spectrum differs from that of chlorobenzene and bromobenzene in that its total intensity falls off with temperature, as shown in figure 4.20. The values of intensity have been corrected as described on p. 4.14, to eliminate the effects of the increase in absorbing impurities due to photochemical activity as the temperature was raised. The relative intensity in the narrow Lorentzian follows a line approximately parallel to that of the total intensity. This indicates that the mechanism causing the narrow Lorentzian is responsible for the decrease in intensity with temperature, whereas the intensity in the broader Lorentzian is approximately constant. The total depolarization ratio and its variation with temperature are shown in figure 4.23. The high value indicates that the anisotropic spectrum was extremely strong in this liquid.

The isotropic spectrum gave a Landau-Placzek ratio of $0.39 \pm .07$, which was independent of temperature within the experimental error. The "background" between the Brillouin lines in the isotropic spectrum was again of the correct order of magnitude and shape to be attributed principally to the antisymmetric components of equation (2.44). It

increased slightly with temperature as the Brillouin lines drew closer together. At low temperatures it was very difficult to measure, since the anisotropic spectrum is very narrow in this liquid, and the isotropic spectrum must be separated from a sharp and intense anisotropic peak. This factor contributed to the uncertainty in low temperature values of the sound velocity, and in intensity measurements.

The hypersonic velocity, shown in figure 4.21, shows a linear variation with temperature within the experimental error, and agreement with the lower temperature ultrasonic results of ref. (41). The ultrasonic results, however, show a 2% deviation from a straight line, and the light scattering results fall below the ultrasonic at higher temperatures and above them at lower temperatures, the discrepancy at the higher temperatures being outside the experimental error. Hence the agreement between the two sets of results is not entirely satisfactory, but more accurate results from both types of measurement are needed to show whether there is a genuine difference between the two. The Brillouin linewidth increases towards lower temperatures, as shown in figure 4.22, but by a small amount which could be due to the increase of frequency-independent bulk viscosity. There are no ultrasonic absorption measurements from which a comparison of the "viscosities" may be made. Hence there is no evidence for a dispersion of greater than 1% in nitrobenzene in the frequency region of 5×10^9 Hz, although measurements of greater accuracy might show a small dispersion.

Table 4.4 gives the actual Brillouin splittings measured, and other parameters used in the calculations. The hypersonic adiabatic compressibility is shown in figure 4.37.

Figure 4.19. Nitrobenzene: variation with temperature of τ_{11s} , τ_{21s} and comparable times.

① $\tau_{11s} = 7.3 \times 10^{-14} \exp \left[\frac{3.69}{RT_0} \right]$

② Times ($\times 10^{-1}$) from static shear viscosity data (52) and using Debye relation. (5.4)

③ τ_{21s}

□ values from Table 4.1

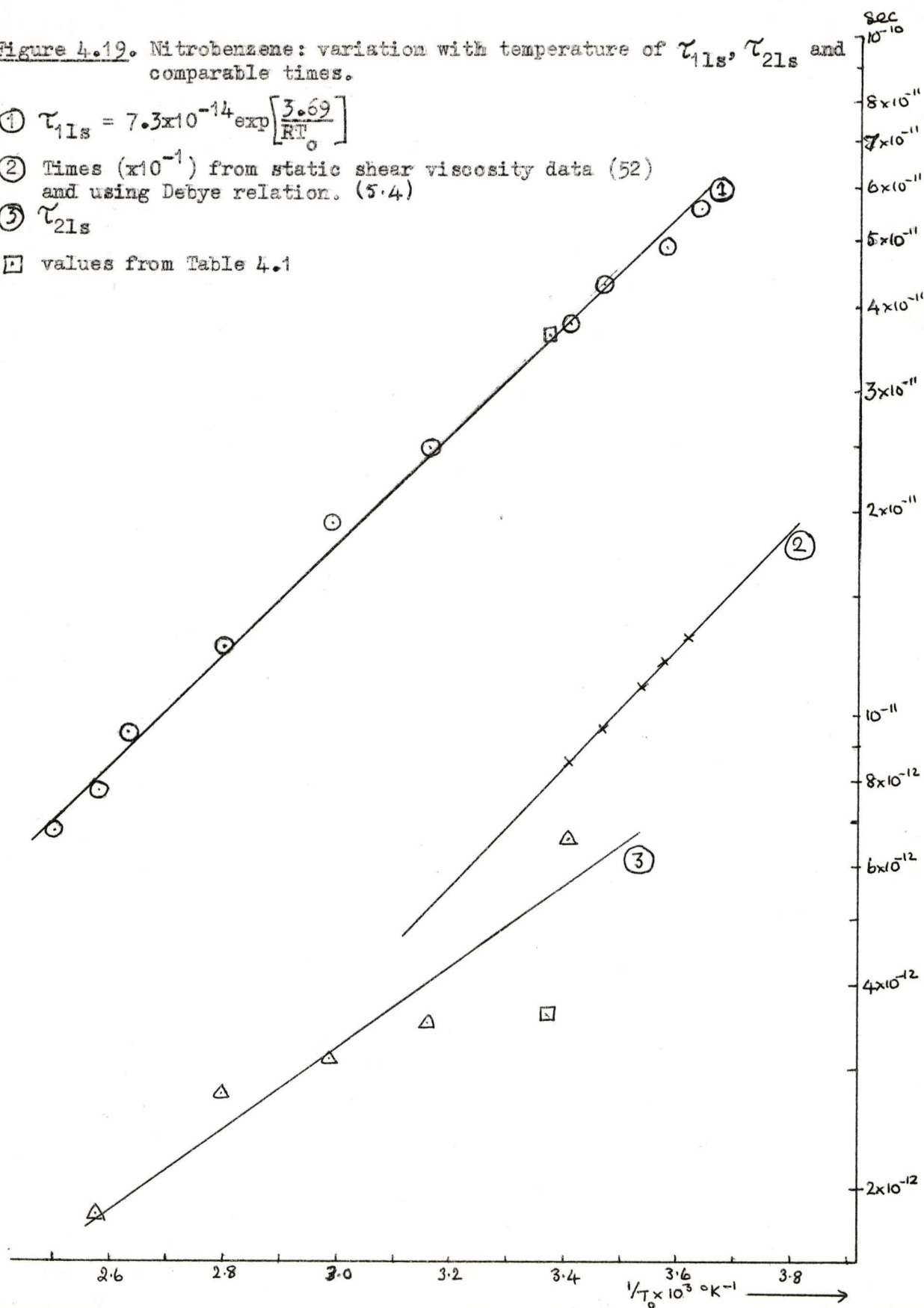


Figure 4.20. Nitrobenzene: intensity of anisotropic spectrum.

- ⊙ total intensity values
X intensity in narrow Lorentzian

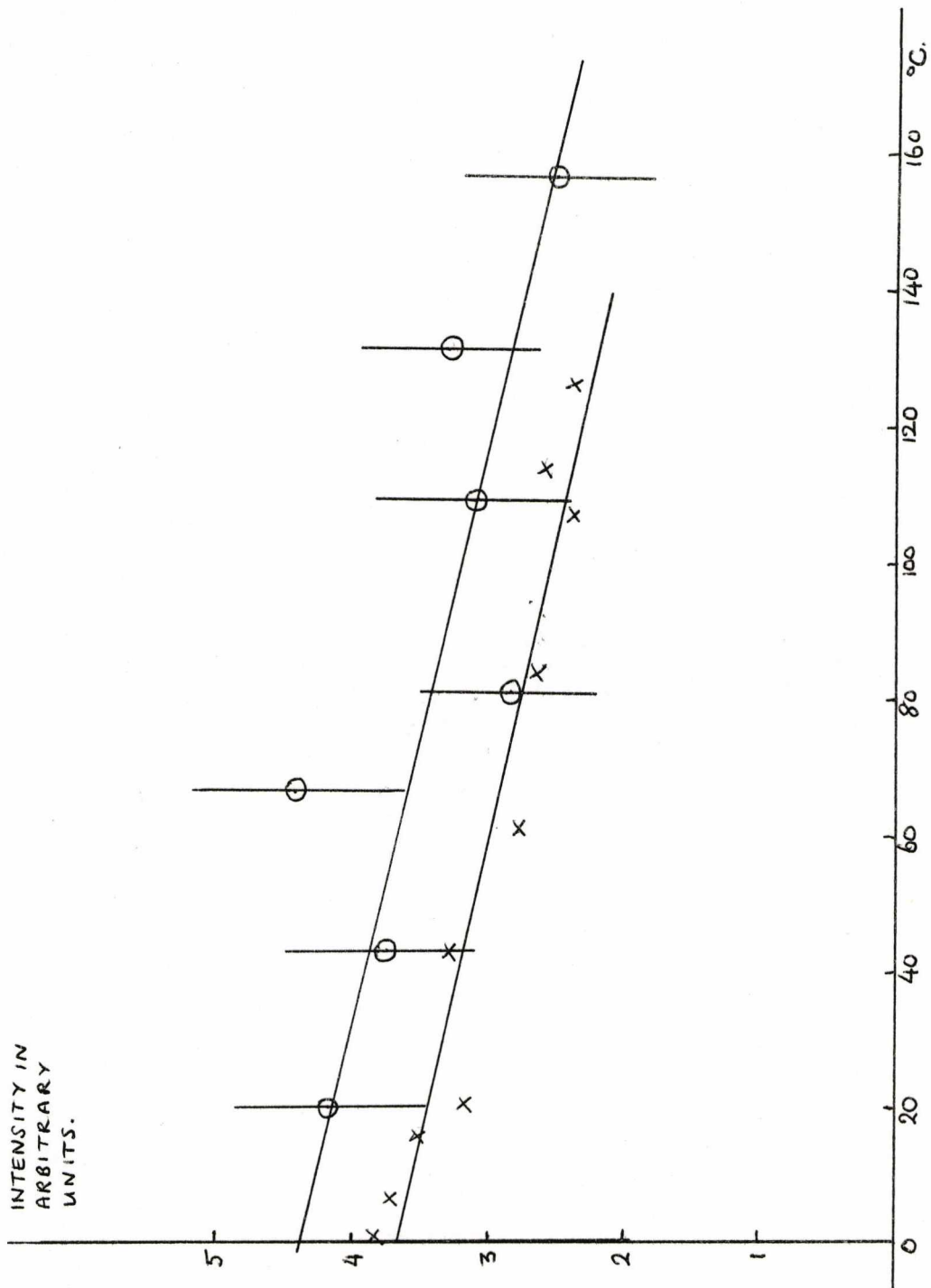


Figure 4.21. Nitrobenzene: velocity of hypersound against temperature.
Frequency $\sim 5 \times 10^9$ Hz at 20°C .

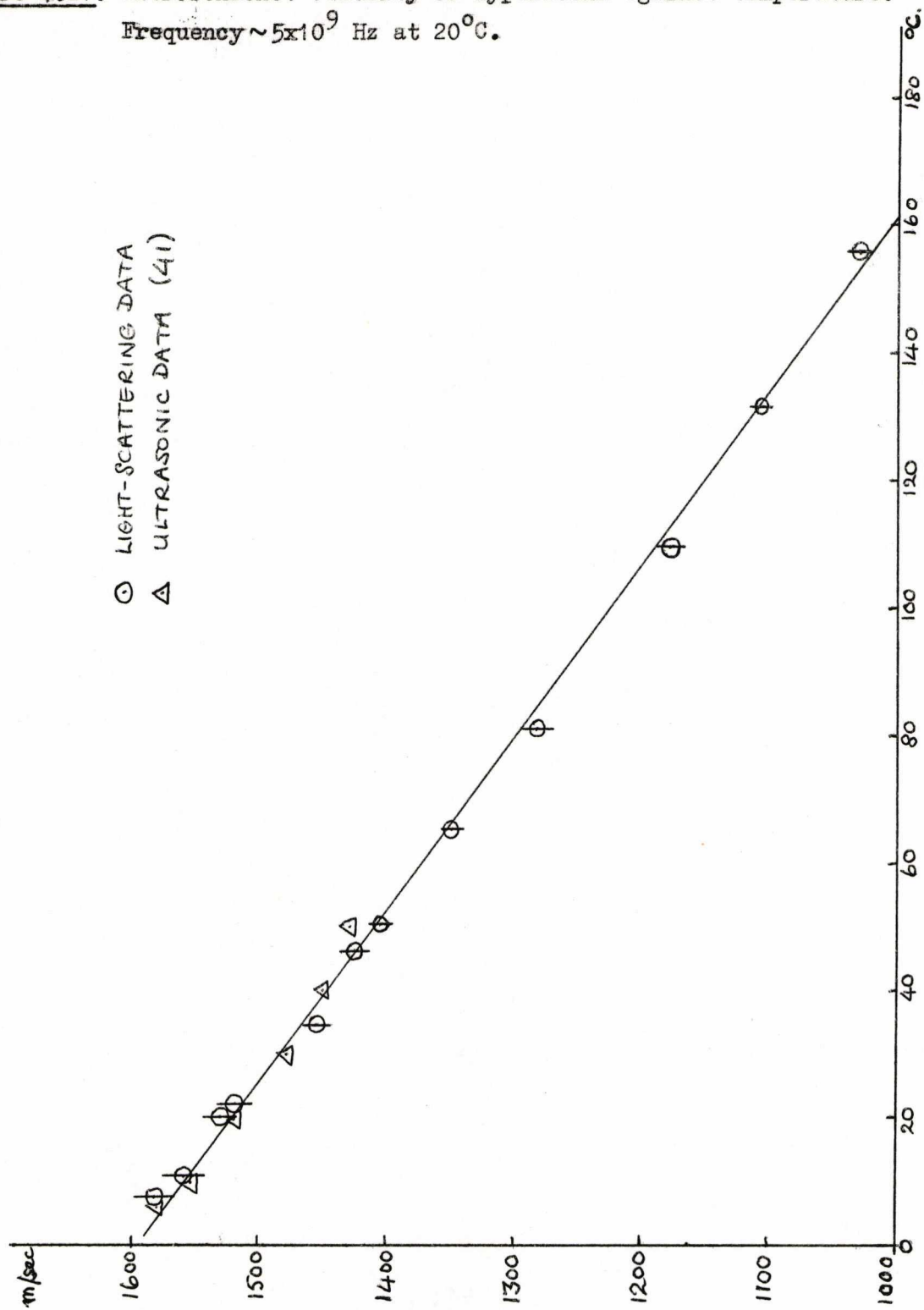
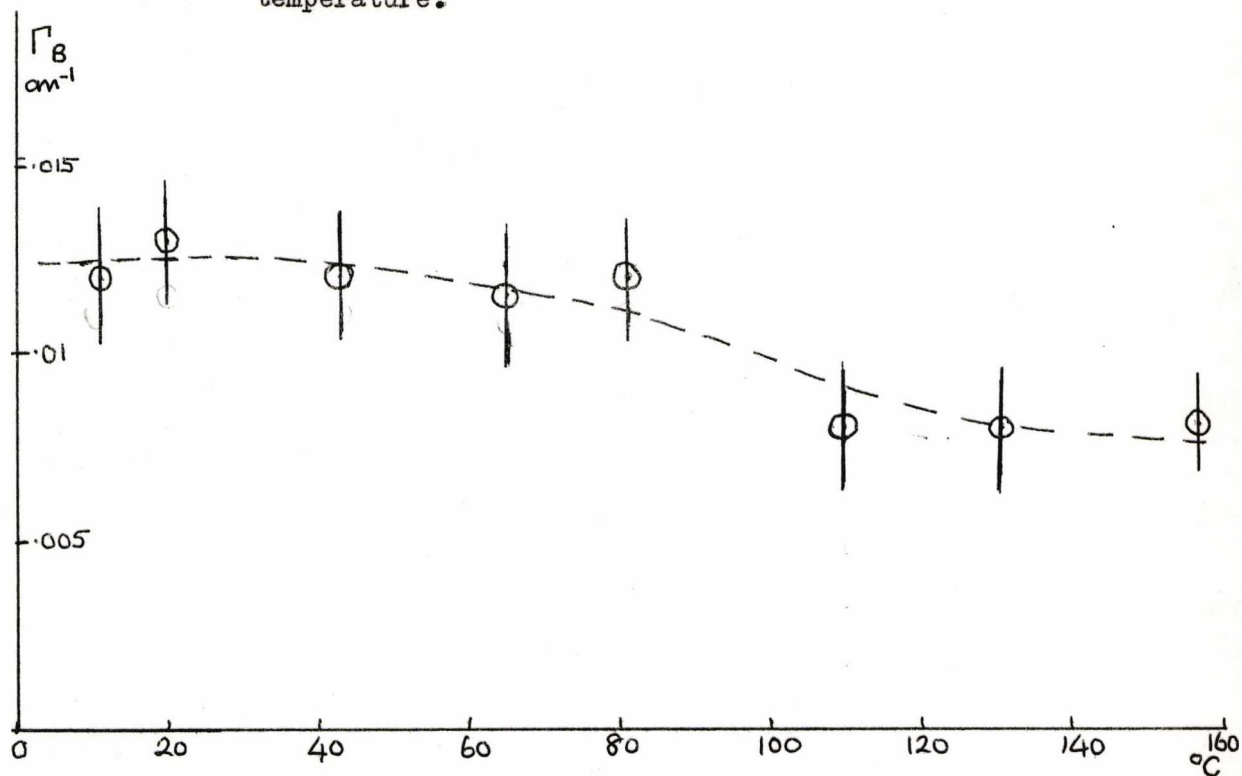


Figure 4.22. Nitrobenzene: variation of Brillouin semi-halfwidth with temperature.



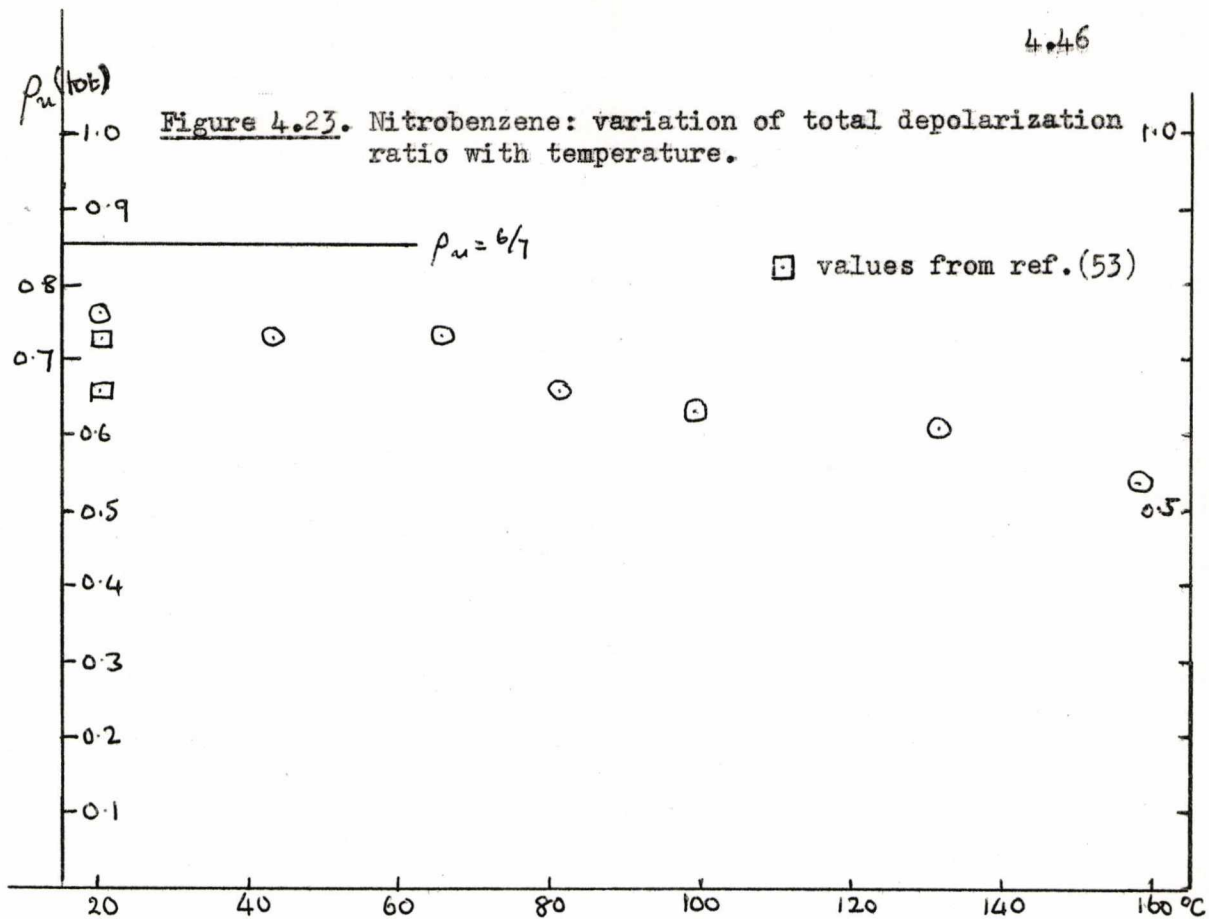


Table 4.5. Nitrobenzene: tabulated results.

Temperature °C.	Brillouin splitting cm ⁻¹ .	Brillouin splitting Hz($\times 10^9$)	Refractive index	Velocity of hypersound m/sec.	Density gm/cc.
7.5	.1826 (2%)	5.48	1.550	1582	1.216
10.3	.1795 (2%)	5.39	1.548	1557	1.213
20.0	.1761 (1%)	5.28	1.544	1531	1.203
21.9	.1747 (1%)	5.24	1.544	1519	1.201
34.4	.1667 (1%)	5.00	1.538	1455	1.189
43.0	.1629 (1%)	4.89	1.534	1426	1.180
50.3	.1602 (2%)	4.81	1.531	1405	1.170
65.2	.1531 (1%)	4.59	1.524	1349	1.158
81.0	.1448 (1%)	4.34	1.517	1282	1.142
109.5	.1320 (1%)	3.96	1.504	1178	1.115
131.5	.1231 (1%)	3.69	1.494	1107	1.093
156	.1138 (1%)	3.41	1.483	1031	1.089

Values of refractive index extrapolated below 15°C and above 25°C from those given in ref. (40). Values of density extrapolated above 50°C from those given in ref. (41).

Aniline.

Aniline is another liquid in which the light-scattering spectrum due to shear-waves has been reported. (31). It is more complex than the liquids discussed so far, in that it is possible for internal rotation of the $-NH_2$ group to occur. Smyth and Grubb (45) attribute 40% of the dielectric relaxation rotation to this cause.

The correlation times from the narrow part of the anisotropic spectrum are shown in figure 4.24, where values from ref. (45) for dielectric relaxation are also shown, besides times calculated from the static shear viscosity using the Debye relation. This liquid is extremely photochemically active; so much so that the impurity content of the sample increased perceptibly during the recording of a single spectrum. It was also very difficult to prepare a dust-free sample. For these reasons, none of the intensity measurements were reliable, since after the correction method of p 4.13 had been used, the results showed such a wide spread that no deductions could be drawn from them. The lineshape, as in experiment I, was far from a single Lorentzian, and the narrow part of the curve accounted for some 50-60% of the total intensity of the anisotropic spectrum.

The results for the velocity of hypersound show a large departure from linearity at low temperatures, which is accompanied by a marked increase in the Brillouin linewidth. (Figures 4.25-26). Unfortunately there are no comparable ultrasonic results. The deviation from linearity is about 5% at $0^\circ C$. This, then, gives evidence for a dispersion region in aniline at about 6×10^9 Hz at $0^\circ C$. It should be noted that the sound velocity in aniline is higher than in any of the other liquids, by about

30%, so that this is a higher frequency than was reached using this method in any of the other liquids.

Values of the hypersonic adiabatic compressibility have again been calculated and are given in figure 4.3]. The Brillouin splittings, and values of the refractive index and density used in the calculations, are tabulated in Table 4.6.

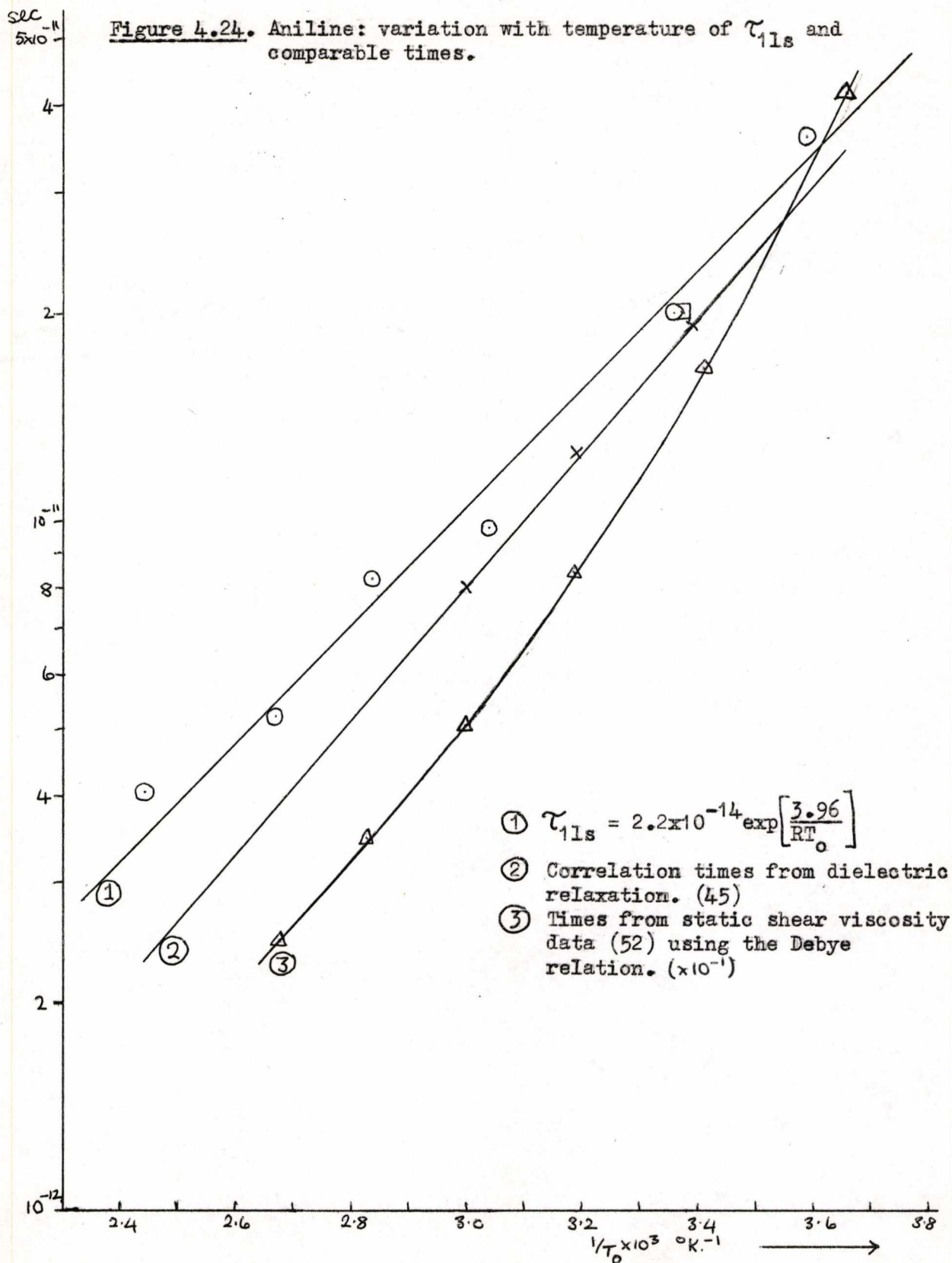


Figure 4.25. Aniline: velocity of hypersound against temperature.
Frequency $\sim 6 \times 10^9$ Hz at 20°C .

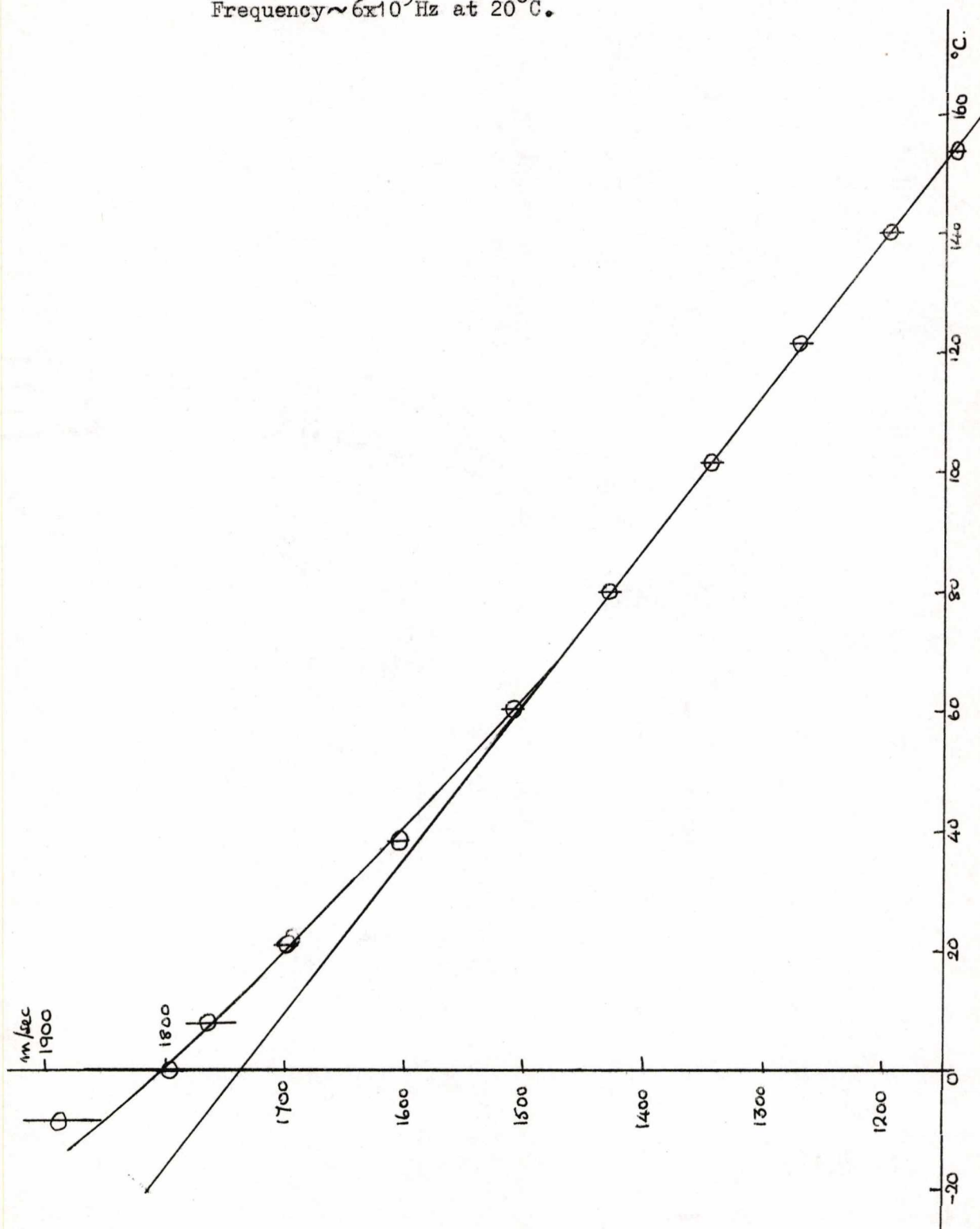


Figure 4.26. Aniline: variation of Brillouin semi-halfwidth with temperature.

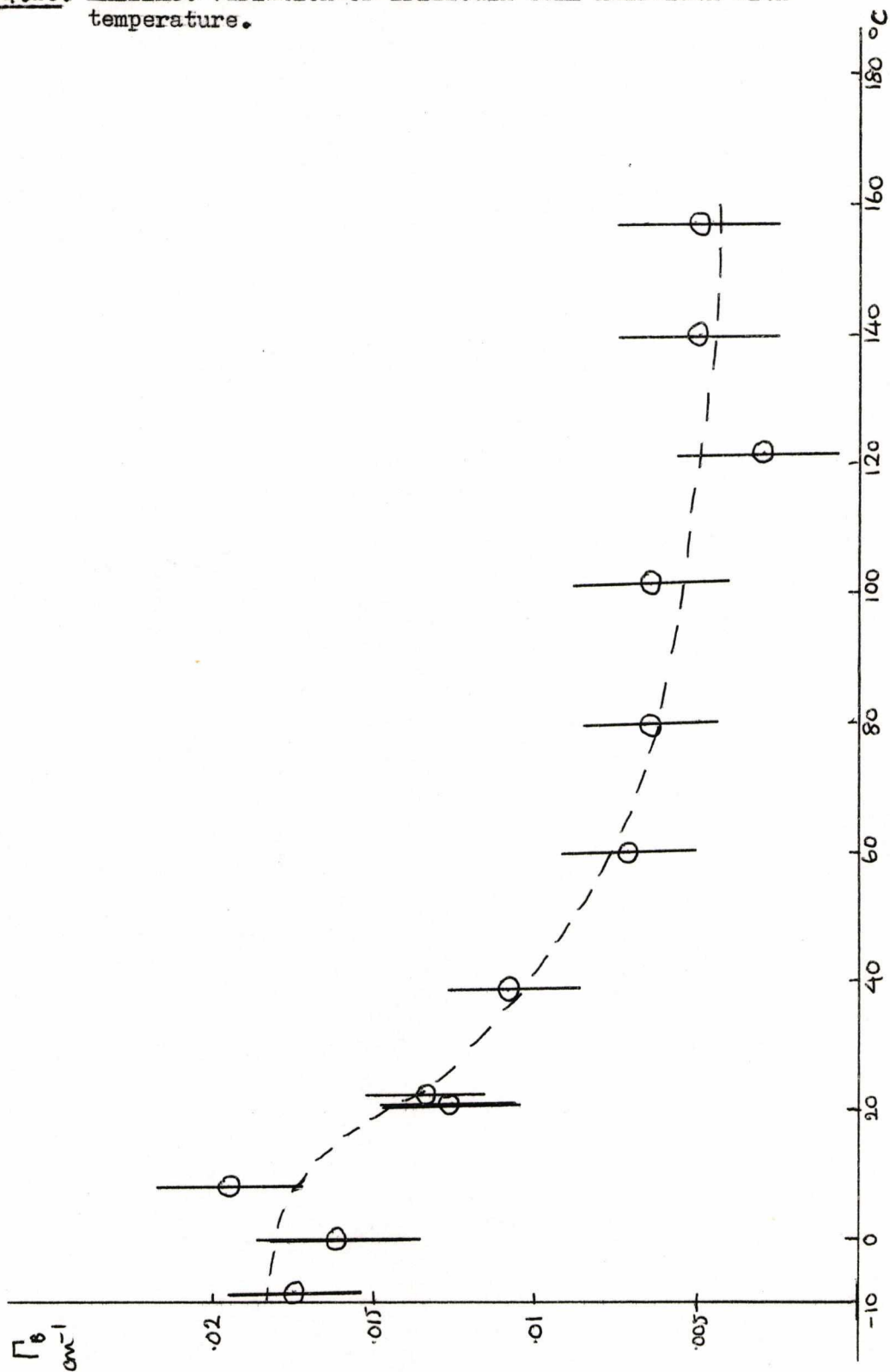


Table 4.6. Aniline: tabulated results, and parameters used in calculation.

Temperature °C.	Brillouin cm ⁻¹ .	splitting Hz (×10 ⁹)	Refractive index	Velocity of hypersound m/sec	Density gm/cc.
-8.4	.2240 (3%)	6.72	1.593	1888	1.046
0	.2124 (1%)	6.36	1.589	1794	1.039
8.0	.2084 (2%)	6.25	1.584	1766	1.032
21.0	.1995 (1%)	5.98	1.578	1698	1.021
38.7	.1876 (1%)	5.63	1.569	1605	1.006
60.3	.1751 (1%)	5.25	1.558	1510	.987
79.8	.1647 (1%)	4.94	1.548	1428	.970
101.4	.1539 (1%)	4.62	1.537	1344	.950
121.4	.1442 (1%)	4.33	1.526	1270	.932
140	.1352 (1%)	4.06	1.517	1196	.914
153.5	.1285 (1%)	3.86	1.510	1142	.902

Values of refractive index extrapolated above 25°C and below 20°C from those given in ref (52). Values of density given in ref. (52) for entire temperature range.

Benzonitrile.

The results for benzonitrile are shown in figures 4.27-4.31. They show no complexities. There is no comparable data from other experimental methods, except that from static shear viscosity, for this liquid.

The intensities of the different components of the spectra have been corrected as described on p.4.14, since this is a liquid in which the impurity content increases with temperature. The total corrected anisotropic intensity decreases slightly with temperature.

This sample showed some extraneous scattering at the incident frequency for some spectra. The lowest value of the Landau-Placzek ratio measured was 0.37. This value was used in calculating the values of the total depolarization ratio, which are shown in Figure 4.31.

With no comparable ultrasonic data, the hypersonic velocity and Brillouin linewidth measurements are rather difficult to interpret. It is possible to draw a straight line through the velocity results, but it is also possible to observe a departure from linearity of about 1.7%. The Brillouin linewidth falls off with temperature as might be expected in the presence of a small dispersion, but this also might be attributed to the frequency-independent "viscosity". Hence these results are inconclusive without comparable ultrasonic data. This illustrates the accuracy required to observe small dispersions using this method.

The shape of the isotropic spectrum again showed satisfactory agreement with equation (2.44) at all temperatures.

The values of Brillouin splitting obtained, and parameters used in the calculations, are given in Table 4.7. The adiabatic compressibility at hypersonic frequencies is shown in figure 4.37.

Figure 4.27. Benzonitrile: variation with temperature of τ_{11s} and comparable times.

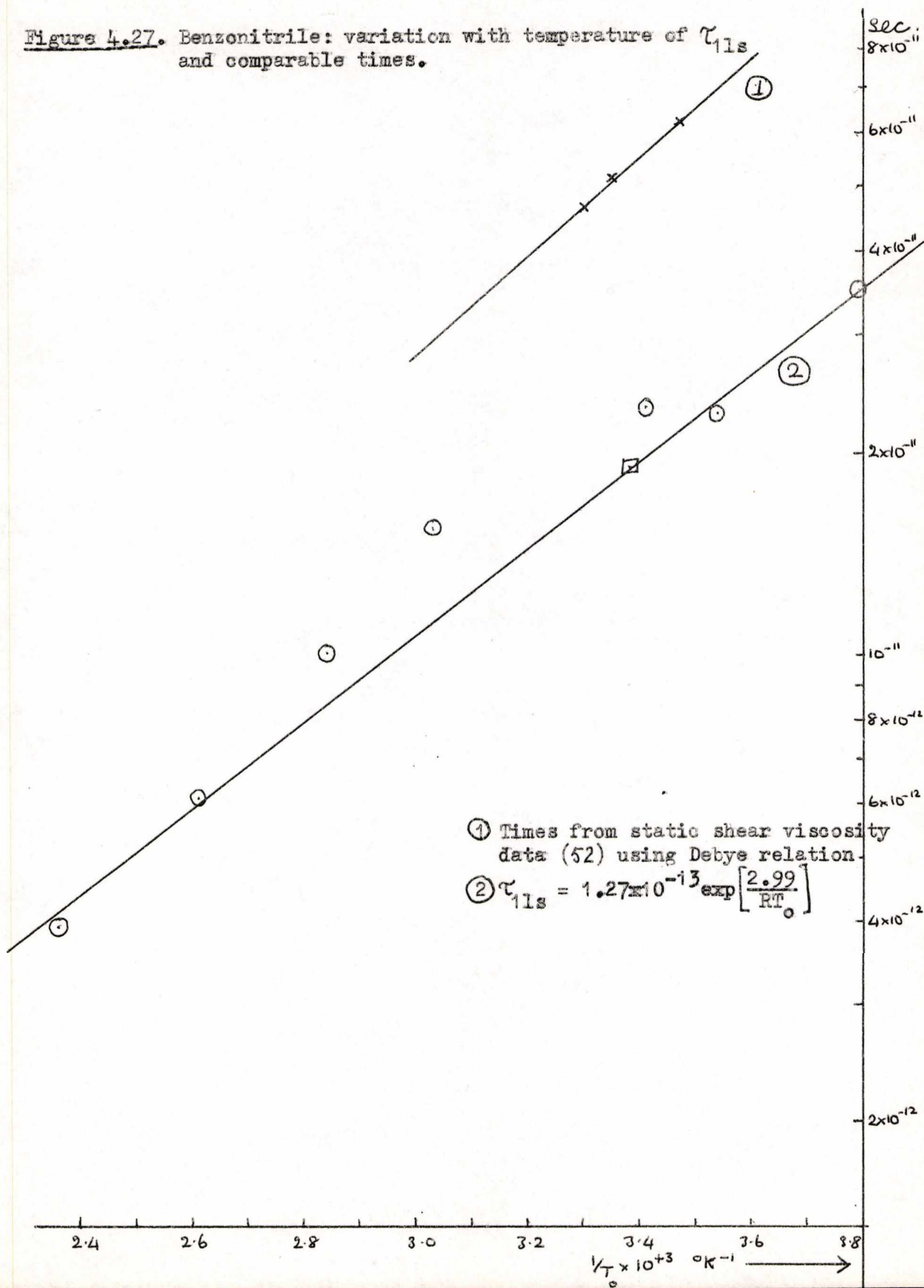


Figure 4.28. Benzonitrile: intensity of anisotropic spectrum.

○ total intensity values
× intensity in narrow Lorentzian

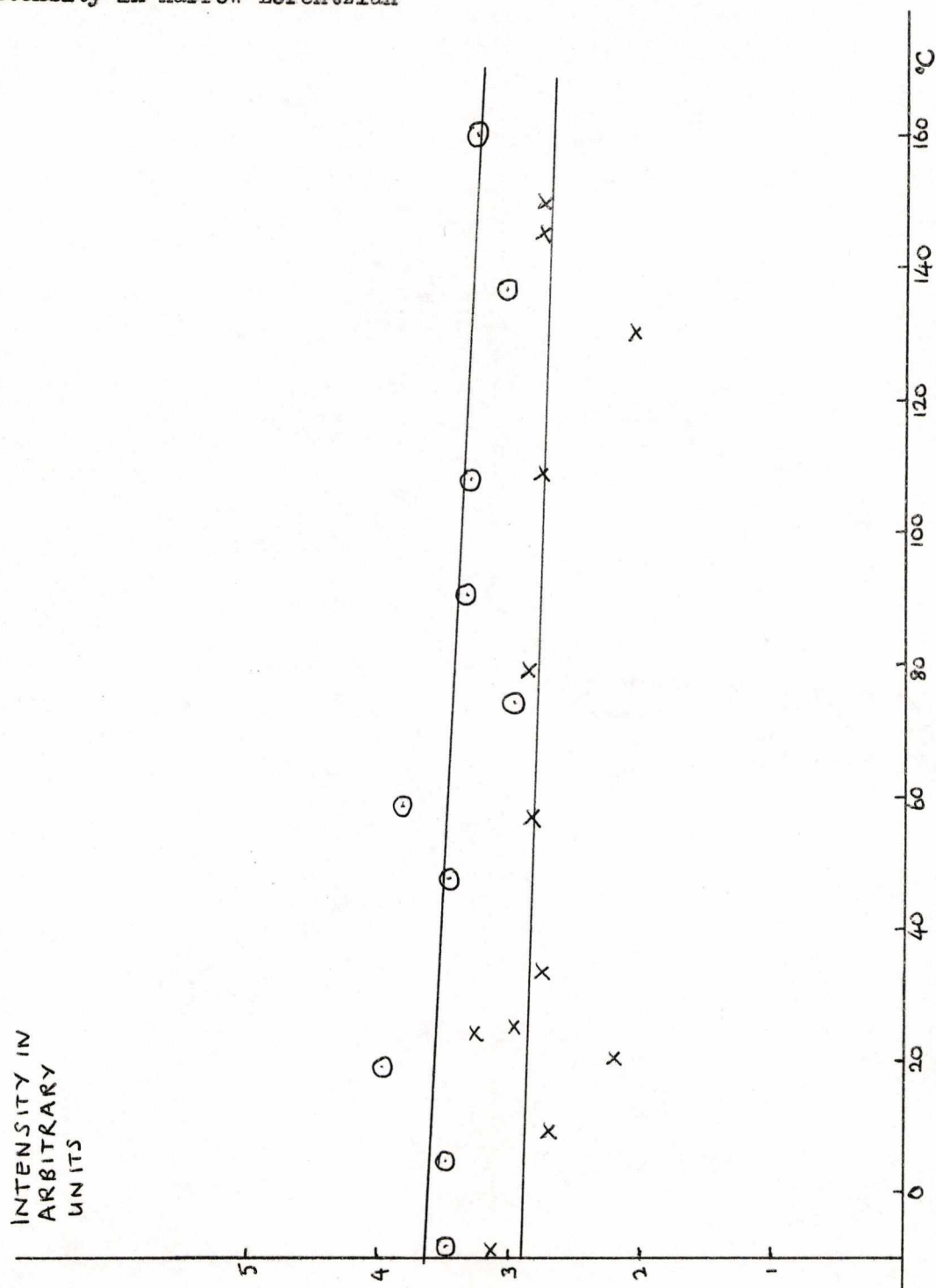


Figure 4.29. Benzonitrile: velocity of hypersound against temperature.
Frequency $\sim 5 \times 10^9$ Hz at 20°C .

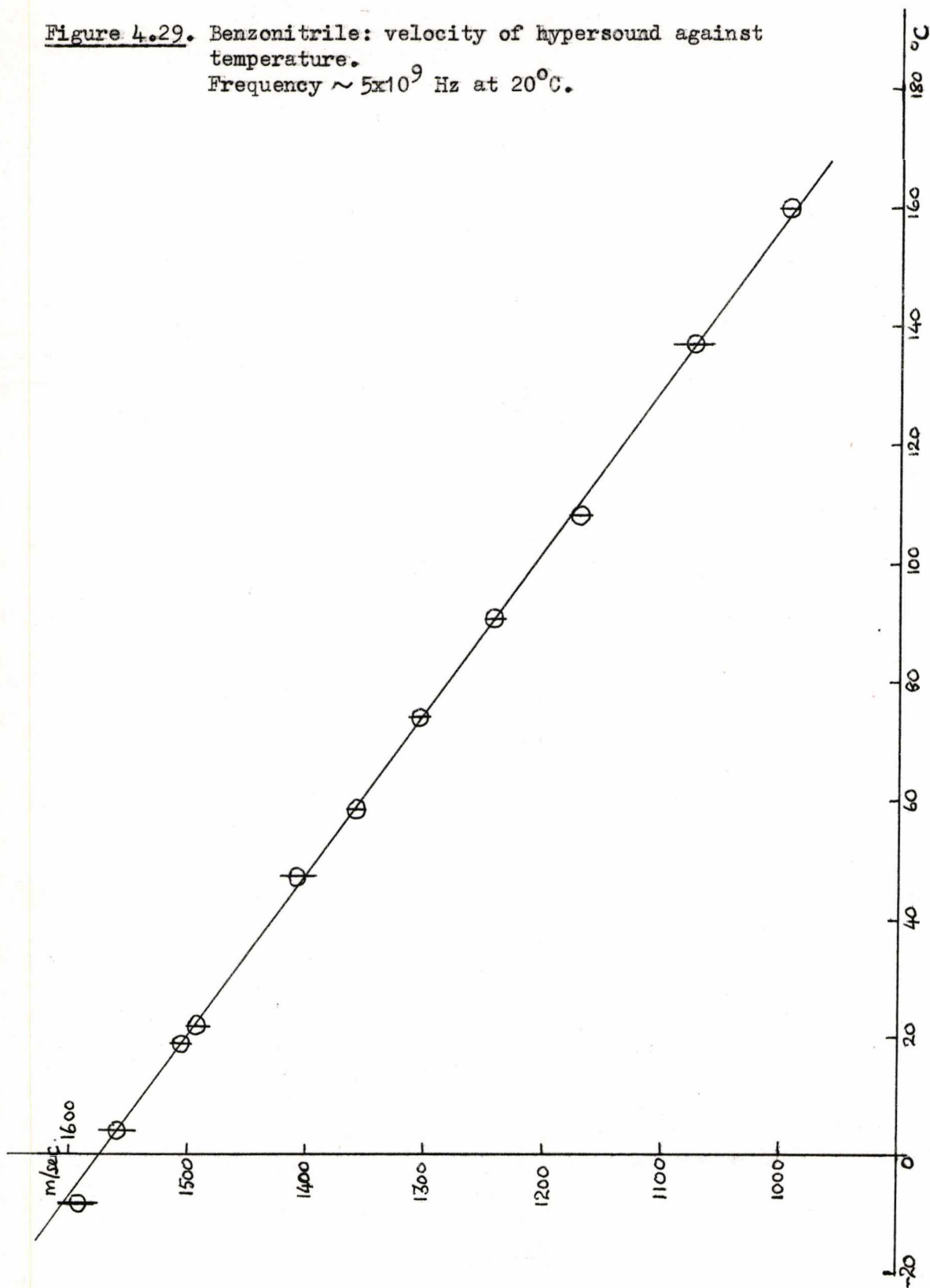


Figure 4.30. Benzonitrile: variation of Brillouin semi-halfwidth with temperature.

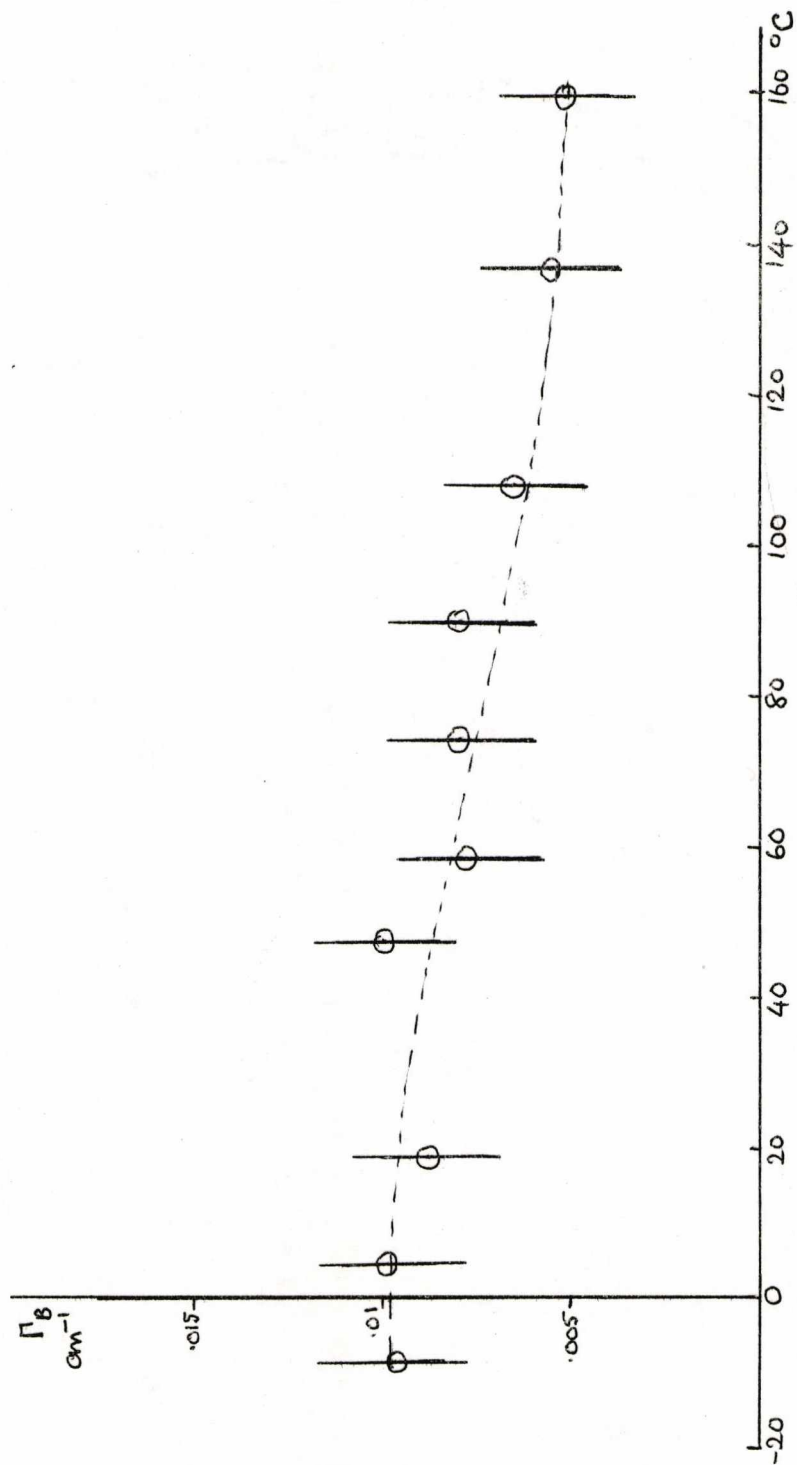


Figure 4.31. Benzonitrile: variation of total depolarization ratio with temperature.

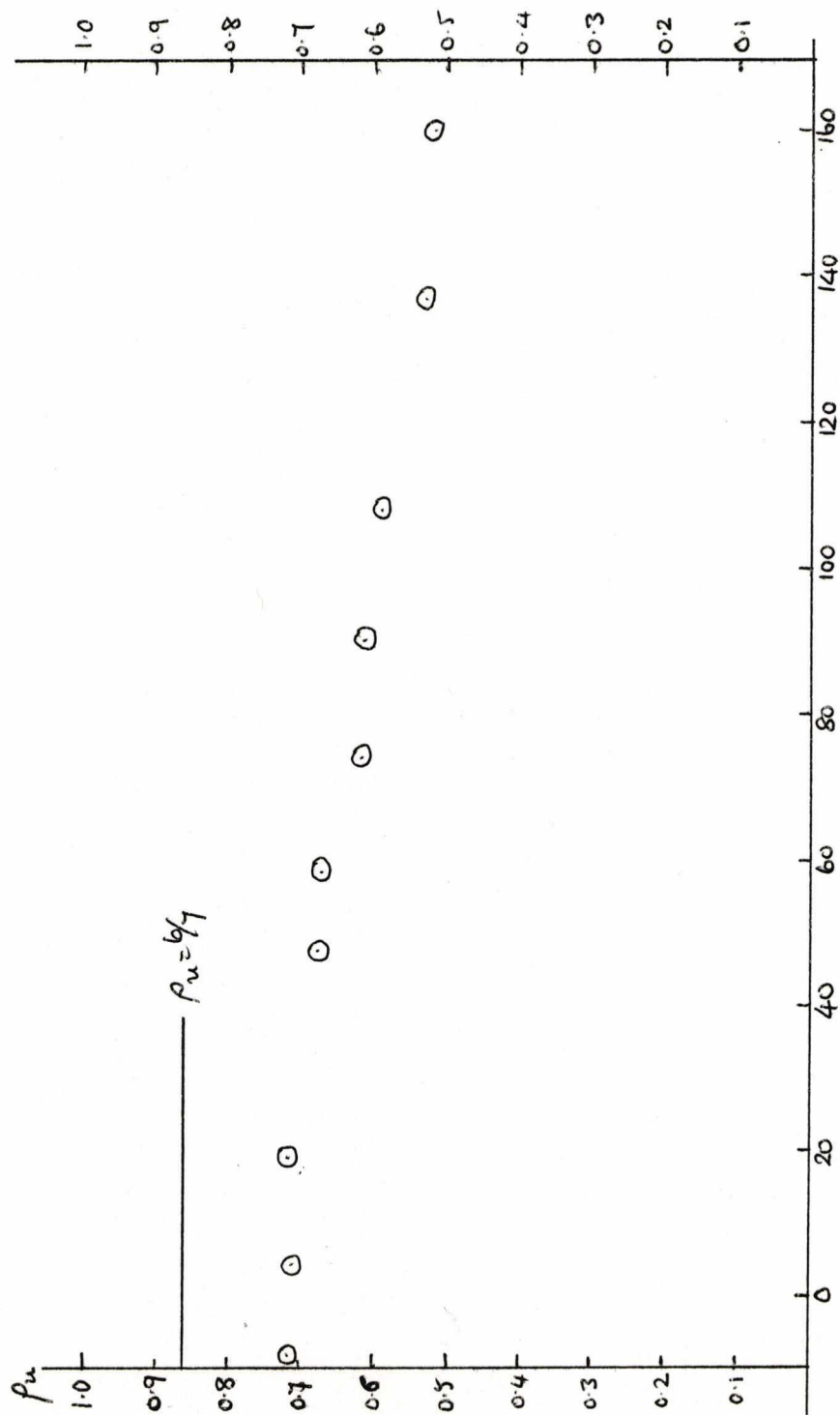


Table 4.7. Benzotrile: tabulated results and parameters used in calculations.

Temperature °C.	Brillouin cm ⁻¹	splitting Hz (×10 ⁹)	Refractive index	Velocity of hypersound m/sec.	Density gm/cc.
-8.3	.1821 (2%)	5.46	1.536	1591	1.030
4.2	.1777 (2%)	5.33	1.530	1560	1.019
19.0	.1710 (1%)	5.13	1.523	1506	1.005
47.5	.1584 (2%)	4.75	1.509	1408	0.980
58.4	.1521 (1%)	4.56	1.504	1358	0.969
74.2	.1456 (1%)	4.37	1.496	1306	0.956
90.2	.1378 (1%)	4.13	1.488	1242	0.941
108	.1290 (1%)	3.87	1.480	1170	0.925
137	.1176 (2%)	3.53	1.466	1076	0.899
160	.1078 (1%)	3.23	1.455	995	0.878

Values of refractive index extrapolated from those given in ref. (52).

Values of density from ref. (52).

Benzoyl chloride.

There is no comparable data for this liquid, neither from ultrasonic measurements nor from experimental methods giving correlation times which may be compared with those from the anisotropic spectrum. Values of the refractive index and density both had to be extrapolated from inadequate data. However, the data thus obtained showed few complexities. This liquid is extremely active photochemically, and the impurity content increased rapidly as the temperature was raised. The intensity measurements have therefore been corrected as described on p. 4.13.

The correlation times obtained from the narrow part of the anisotropic spectra, and the total intensity in the anisotropic spectra, are shown in figures 4.32 and 4.33. The anisotropic intensity was independent of temperature, and the lineshape was extremely complex, in agreement with the results of experiment I. (Figures 4.2, 4.3) The narrow Lorentzian contained only 30-40% of the anisotropic intensity.

The velocity of hypersound showed a linear variation with temperature, and the Brillouin linewidth was approximately constant with temperature, increasing slightly as the temperature was raised. This could indicate the existence of a dispersion region below 3×10^9 Hz, although greater accuracy would be required in measurements of the Brillouin linewidth to establish this.

Benzoyl chloride is particularly noteworthy because of its very high total depolarization ratio (See figure 4.36). This stems from the fact that the anisotropic depolarization ratio (that of the anisotropic spectrum alone) is itself greater than 6/7, the limiting value predicted

from the considerations on p 2.8 for scattering from a symmetric dielectric constant tensor of zero trace. The value of $\rho_u(\text{anis})$ was independent of temperature and equal to 0.96 ± 0.02 . The intensity of the anisotropic spectrum was so much greater than that of the isotropic spectrum, that $\rho_u(\text{tot})$ was also greater than $6/7$. These results will be discussed further in connection with the interpretation of the anisotropic spectra.

The Landau-Placzek ratio had a value 0.36 ± 0.03 . The actual values of Brillouin splitting obtained, and the parameters used in the calculations, are given in Table 4.8. The temperature-dependence of the adiabatic hypersonic compressibility is shown in figure 4.37.

Figure 4.32. Benzoyl chloride: variation of τ_{11s} with temperature.

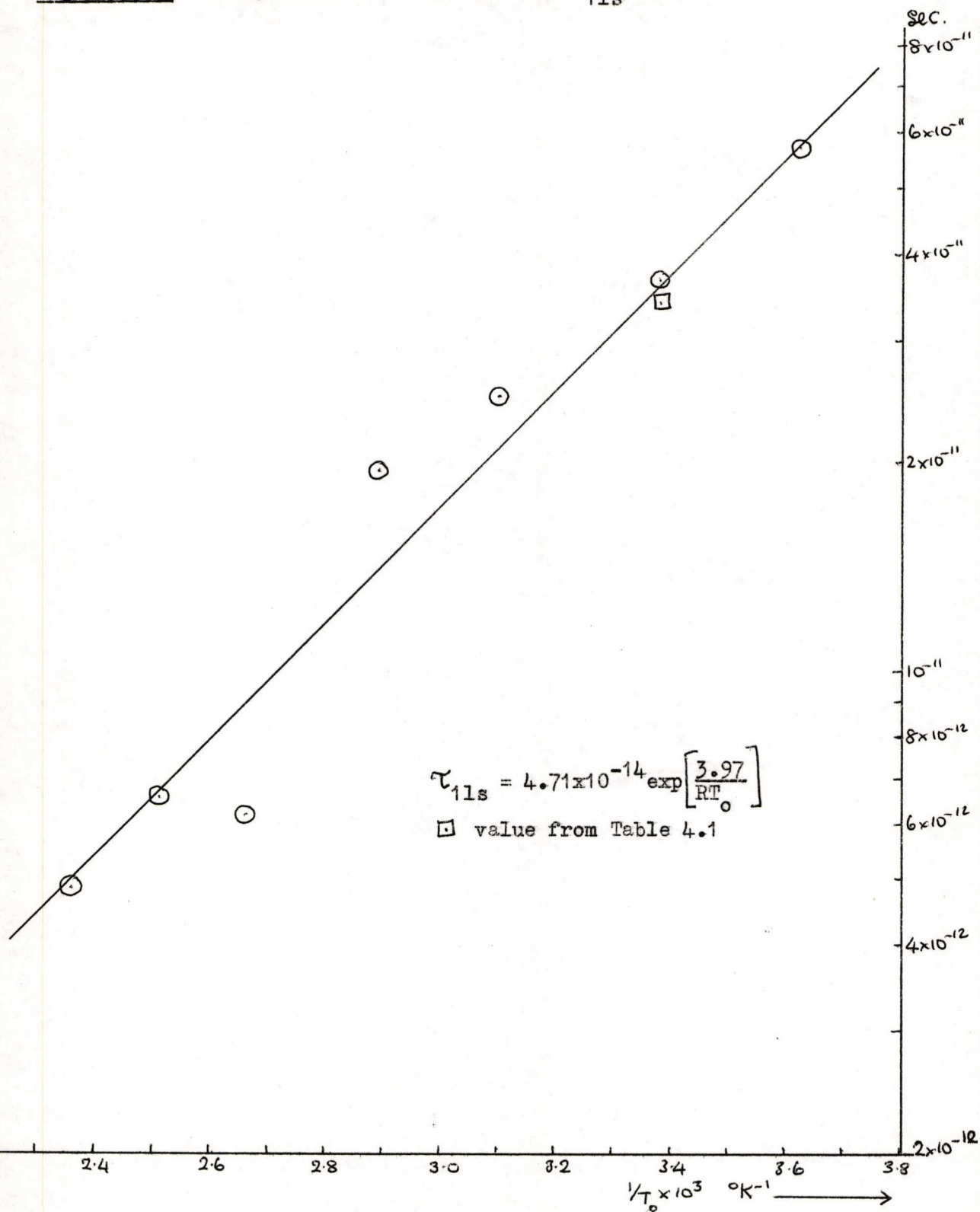


Figure 4.33. Benzoyl chloride: intensity of anisotropic spectrum.

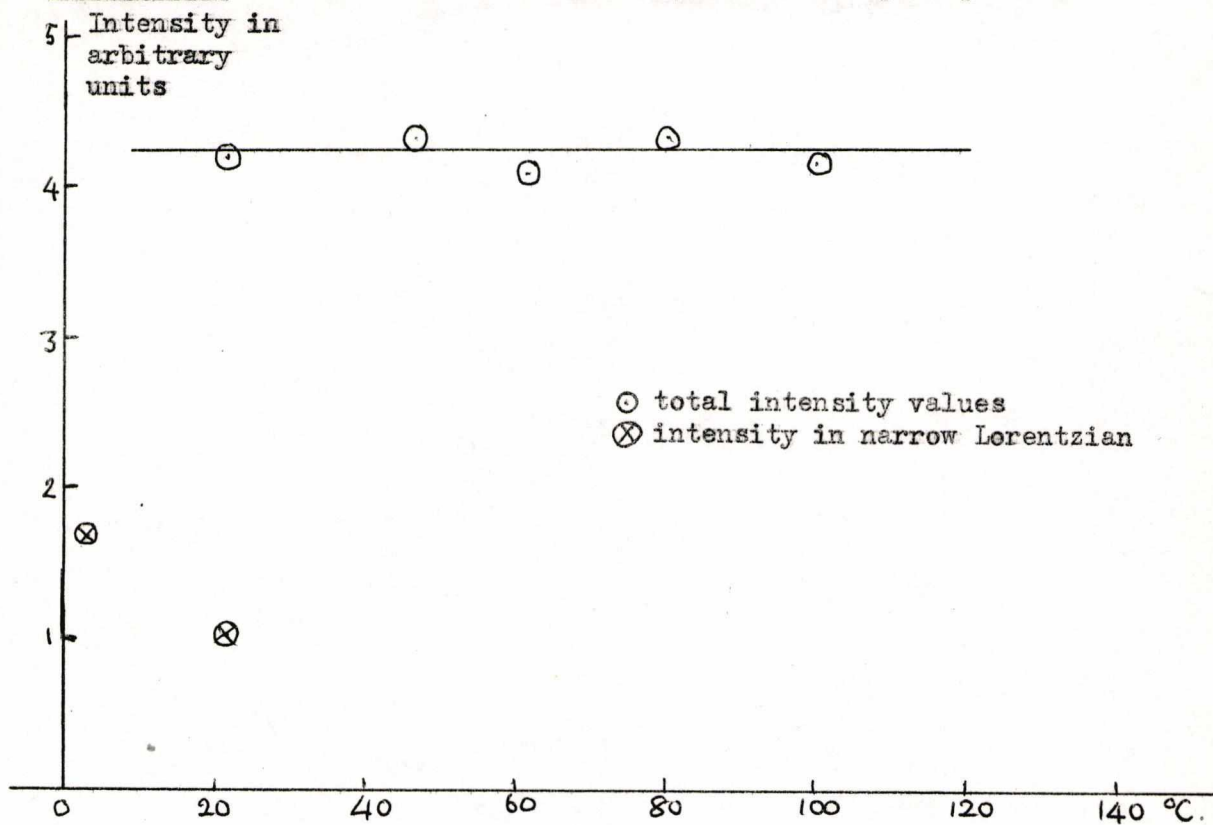


Figure 4.34. Benzoyl chloride: velocity of hypersound against temperature.
Frequency $\sim 5 \times 10^9$ Hz at 20°C .

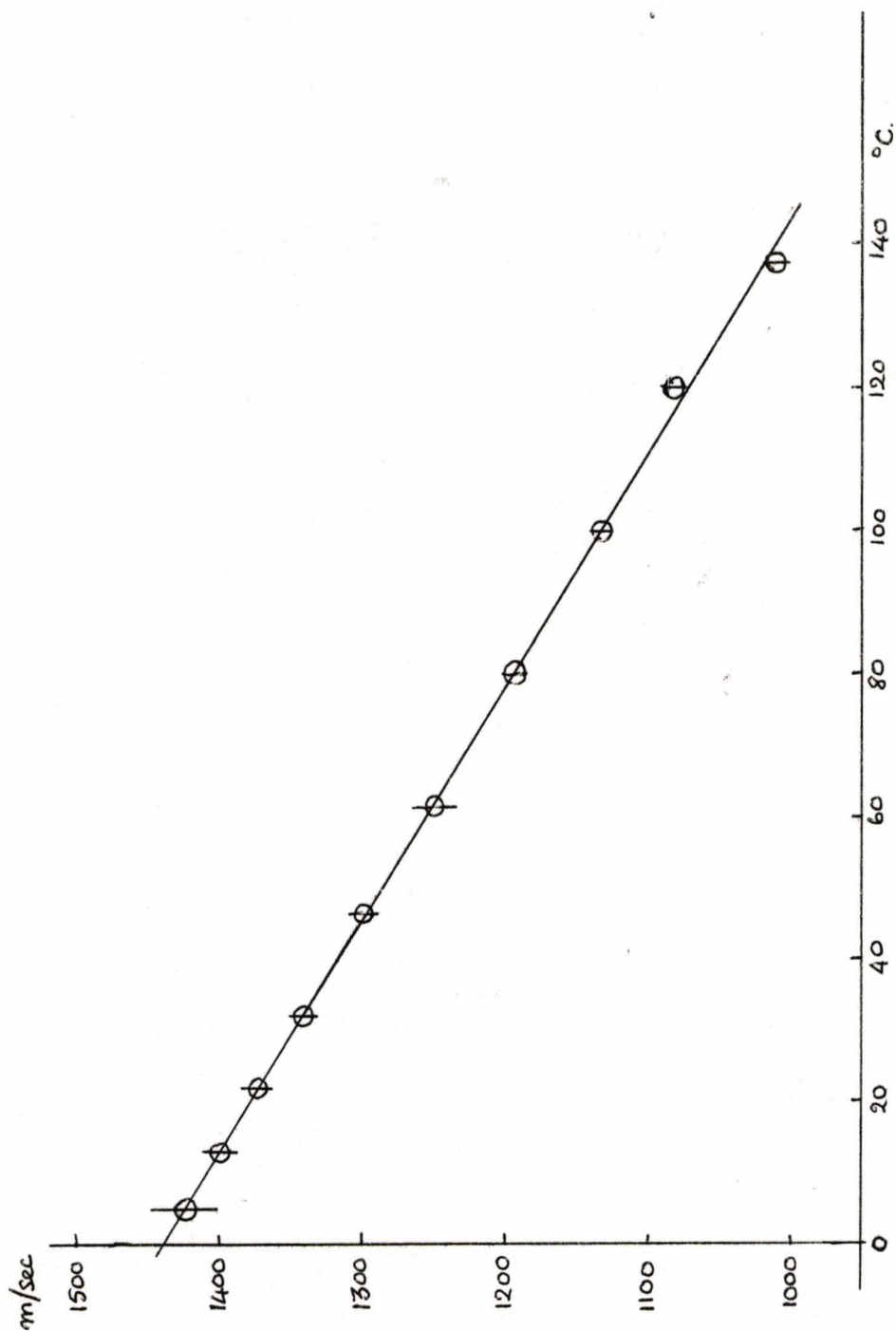


Figure 4.35. Benzoyl chloride: variation of Brillouin semi-
linewidth with temperature.

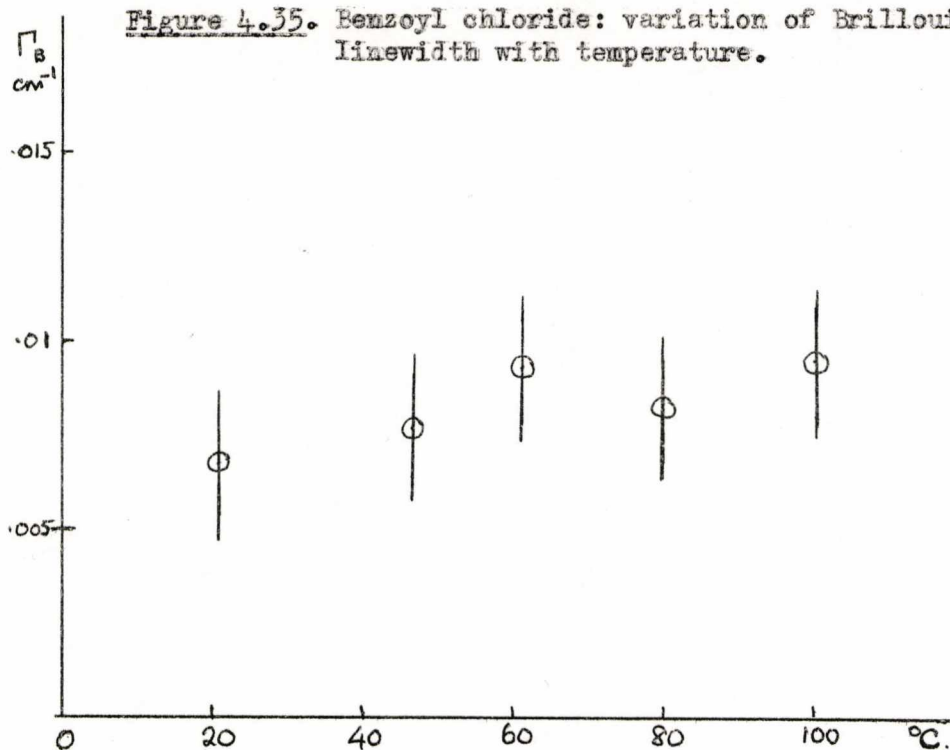


Figure 4.36. Benzoyl chloride: variation of total depolarization
ratio with temperature.

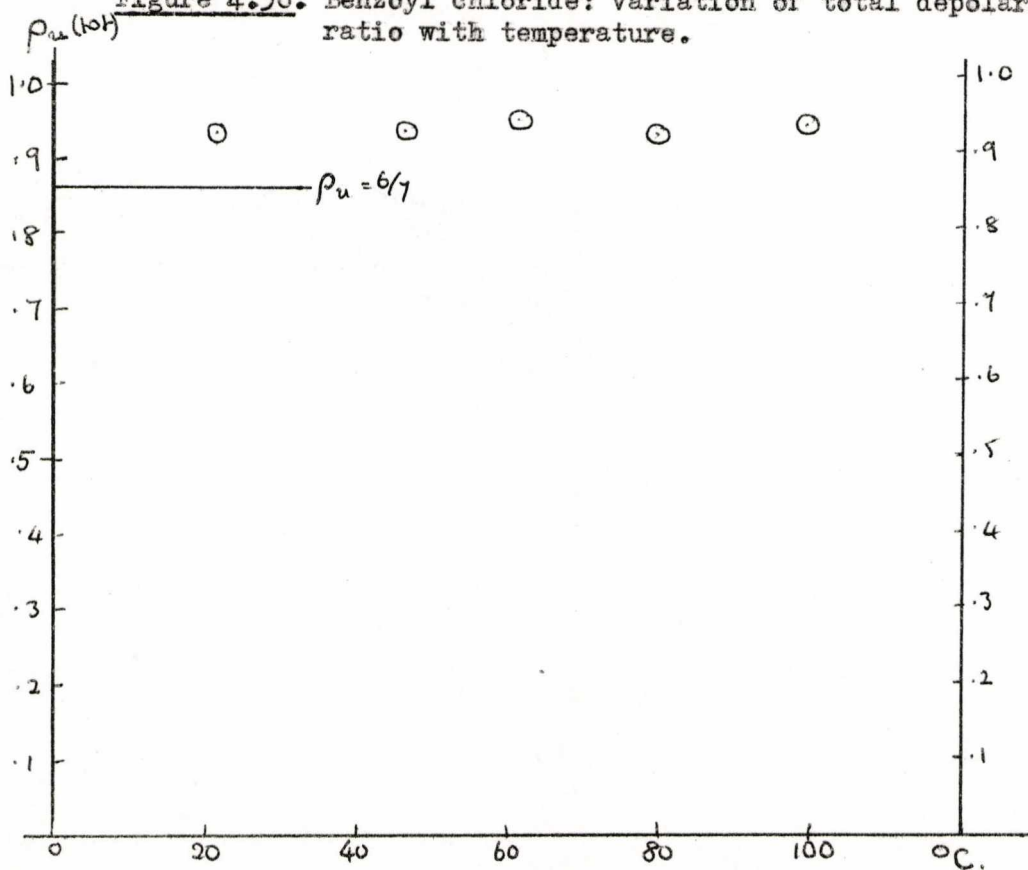


Table 4.8. Benzoyl chloride: tabulated results and parameters used in calculations.

Temperature °C.	Brillouin splitting cm ⁻¹	splitting Hz (×10 ⁹)	Refractive index	Velocity of hypersound m/sec.	Density gm/cc.
5.0	.1662 (2%)	4.99	1.567	1424	1.237
12.9	.1628 (1%)	4.88	1.560	1401	1.223
21.9	.1588 (1%)	4.76	1.552	1374	1.298
31.7	.1542 (2%)	4.62	1.543	1341	1.190
46.4	.1482 (1%)	4.44	1.530	1299	1.155
61.4	.1413 (2%)	4.24	1.517	1250	1.139
79.9	.1335 (1%)	4.01	1.501	1194	1.111
99.9	.1251 (1%)	3.75	1.483	1132	1.077
120	.1181 (1%)	3.54	1.466	1082	1.044
137.5	.1093 (1%)	3.28	1.450	1011	1.015

Values of density extrapolated from those given in ref. (52) and as quoted by British Drug Houses, Ltd. Values of refractive index extrapolated from those given in ref.(40).

Figure 4.37. Hypersonic adiabatic compressibility for the six liquids, obtained using the relation $\beta_S = 1/(v_s^2 \rho_0)$

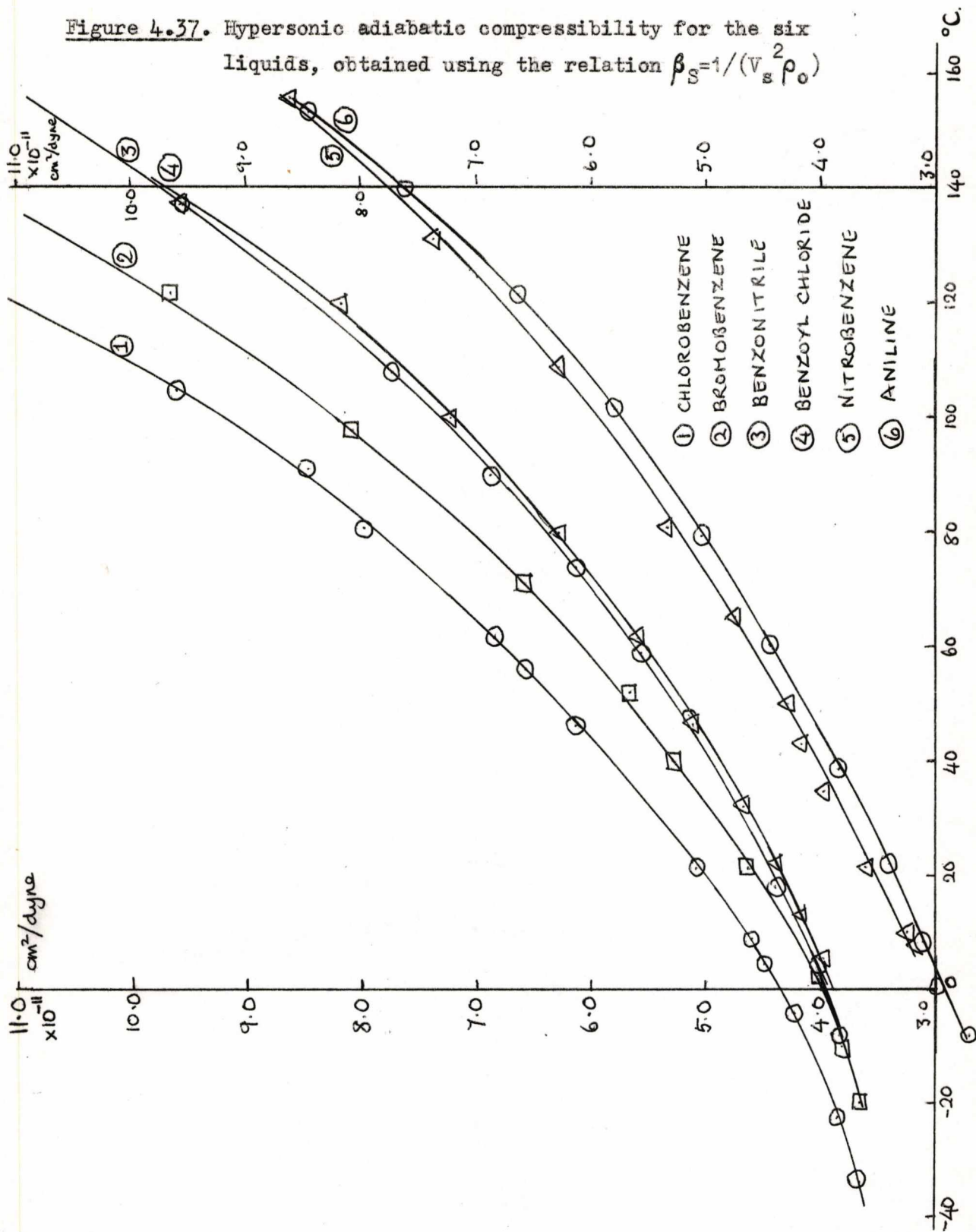


TABLE 4.9. TABULATED RESULTS AND DATA; WITH

A

COMPARABLE RESULTS FROM OTHER TECHNIQUES FOR ALL SIX LIQUIDS AT 20°C

LIQUID	RESULTS FROM STATIC SHEAR VISCOSITY DATA			DIELECTRIC RELAXATION		NUCLEAR MAGNETIC RESONANCE		NUCLEAR QUADRUPOLE RESONANCE		LIGHT-SCATTERING RESULTS 20°C			
	η cp.	τ_{η} sec.	$E_{a\eta}$ kcal/mole	$\tau_D/3$ sec.	E_{aD} kcal/mole	τ_d sec.	E_{ad} kcal/mole	τ_a sec.	E_{aq} kcal/mole	τ_{12s} sec.	E_{a12s} kcal/mole	τ_{2ts} sec.	E_{a2ts} kcal/mole
C ₆ H ₅ Cl	0.799 [52]	3.4×10^{-11}	2.92	0.4×10^{-11} [8]	2.3	0.4×10^{-11} [51]	2.3	0.3×10^{-11} [51]		0.92×10^{-11}	2.76		
C ₆ H ₅ Br	1.21 [41]	5.24×10^{-11}	2.79	0.6×10^{-11} [8]	2.65	0.49×10^{-11} [49]	2.55	0.5×10^{-11} [48]		1.20×10^{-11}	1.29	1.12×10^{-12}	4.04
C ₆ H ₅ NO ₂	2.03 [52]	8.52×10^{-11}	4.09	1.6×10^{-11} [8]				$>0.3 \times 10^{-11}$ [46]	3.2	3.75×10^{-11}	3.69	5.7×10^{-12}	2.45
C ₆ H ₅ NH ₂	4.40 [52]	16.7×10^{-11}	non-Arrh. (Fig 4.24)	0.68×10^{-11} [45]	4.48					2.31×10^{-11}	3.96		
C ₆ H ₅ CN	1.30 [52]	5.6×10^{-11}	3.42					1.0×10^{-11} [34]		1.97×10^{-11}	2.99		
C ₆ H ₅ COCl										3.8×10^{-11}	3.97		

B
TABLE 4.9 (continued). TABULATED RESULTS AND DATA, WITH
COMPARABLE RESULTS FROM OTHER TECHNIQUES FOR ALL SIX LIQUIDS AT 20°C.

LIQUID	LANDAU- PLACZEK RATIO $\gamma-1$	$\rho_u(\text{tot})$ at 20°C	$\rho_u(\text{anis})$ at 20°C	Hypersonic longitudinal viscosity at 20°C eq. (4.5b) cp	Ultrasonic longitudinal viscosity at 20°C eq. (4.5b) cp	MELTING POINT °C.	BOILING POINT °C.	DIPOLE MOMENT esu / cm ($\times 10^{-18}$)	MOLECULAR WEIGHT	AVERAGE VOLUME PER MOLECULE (\AA^3)	
										AT 20°C	AT MELTING POINT
C_6H_5Cl	$0.55 \pm .05$	0.59	0.857	91	176 [41]	-45	132	1.58 [56]	112.5	170	160
C_6H_5Br	$0.36 \pm .03$	0.59	0.857	94	177 [41]	-37	155.6	1.54 [56]	156.9	175	166
$C_6H_5NO_2$	$0.39 \pm .07$	0.75	0.857	117		5.7	210.8	3.98 [56]	123	170	168
$C_6H_5NH_2$			0.857	94.5		-6.2	184	1.53 [56]	93	154	151
C_6H_5CN	$0.37 \pm .03$	0.72	0.857	78		-13	190.7	4.39 [56]	103	171	166
C_6H_5COCl	$0.36 \pm .03$	0.94	0.96 \pm .02	68		-1	140.6	3.67	140.5	194	188

CHAPTER 5.Interpretation of results.Section 1. The isotropic spectrum.

The isotropic spectra of the individual liquids have been discussed in some detail in chapter 4, as the results were presented. Several features have emerged from all the results.

The frequency of hypersound changes with temperature in each case from about 3×10^9 Hz to 5×10^9 Hz. The velocity of hypersound changes linearly with temperature in all cases, except where there is additional evidence, from the dependence of the Brillouin linewidth on temperature, that a dispersion region is being traversed. There is evidence for a dispersion in aniline of about 5% centred at a frequency of about 6×10^9 Hz at $0-10^\circ\text{C}$. Results for nitrobenzene and benzonitrile are ambiguous, suggesting that there may be small dispersions of about 1% in these liquids in this frequency range, but the experimental accuracy of 1% is insufficient to establish this conclusively. To examine such dispersion regions, greater accuracy is required in measuring both the Brillouin splitting and the Brillouin linewidth. These last measurements are limited by the linewidths of the multimode lasers used in these experiments. It is important to know the temperature-dependence of the ultrasonic velocity and absorption coefficient to interpret the results.

For chlorobenzene and bromobenzene, values of the ultrasonic absorption coefficient over a range of temperatures were known from the literature (41). From these, values of the "bulk viscosity", defined using the relation

$$2\alpha_s = \frac{2\Gamma_s}{v_s} = \frac{\omega^2}{v_s^3 \rho} \left[\frac{4}{3} \eta + \zeta \right] \dots\dots\dots (5.1)$$

were calculated. (See equations (4.5), (4.5b)).

Here V_s is velocity of sound

α_s is sound absorption coefficient in cm^{-1}

Γ_B is Brillouin semi-linewidth.

$\frac{4}{3}\eta + b$ is "bulk viscosity".

Values of the "bulk viscosity" calculated using this equation from the hypersonic and ultrasonic results at 20°C , are given in Table 4.9, with values of the static shear viscosity.

The values of "bulk viscosity" are considerably larger than those of the static shear viscosity, for all the liquids. For chlorobenzene and bromobenzene, there is an appreciable difference between the "bulk viscosity" observed in hypersonic and ultrasonic frequency regions. This suggests that a dispersion region has occurred at a frequency lower than 3×10^9 Hz. The expected frequency region for such a dispersion has been calculated for chlorobenzene, and found to be about 1×10^9 Hz. For bromobenzene it would be somewhat lower. The temperature-dependence of the "bulk viscosity" change associated with this dispersion, suggests that the cause of the dispersion is a relaxing internal specific heat. In view of the similar molecular structure of the other liquids studied, it is to be expected that such a dispersion region would occur in all cases, at a frequency below 3×10^9 Hz.

The form of the spectrum in all cases may be accounted for by the Rayleigh line, two Lorentzian Brillouin lines, and antisymmetric terms due to absorption of the sound-waves, centred at the Brillouin frequency, any Mountain line present being weak and difficult to identify. It is very important to include the antisymmetric terms in analysing the

spectrum, particularly in searching for a Mountain line. They may cause the Rayleigh line to appear broadened, due to additional intensity in the centre of the spectrum.

The values of the Brillouin intensity, where these could be measured, were in agreement with the relation (see equation (2.22))

$$I_B \propto \rho_0^2 kT_0 \beta_S \dots\dots\dots(5.2)$$

where I_B is Brillouin intensity.

The values of the adiabatic compressibility at hypersonic frequencies are shown in figure 4.37 for all the liquids. They may be used to give an approximate comparison of the molecular environments and relative strengths of the intermolecular forces. Since there is no evidence for a dispersion of greater than 2% except in aniline at low temperatures, it may be assumed that the compressibility values are the same as at low frequencies.

The adiabatic compressibility is related to the radial distribution function by the equation

$$\beta_S \gamma = \frac{1}{kT_0} \lim_{q \rightarrow 0} \left[1 + \rho_0 \int (g(r) - 1) \exp(iq \cdot r) dr \right] \dots\dots (5.3)$$

from equation (1.6).

From figure 1.1, it may be seen that the variation with temperature of this integral is governed principally by the variation of the number of "holes" in the first "shell" of neighbours, or the average volume per molecule apart from that occupied by the molecule itself. This volume will be determined by the intermolecular forces at a given temperature, and will tend to be larger if the attractive forces opposing expansion

are weaker. Compression will be limited by the repulsive core of the intermolecular potential. The total intermolecular potential contains contributions due to Van der Waals dispersive forces, dipole-dipole interactions, dipole-induced dipole interactions, and so on. Values of the permanent dipole moment of the molecules are given in Table 4.9.

The relative strength of the intermolecular forces may be estimated approximately by a comparison of the melting and boiling points. (See Table 4.9). Chlorobenzene and bromobenzene are furthest from their melting points at room temperature, and have the highest compressibilities. They also have dipole moments which are smaller than those of the other liquids (with the exception of aniline). This factor clearly contributes to their low melting points and higher compressibility. The other liquids are less compressible and have higher melting and boiling points, consistent with the fact that their intermolecular forces are stronger. There may well be hydrogen-bonding in aniline, so that the molecules are bound close together and the compressibility is low.

This discussion illustrates the fact that dipole-dipole interactions and hydrogen bonding, if present, are important factors in determining the characteristics of a liquid, but these considerations are insufficient to explain, for example, why the compressibility of nitrobenzene is lower than that of benzonitrile.

Further evidence for hydrogen-bonding in aniline is given by the non-Arrhenius temperature-dependence of the static shear viscosity. It would seem reasonable that a liquid in which the spectrum of light scattered from shear-waves has been reported (31), must have strong non-central intermolecular forces. This will be further discussed in the third section.

Section 2. The anisotropic spectrum.

In chapter 2, the anisotropic spectrum has been discussed from the macroscopic and microscopic viewpoints. It has been shown that there are two possible causes of off-diagonal elements of the induced polarizability tensor of the medium. One is the intrinsic anisotropy of the individual molecules, and the other the shear stresses and deformations which exist even in an atomic liquid. The microscopic theory takes into account the anisotropic polarizability of individual molecules, whereas the shear stresses and deformations are considered more conveniently from a macroscopic viewpoint.

Considerable confusion has arisen in trying to relate these two viewpoints. Clearly an important question is: how is the existence of stress and deformation in the liquid related to the orientation of the molecules? Is it possible for a molecule to rotate without affecting the shear deformation of the surrounding liquid?

In answering this question, it is useful to consider the part played by molecular reorientation in shear viscous flow, since the mechanisms causing this are closely related to those causing shear stress and deformation. A useful contribution to this problem has been made by Curtis et al (8), who performed dielectric relaxation measurements on a number of molecules in different environments. They make the point that shear viscosity depends on both translation and rotation of the molecules, and show that for a nearly spherical molecule, a large increase in shear viscosity has little effect on the reorientation time of the molecule. Clearly in a liquid of such molecules, reorientation plays a relatively unimportant part in viscous flow. However, a large dipole-dipole inter-

action, which is strongly orientation-dependent, has a marked effect on the molecular reorientation time. A very non-spherical shape could have a similar effect, if the molecules were close enough together on average for rotation to be hindered. Clearly an important parameter in determining the importance of the molecular shape, is the average "free volume" per molecule, or that part of the average volume per molecule which is not occupied by the molecule itself. The repulsive core of the interatomic potential acts over a very short range, whereas the dipole-dipole interaction decreases with distance r , as r^{-3} . In the case of either being important, molecular rotation would play an important, or even dominant part in viscous flow.

Shear stresses, then, arise not only as a result of molecular reorientation, but as a result of distortion of the electron cloud of the molecules, due to the presence of their neighbours. It is therefore possible for a nearly spherical molecule to rotate "independently" and the presence of shear-waves to still be observed. However, the more non-spherical the molecule and non-central the intermolecular interactions, the more both shear stress and viscous flow will be dominated by the rotation of the molecules.

Values of the static shear viscosity may be used to derive reorientation times τ_η , using the Debye relation

$$\tau_\eta = \frac{4\pi a^3}{3} \frac{\eta}{kT_0} \dots\dots\dots (5.4)$$

This is the time appropriate to the $l=2$ Legendre component of the orientation correlation function, for the rotation of a macroscopic sphere of radius a in a medium of shear viscosity η . The values of $\frac{4}{3}\pi a^3$ used were the average volume per molecule at 20°C, and the results for τ_η are

therefore too large, since the "free volume" per molecule has been ignored. However the temperature-dependence of the logarithmic plot of this time gives a value of E_a (see equation (2.102)) which may be compared directly with values from other types of measurement. Such values of τ_n and E_{an} have been calculated from the static shear viscosity, where available in the literature, and included in Table 4.9.

In comparing values of τ and E_a derived from shear viscosity data, dielectric relaxation measurements, and light-scattering, it is important to consider the exact quantity that is being measured.

By dielectric relaxation, and other techniques which study the molecular motion via the permanent dipole moment of the molecule, times are obtained which characterize the reorientation of the molecule about a minor axis. In studying that part of the light-scattering spectrum which is due to molecular reorientation, if such a part may be separated, we observe the decay of fluctuations in the induced polarizability. The induced polarizability, although its principal direction is parallel to the direction of the permanent dipole moment for these molecules, (fig. 4.4) has strong components in the other two perpendicular directions. (Ref. (36)). Hence if reorientation is not equally probable about all molecular axes, a time for molecular reorientation derived from light-scattering may well be different from that derived from dielectric relaxation. In general, in view of the direction of the major axis for moment of inertia of these molecules, one would expect it to be shorter.

The polarizability of the molecules will be affected by any force which distorts the electron cloud, and its time-dependence by the decay of such forces, as well as by molecular reorientation. Hence the correlation times obtained from light-scattering are directly comparable with

those obtained using equation (5.4), since the mechanism of shear viscosity is also governed by all these factors. The close relation between shear stress and shear viscous flow has also been referred to in the above discussion. The static shear viscosity η is related to the shear modulus at infinite frequency μ_{∞} through the Maxwell relation

$$\mu_{\infty} \tau_{\mu} = \eta \quad \dots\dots\dots (5.5)$$

where τ_{μ} is the Maxwell relaxation time for the shear modulus.

The values of τ_{11s} from light-scattering all show an Arrhenius temperature-dependence, within the experimental error, and the values of τ_{η} calculated from equation (5.4), with the exception of aniline, show this temperature-dependence also. The times τ_{η} are larger than the times τ_{11s} in all cases, for reasons which have been discussed above. (p. 5.6, line 26). The values of E_{a11s} and $E_{a\eta}$ show agreement to about 10-15% for chlorobenzene, nitrobenzene and benzonitrile. Aniline shows non-Arrhenius viscosity behaviour, but there is agreement to the same order of accuracy at high temperatures for this liquid also. (See fig. 4.24). Bromobenzene is the only liquid where E_{a11s} and $E_{a\eta}$ are significantly different (by about 50%). There is no shear viscosity data for benzoyl chloride.

It appears then, that in chlorobenzene, nitrobenzene, benzonitrile and aniline (except at low temperatures) the narrow part of the anisotropic spectrum is characterized by a time which has the same temperature-dependence as the shear viscosity. This implies that the same molecular mechanism is involved in the decay of shear polarizability and in shear viscous flow. It remains to consider how these processes are related to molecular reorientation in these liquids.

The relations between the correlation times obtained from light-scattering, nuclear magnetic and quadrupole resonance, and dielectric relaxation, have already been discussed on pp. 4.7-9. This discussion may now be extended by considering the relations between the values of E_a obtained from the different methods. In the cases of nitrobenzene and aniline, the values of E_a obtained from molecular reorientation, the narrow part of the anisotropic spectrum of scattered light, and static shear viscosity data, show agreement to within about 20%. (The nuclear magnetic quadrupole value for nitrobenzene has an error of about 30%). These are highly polar molecules with strong non-central interactions, and as indicated by their low compressibility, they do not have a large free volume in which to rotate. It therefore appears that the molecules of these liquids are not able to rotate independently of their neighbours, and the viscosity is dominated by molecular reorientation. These are both liquids in which the central part of the spectrum has been attributed to scattering from the shear waves of Rytov's theory. (31) If this interpretation is correct, the confusion between microscopic and macroscopic approaches is resolved if one asserts that the shear waves of Rytov's theory, in these liquids, decay principally by molecular reorientation, so that the central region of the spectrum is the sum of two curves of the same width. The first is due to the statistical variations in orientation of different individual molecules in the liquid, and the second that predicted by Rytov's theory and shown in figure 2.5.

We have no measurements of the temperature-variation of the intensity of the anisotropic spectrum for aniline, but that observed for nitrobenzene is in agreement with the above assertion. (Figure 4.43).

The intensity contained in the narrow Lorentzian decreases by a factor of $1/3$ or $1/2$ in the temperature range from $0-100^{\circ}\text{C}$. If equation (2.104) is used to calculate the expected decrease in intensity of the spectrum due to shear waves in this temperature range, the result is a decrease by a factor of 15. The experimental results can be explained if at room temperature about half the intensity in the narrow Lorentzian is due to scattering from shear waves.

On these grounds it might be expected that the anisotropic spectrum for nitrobenzene should be close to a single Lorentzian, as is in fact the case. Aniline, however, in which the spectrum due to shear waves has also been reported, has a spectrum of complex shape, in which the narrow Lorentzian contains only 50-60% of the total anisotropic intensity. However, if there is hydrogen-bonding in this liquid, additional complexity of the spectrum is not surprising. Benzonitrile is more directly comparable to nitrobenzene, since this too is highly polar and has a weak second Lorentzian. The intensity of the anisotropic spectrum of benzonitrile decreases by about 10% over the entire temperature range, and it is not clear which Lorentzian, if either, is associated with this intensity change. (Figure 4.28).

Those theories of the anisotropic spectrum which include only the anisotropy of individual molecules, and ignore correlations in orientation between molecules, predict that the intensity of the anisotropic spectrum should be dependent on the temperature only through the density. (p.2.34) The intensity should thus remain approximately constant with temperature, decreasing by about 10% over the entire range. This behaviour has been observed for benzonitrile. The anisotropic intensities of chlorobenzene, bromobenzene and benzoyl chloride are also approximately independent of

temperature. (Figures 4.7, 4.14, 4.33). It is clear that the difference between the spectra of nitrobenzene, and benzonitrile and benzoyl chloride, cannot be explained in terms of the dipole-dipole interactions between the molecules of the liquids, since the permanent dipole moments of the three molecules are very similar. Also this agreement with the predictions of the "self-scattering" theory does not imply that the assumptions of this theory are justified. Nothing has been said about the temperature-dependence of the intensity if the terms describing intermolecular correlation in orientation are included. We have seen also (pp 5.5-6) that shear stresses may well depend on factors other than orientation of the molecules.

The question may then be asked: may the spectrum of light scattered from shear waves be distinguished in the anisotropic spectra of benzonitrile, chlorobenzene, bromobenzene and benzoyl chloride? There are two possible answers to this question consistent with the experimental temperature-dependence of the anisotropic spectral intensities.

- 1). The value of X (defined by equation (2.89)) is so small that the intensity scattered by shear waves is negligible compared with that scattered by individual molecules.
- 2). The value of E_a for the decay of shear waves is so small that equation (2.104) predicts an intensity approximately independent of temperature. This would occur if E_a is much less than 0.5 kcal/mole, (or the value of RT_0 at room temperature). Such a low value of E_a would imply a short time for the decay process to occur. Hence shear waves would be responsible for the wings of the spectrum.

The values of E_a derived from methods measuring the reorientation of

single molecules (dielectric relaxation, nmr, nqr), from static shear viscosity values, and from the narrow Lorentzian of the anisotropic spectrum of scattered light, may be compared for chlorobenzene and bromobenzene.

In the case of chlorobenzene, $E_{a\eta}$ and E_{a11s} agree to within 10%, whereas E_{aD} and E_{ad} have a smaller value. This indicates that for this liquid, shear viscous flow and the decay of molecular polarizability fluctuations are closely related, and take place by a more complex mechanism than molecular reorientation alone. Bromobenzene shows close agreement (to about 10%) between $E_{a\eta}$, E_{aD} and E_{ad} , indicating that molecular reorientation is intimately connected with viscous flow. However, E_{a11s} is smaller than these values by about 50%. It is possible that in this liquid, the molecules are so non-spherical that reorientation about a major axis is preferred to that about a minor axis. Polarizability fluctuations may decay by a molecular process involving rotation of the molecules about their major axes, since the induced polarizability along all molecular axes is comparable in magnitude (see p 5.14) (This argument would not apply to the same extent to nitrobenzene and aniline, in view of their complex shape.) If relative reorientation of the molecules is difficult, it might be expected that shear-waves were fairly strong in this liquid, and hence responsible for the broader Lorentzian in the light-scattering spectrum.

Hence it appears that the narrow component of the anisotropic spectrum is principally caused by the statistical variations in orientations of individual molecules. Such fluctuations decay by a process closely related to that of viscous flow. In the liquids studied in this work, the decay is caused largely, but not exclusively, by molecular reorientation.

Shear-waves are observable through the change in induced polarizability due to distortion of the electron cloud of the molecules. The only effect of

dipole-dipole interactions or molecular shape factors upon them is to influence their mode of decay. Since the dispersive forces leading to distortion of the electron cloud are short-range, it would appear reasonable that the time for shear-wave decay is governed by the time for the molecules to move apart. If this time is shorter than the time for molecular reorientation, then shear waves may contribute to the wings of the spectrum. The experimental results are inconclusive on this point.

Nitrobenzene, and possibly aniline, may not be described in this way, since shear-waves in these liquids decay by molecular reorientation, and so contribute to the central region of the spectrum. There is no obvious reason why these liquids should differ from benzonitrile, for example. An important parameter is clearly the "free volume" per molecule which is available for reorientation. The second Lorentzian in nitrobenzene may be due to molecular vibration.

It is possible that the theory of Rytov, describing the effects of the dependence of dielectric constant on shear deformation, may describe part of the spectrum in either its original (p 2.39) or its modified (p 2.44) form. In the case of nitrobenzene, Rytov's τ_1 would be equated with the time for molecular reorientation. (Note that this is the Maxwell relaxation time for the shear modulus). In this case his theory would hold in its original form. If, however, the shear-waves decay by a mechanism other than reorientation, it is necessary to introduce the dependence of dielectric constant on low-frequency shear deformation by means of Rytov's modified theory. (Assumptions given by equations (2.98), (2.108)). In such a case, Rytov's τ_2 would be equated with the time for molecular reorientation. The spectrum due to the statistical fluctuations in orientation of individual molecules, would

be added to that predicted by Rytov. The magnitude of the spectrum due to shear waves compared with that due to the anisotropy of individual molecules, depends on the effect of the local field on the polarizability of the molecules.

Section 3. General discussion.

The effect of the local field on the anisotropy of the polarizability may be calculated, by comparing values of Δ^2 obtained using equation (2.3) for the liquid, with those obtained using equation (2.5) for the free molecules, where values of $\alpha_1, \alpha_2, \alpha_3$ are available in the literature. Kielich (36) gives values for the induced polarizability along the three principal molecular axes, for benzene and nitrobenzene. Results for the other liquids do not seem to be readily available. In table 5.1, values of the anisotropy calculated using these equations, are presented.

TABLE 5.1.

Liquid	Polarizabilities (10^{24} cm^3)			Δ^2 free molecule eq(2.5)	Δ^2 from ρ_u (tot) for liquid eq(2.3)	
	α_1	α_2	α_3			
C_6H_6	12.31	12.31	6.35	.037		
$\text{C}_6\text{H}_5\text{NO}_2$	17.16	14.19	7.41	.0499	.057	(20°C)
					.049	(156°C)
$\text{C}_6\text{H}_5\text{CN}$.038	(0°C)
					.045	(160°C)
$\text{C}_6\text{H}_5\text{Br}$.030	(20°C)
					.034	(140°C)
$\text{C}_6\text{H}_5\text{Cl}$.027	(20°C)
					.031	(120°C)

The anisotropy for the benzene molecule must give a lower limit for the anisotropy of the other molecules. These results then show that in general, the effect of the local field in the liquid is to reduce the anisotropy of the polarizability, and as the temperature is raised, and the molecules are on average further apart and may rotate more independently, the anisotropy calculated using the depolarization ratio increases. In nitrobenzene, however, the local field in the liquid enhances the molecular anisotropy, and as the temperature is raised, the anisotropy decreases to a value close to that for a free molecule. This adds to the evidence for strong correlations in orientation of neighbouring molecules in nitrobenzene, and to the evidence that the molecular motion in nitrobenzene is rather different in character from that in the other benzene derivatives in Table 5.1.

The very high value of the depolarization ratio in benzoyl chloride remains unexplained. If the polarizability tensor had an antisymmetric component (equation (2.6)), then the depolarization ratio of the anisotropic spectrum would be greater than the limiting value $6/7$. (See p. 2.7). However, since a liquid is an isotropic medium, and the frequency change in scattering is low, being caused by molecular motions which are very slow compared with the frequency of the light, the dielectric constant tensor must be symmetric. (Ref. (60), 493). The only possible exception to this would be if the frequency of the incident light were close to a frequency region where benzoyl chloride is strongly absorbing. In view of the high level of photochemical activity in this liquid, this explanation is a possibility. The introduction of a field-dependent term into the polarizability equation (2.6) would not increase the limiting

depolarization ratio above 6/7. (65), (66).

It has been suggested that the width of the narrow Lorentzian in the anisotropic spectrum of aniline and nitrobenzene, corresponds to the Maxwell relaxation time of the shear modulus. This width may therefore be compared directly with the frequency of dispersion regions observed by means of the isotropic spectrum, at the appropriate temperature. The semi-width of the anisotropic spectrum of aniline at 15°C is 6×10^9 Hz, which is the frequency at which the absorption of hypersound is a maximum at approximately this temperature. (Figures 4.25, 4.26) Hence the dispersion in aniline may be attributed to structural relaxation. Further evidence for this interpretation is the rapid decrease in Brillouin semi-line width at temperatures above the absorption peak. Assuming that the relaxation times for shear and compressional moduli vary with temperature in the same way, the relaxation time at 20°C is 2.3×10^{-11} sec. (From figure 4.24).

A similar comparison may be made for nitrobenzene. The half-width of the narrow Lorentzian is the same as the frequency of hypersound at about 35°C, its value being 5×10^9 Hz. This is also the temperature-region at which the Brillouin line width is a maximum. Hence it appears very likely that there is a small structural dispersion in nitrobenzene in this region. The Maxwell relaxation time at 20°C is 3.7×10^{-11} sec.

Since the mode of shear wave decay for the other liquids has not been established, such a comparison may not be made. However, the values of τ_{1s} are a lower limit to the Maxwell relaxation time. Hence structural relaxation in these liquids occurs at or above the highest frequencies attained in this work.

Section 4. Survey of field.

There are a number of questions which have arisen in the course of this work, which may lead to interesting fields of future research.

In the study of hypersound, the temperature-variation method is valuable in that structural dispersions may be brought within the frequency range of the light-scattering technique. However, thermal relaxation times vary only slowly with temperature, and it is clearly desirable to use both variation of temperature and of frequency to scan the dispersion regions more thoroughly. If the frequency of phonons studied at a scattering angle of 90° is 5×10^9 Hz, that at 5° , in the absence of dispersion, is 3×10^8 Hz, that at 2° is 1.2×10^8 Hz, while that at 175° is 7×10^9 Hz. (Eq. (2.26)). The frequency of phonons studied could only be increased above this upper limit by use of incident radiation of a shorter wavelength. The measurement of forward scattered light at very small scattering angles represents considerable experimental difficulties, but a lower limit of 5° , corresponding to 3×10^8 Hz, could reasonably be attained. It is clearly desirable that accurate ultrasonic results should be available for the liquids to be studied, and that the entire frequency range between the maximum for the ultrasonic method and the maximum for the light-scattering technique be spanned. Independent variation of temperature and frequency would give a more complete picture of the various processes taking place in the liquids.

Measurements of the Brillouin linewidths have been severely limited in accuracy by the use of multimode lasers. This difficulty should be overcome as single-mode lasers of comparable power become available. This would represent a considerable advance in the interpretation of the entire isotropic spectrum, since antisymmetric Brillouin components and weak

Mountain lines would be more easy to distinguish.

The dependence on temperature of the sound-velocity and absorption coefficient at low and high frequencies in the absence of dispersion is of itself an interesting study, since even the linear temperature-dependence of $V_{s,0}$ has not been adequately explained theoretically.

In the study of the anisotropic spectrum, the use of single-mode lasers would also represent a significant advance, since then the central "dip" due to shear-waves, if present, should be readily observable. Apart from this observation of the "dip", shear-waves would be very difficult to identify, unless they represent a significant proportion of the central region of the spectrum. The temperature-dependence of the anisotropic intensity may not be adequate to identify them if the time for them to decay is very short, and hence the energy to do so low.

The Fabry-Perot is clearly not a suitable instrument for the study of the wings of the line, and measurements should be taken in conjunction with those from a monochromator, which allows a wide range of frequencies to be studied, but has poor resolution for the measurement of the central region of the anisotropic spectrum.

The environment of the molecules may be changed in various ways to facilitate interpretation of different parts of the spectrum. A mixture of liquids of high and low polarity, or of different-shaped molecules, may be used to study the effects of intermolecular correlation in orientation. Optically isotropic molecules may be used to study the spectrum due to shear waves only. Alternatively the sample could be placed in a static or alternating electric field so that the effect of imposed orientation of the molecules could be seen, or dielectric relaxation measure-

ments could be taken at the same time. Such measurements might provide some suggestion as to the cause of the observed anomalies in the effect of the liquid local field in nitrobenzene (and aniline), since these do not depend on permanent dipole moment alone.

Measurements at different intensities of incident light would indicate whether hyperpolarizability is of importance in the light scattering from any of these liquids. Such measurements, particularly in conjunction with monochromator measurements of the entire spectrum, might enable the high depolarization ratio of liquids like benzoyl chloride to be explained.

Clearly it is important that a thorough study be undertaken of pure liquids and binary mixtures, using small molecules of known properties and shape, so that the results of such measurements may be interpreted unambiguously. Besides this, however, the light-scattering technique is applicable to a number of other fields. A certain amount of work has been done in the following fields: critical point phenomena (67,68,69), the study of liquid crystals (70) and liquid surfaces (71), the study of glasses and phase transitions (72), the scattering of light from biological macromolecules (73), and the study of turbulent flow in liquids and gases, (74). Provided, then, that the results of light-scattering experiments in liquids may be unambiguously interpreted, the technique holds considerable promise for development in a number of fields.

List of references.

1. Frenkel J., 1946, "Kinetic Theory of Liquids", Oxford University Press.
2. Egelstaff P.A., and Schofield P., 1965, Contemp.Phys., 6, 274.
3. Egelstaff P.A. and Schofield P., 1965, Contemp.Phys. 6, 453.
4. Egelstaff P.A., 1965, Brit.J.Appl.Phys., 16, 1219.
5. Egelstaff P.A., "An introduction to the liquid state." Academic Press, 1967.
6. Van Hove L., 1954, Phys Rev. 95, 249.
7. Cummins H.Z., Knable N., Yeh Y., 1964, Phys.Rev.Lett., 12, 150.
8. Curtis, A.J., McGeer, P.L., Rathmann G.B., Smyth C.P., 1952, J. Am. Chem. Soc. 74, 644.
9. Bommél, H.E., Dransfield K., 1960, Phys. Rev. 117, 1245.
10. Pinkerton, J.M.M., 1949, Proc.Phys.Soc. London B62, 129.
11. Herzfeld K.F., Litovitz T.A. "Absorption and Dispersion of Ultrasonic Waves", Academic Press, 1959.
12. Kono R., McDuffie G.E., Litovitz T.A., 1966, J.Chem.Phys., 44, 965.
13. Montrose C.J., Litovitz T.A., Symposium on neutron inelastic scattering, Copenhagen, 20-25 May, 1968.
14. Landau L.D., Lifshitz E.M., "Statistical Physics", Pergamon Press, 1959.
15. Einstein A., 1910, Ann.Physik, 33, 1275.
16. Montrose C.J., Solovyev V.A., Litovitz T.A., 1968, J.Acoust.Soc.Am., 43, 117.
17. Coumou D.J., Mackor E.L., Hijmans J., 1964, Trans.Farad.Soc., 60, 1539, 2244.
18. Fabelinskii I.L., 1968, "Molecular Scattering of Light", (New York, Plenum Press)
19. Landau L.D., Lifshitz T.A., "Fluid Mechanics", Pergamon Press, 1959.
20. Mountain R.D., 1966, J.Res.Natl.Bur.Std., 70A, 207.
21. Cummins H.Z., Gammon R.W., 1966, J.Chem.Phys., 44, 2785.
22. Gornall W.S., Stegeman G.I.A., Stoicheff B.P., Stolen R.H., Volterra V., 1966, Phys.Rev.Lett., 17, 297.
23. Knaap H.F.P., Gornall W.S., Stoicheff B.P., 1968, Phys. Rev., 166, 139.
24. Rank D.H., Kiess E.M., Fink U., 1966, J.Opt.Soc.Am., 56, 196.
25. Rank D.H., McKelvey J.P., 1949, J.Opt.Soc.Am., 39, 762.
26. Zwanzig R., 1965, J.Chem.Phys., 43, 714.

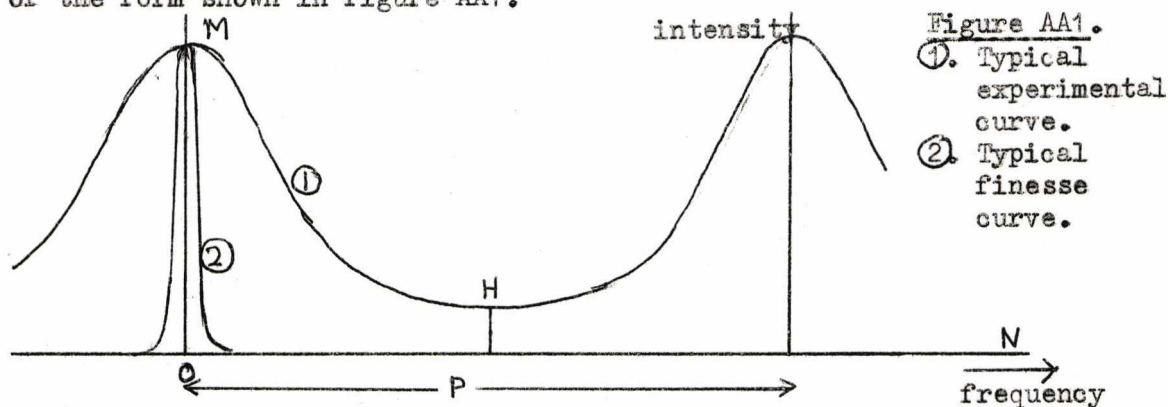
27. Pinnow D.A., Candau S.J., Litovitz T.A., ~~to be published.~~
1968, *J. Chem. Phys.*, 49, 347.
28. Pecora R., Steele J., 1965, *J. Chem. Phys.*, 42, 1872.
29. Leontovich M.A., 1941, *Izv. Akad. Nauk. SSSR Ser. Fiz.* 5, 148.
1941, *J. Phys. (USSR)*, 4, 499.
30. Rytov S.M., 1958, *Sov. Phys. J.E.T.P.*, 6, 130, 401, 513.
31. Stegemann G.I.A., Stoicheff B.P., 1968, *Phys. Rev. Lett.*, 21, 202.
32. Starunov V.S., 1963, *Opt. i Spektroskopiya* 18, 300.
1963, *Opt. and Spectry.* 18, 165.
33. Zaitsev G.I., Starunov V.S., 1967, *Opt. and Spectry.*, 22, 221.
34. Szöke S., Courtens E., Ben-Reuven A., 1967, *Chem. Phys. Lett.* 1, 87.
35. Bhatia A.B., Tong E., 1968, *Phys. Rev.* 173, 231.
36. Kielich S., 1967, *J. Chem. Phys.* 46, 4090.
37. Starunov V.S., Tiganov E.V., Fabelinskii I.L., 1967, *Zh. E.T.F.*, 5, 317.
38. Kielich S., 1958, *Bull. Acad. Polon. Sci. Sér. Sci. Math. Astron. Phys.*, 6, 215.
39. Leidecker H.W., LaMacchia J.T., 1968, *J. Acoust. Soc. Am.*, 43, 143.
40. Timmermans, "Physico-Chemical Constants of Pure Organic Compounds"
(Brussels: Elsevier), 1950.
41. Nozdrev V.F., "The use of ultrasonics in molecular physics", Pergamon Press, 1965.
42. Mason W.P., "Physical Acoustics" vol. III, Academic Press 1965.
43. Craddock H.C., Jackson D.A., Powles J.G., 1968, *Molec. Phys.*, 14, 373.
44. Rouch J., Locket R., Rousset A., 1967. *C. r. hebd. Séanc. Acad. Sci. Paris*,
265, 253.
45. Smyth C.P., Grubb E.L., 1961, *J. Am. Chem. Soc.*, 83, 4879.
46. Moniz W.B., Gutowsky H.S., 1963, *J. Chem. Phys.* 38, 1155.
47. Powles J.G., Figgins R., 1967, *Molec. Phys.*, 13, 253.
48. Powles J.G., Rhodes M., Strange J.H., 1966, *Molec. Phys.*, 11, 515.
49. Powles J.G., Figgins R., 1966, *Molec. Phys.*, 10, 155.
50. Pinnow D.A., Candau S.J., LaMacchia J.T., Litovitz T.A., 1968, *J. Acoust. Soc. Am.*, 43, 131.
51. Figgins R., Rhodes M., to be published in *Molec. Phys.*
52. Chemical Rubber Co. Handbook of Chem. and Phys. 48th ed. 1967-1968.

53. Cabannes J., Roussët A., 1937, Tables Annuelles de Constantes et Données Numériques, "Diffusion de la Lumière".
54. Born M., Wolf E., 1964, "Principles of Optics", (New York, Macmillan), §§9.4ff.
55. Glasstone, "Textbook of Physical Chemistry", Macmillan, 1955.
56. Gould E.S., "Mechanism and Structure in Organic Chemistry", New York, 1960.
57. Sharrah, 1960, J.Chem.Phys., 32, 241.
58. Craig P.P., Sutin N., 1963, Phys. Rev. Lett., 11, 460.
59. Rayleigh, 1881, Phil.Mag., 12, 81
60. Landau L.D., Lifshitz T.A., "Electrodynamics of Continuous Media", Pergamon Press, 1959.
61. Ben-Reuven A., Gershon N.D., to be published.
62. Nyquist H., 1927, Phys.Rev., 29, 614; 1928, Phys.Rev., 32, 110.
63. Rytov S.M., 1967, Sov.Phys.J.E.T.P., 27, 147.
64. Simic-Glavaski B., to be published.
65. Buckingham A.D., Stephen M.J., 1957, Trans.Farad.Soc., 53, 884.
66. Cyvin, S.J., Rauch J.E., Decius J.C., 1965, J.Chem.Phys., 43, 4083.
67. Alpert, S.S., Yeh Y., Lipworth E., 1965, Phys.Rev.Lett., 14, 486; 1967, Phys.Rev.Lett. 57, 1164.
68. Ford, N.C.Jr., Benedek G.B., 1965, Phys.Rev.Lett. 15, 649.
69. Kolpakov, Yu.D., Skripov V.P., 1965, Opt. and Spectry., 19, 342.
70. de Gennes, 1968, Comptes Rendues Acad.Sci. B 266, 15.
71. Katyl, R.H., Ingard K.U., 1967, Phys.Rev.Lett., 19, 64.
72. Peticolas, Stegemann, Stoicheff, 1967, Phys.Rev.Lett., 18, 1130.
73. Dubin S.B., Lunacek J.H., Benedek G.B., 1967, Proc. Nat.Acad.Sci., 57, 1164.
74. Pike E.R., Jackson D.A., 1968, J.Sci.Instr. 1, 727.
75. Craddock H.C., Jackson D.A., 1968, Brit.J.Appl.Phys. (J.Phys.D), ser 2, vol.1., 1575.
76. Akhmanov S.A., Krindach D.P., Sukhorukov A.P., Khocklov R.V., 1967, Zh.Eksper.Teór.Fiz.Pis'ma, 6, 509.
77. Tseiderberg N.V., 1965, "Thermal Conductivity of Gases and Liquids", (London:Edward Arnold), pp.199 ff.
78. Gordon J.P., Leite R.C.C., Moore R.S., Porto S.P.S., Whinnery J.R., 1965, J.Appl.Phys., 36, 3.

Appendix A. Computational Analysis of Spectra.

The programs to be described were written in Algol for use on the University's Elliot 803 and 4130 computers.

There are two effects to be allowed for in the derivation of the true anisotropic spectrum from the curve obtained from the Fabry-Perot interferometer. The first is the instrumental broadening of the spectrum, and the second the effect of overlap of successive orders of the Fabry-Perot. The experimental curve before these corrections have been made is of the form shown in figure AA1.



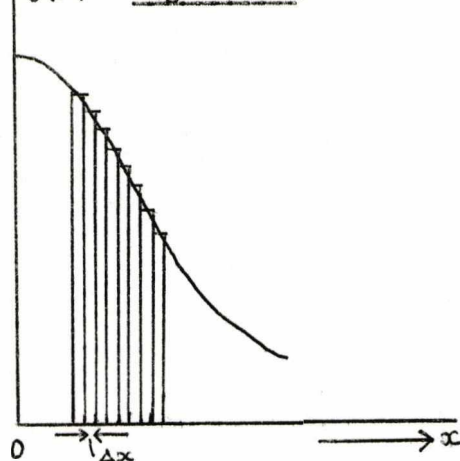
N is the noise-level, and P the distance between successive peaks, given in cm^{-1} by $1/2t$, where t is the width of the Fabry-Perot spacer. A finesse curve of typical shape and width is shown for comparison.

The first program is for the numerical deconvolution of the experimental curve with the finesse curve, which is assumed to be Lorentzian. As has been discussed in chapter 3, if very small spacers are used (less than 1 mm) the assumption of Lorentzian finesse shape is valid. If slightly larger spacers are used, the linewidths obtained making this assumption may be approximately corrected using the results of (39), and the observed finesse shape. Otherwise the program could be modified by using a non-Lorentzian finesse shape. The second program is to allow for the effects of overlap of successive orders.

Program I. Deconvolution of experimental data with Lorentzian.

The basic procedure for numerical convolution of an assumed true lineshape with a finesse curve is as follows. The true curve, $B(x)$, is first represented digitally, as a series of intensities $B'(x')$ at successive values of x , Δx apart, choosing Δx to be as small as is practicable. It is then assumed that the area under the curve is made up of the sum of

$B(x)$ Figure AA2.



the areas of all the rectangles, heights $B'(x')$, width Δx . (See figure AA2).

The effect of the finesse broadening on an individual rectangle, will be to replace it by a curve of the same area (or one reduced by a constant factor), centred at the same point, but having the shape and width of the finesse curve $F(x)$. Hence the convoluted curve, $S(x')$, may be found by summing the contributions to the intensity at each point x' from the convoluted curves of all the neighbouring rectangles.

It is not possible to perform this procedure in reverse, i.e., to find $B(x)$ given $S(x)$ and $F(x)$. Hence it is necessary to assume values of $B'(x')$, calculate $S(x')$, and compare the result with the experimental values $E(x')$. If the fit is not good, the assumed values of $B'(x')$ must be corrected. In this program, the experimental curve itself is used as a first approximation to $B(x)$. In the calculation, terms from the individual Lorentzians are included down to 0.2% of the experimental intensity at $x=0$. When the values of $S(x')$ have been calculated, the values of $B'(x')$ are corrected proportionally, being replaced by $B'(x') \cdot E(x') / S(x')$, so that the correction becomes successively smaller. This calculation is

repeated until $E(x')$ and $S(x')$ differ by only 0.2% of $E(0)$ for all values of x' . (This accuracy was selected because it was the experimental accuracy for measurement of $E(x')$.) The program takes into account, when the Lorentzians are being calculated, the reflection of the curve about every point M and H. (Fig. AA1).

In this program, the interorder spacing, P , was defined to be 100 units, and Δx had the value 2 units, so that 26 values of $B'(x')$ are calculated, between and including those at M and H.

The program was found to give satisfactory results except when the gradient of the experimental curve is too steep, as may occur for very sharp peaks. In this case a value of $B'(x')$ may be overestimated, and the next one underestimated, and the sum of the components due to the two still give a good fit to $E(x')$. This may occur at any part of the curve, but it is not serious except in the region of a sharp peak, since deviations of $B(x)$ from a smooth curve are small unless the gradient is large. In this work, since results from several Fabry-Perot spacers were used for each liquid, the whole curve for the smallest spacer could be determined quite easily. If a single sharp peak were being analysed, then the value of Δx must be reduced. These considerations show the value of recording the spectra in digital form.

The use of this program then enabled the deconvolution of the experimental curve with the finesse curve without any assumption about the mathematical form of the true anisotropic lineshape.

Program II. Correction of experimental results for the effects of overlap of successive Fabry-Perot orders.

If the true anisotropic spectrum is again $B(x)$, then the observed curve obtained after resolution by the Fabry-Perot, $I(x)$, is given by

$$I(x) = B(x) + \sum_{n=1}^{\infty} [B(nP + x) + B(nP - x)] \quad \dots\dots\dots(AA1)$$

The number of terms in the series that must be considered in allowing for the overlap depends on the rate of decrease of the intensity in the wings. This is an unknown quantity, and to derive the lineshape computationally, some assumption must be made about the mathematical form of $B(x)$. This program derives the basic lineshape assuming a sum of two Lorentzians, or the sum of a single Lorentzian and a constant background intensity in the case where the broader Lorentzian cannot be resolved. The widths of the two Lorentzians are guessed at the outset, the narrow one reasonably accurately, and fed into the computer as data, together with guessed values of a step-length suitable for the adjustment of each. These widths will then be adjusted by the computer to give a best least-squares fit to the experimental data.

As in program I, the experimental curve is fed in in digital form. The interorder spacing, P , was assumed to be 10 units, and Δx 0.5 units, so that 11 data values are used, between and including M and H . (See figs. AA1, AA2).

The program is comprised of three procedures. The first, procedure "Curve", is given the width and height of one Lorentzian, and calculates from these the sum given in equation (AA1) for one Lorentzian, at the values of x' at which the experimental intensity has been measured. It takes into account terms down to 0.01% of the peak height. This high accuracy was found to be necessary from tests on curves with known parameters.

The second, procedure "Function", performs the procedure "Curve" for each of the two widths given as data, and peak heights for the two

Lorentzians of unity. It then uses the values of $I(x')$ at two points, M and H, to calculate the correct peak heights needed to fit the experimental curve at these two points. It normalises the values of $I(x')$ to agree with these peak heights, and then evaluates the mean-square deviation of the sum of the two curves $I(x')$ from the experimental data.*

The third procedure is a standard procedure "Simplex", which adjusts the widths of the two Lorentzians, T_1 , T_2 , and minimizes the mean-square deviation.

If, in the process of the adjustment, the width of one of the Lorentzians becomes greater than 10 units, or the interorder spacing, then procedure "Curve" sets the intensity at all values of x to a constant value, the rest of the program operates as before, and the results are printed out as a single Lorentzian plus a constant.

If it is suspected that there is dust in the sample, or extraneous scattering at the incident frequency, the experimental value of the intensity at M may be unreliable. An additional parameter may then be introduced, through which the program is instructed to ignore the first reading from the point of view of calculation and comparison. It then uses the second intensity value as its reference point in procedure "Function", or in very contaminated samples the first two intensity values may be ignored.

The results output from the program then give the peak heights, A, B, of the two Lorentzians, and their widths T_1, T_2 . The overlapped curve is also given for comparison with the experimental, and the true curve

* * * * *

*It is possible to guess the height values also, but this greatly lengthens the time needed to run the program.

at values of x up to 30 units.

This program was extensively tested using curves of known parameters. The tests had the following results.

The width of the narrow Lorentzian could be measured to an accuracy of 5%. This was so for semi-widths down to about 0.3 units, even if the first experimental point was ignored, or the second experimental point was inaccurate to 5% of the peak height. (The gradient of the curve in this region was sometimes steep enough to cause large errors on this point.) Unless the narrow Lorentzian was broader than about 4 units (full-width), ignoring the first two points increased the error considerably. Hence experimental values of T_1 were reliable to 5%, except where the sample became very contaminated.

The accuracy of the parameters of the broader Lorentzian depended on the height and width of the curve. If the ratio of the peak-heights of broad and narrow Lorentzian was greater than about 0.1, the parameters could all be measured to about 5%. For ratios of less than 0.1, which often occurred experimentally, large errors were introduced in the measurement of T_2 , particularly as this approached 10 units.

The accuracy of the relative area of the curves depended on the accuracy of the individual parameters, and was therefore least when the curves were well-resolved.

Small random errors did not affect the analysis, but a systematic error on the noise level of 3% peak height, caused a 10-20% error in T_2 .

In practice, enough curves were taken for each liquid, to enable the effects of contamination and the other errors mentioned above, to be detected, and allowance for them to be made.

Appendix B. Thermal Defocussing in Liquids and Solids.

It was observed that in some liquids, the laser beam could not be focussed to a single coherence area, but was "defocussed" by the liquid, which caused the beam to diverge. The beam, when thrown onto a screen, exhibited circular interference fringes, which increased in diameter over a period of seconds, attaining an equilibrium size. In some liquids the fringes then became vertically flattened.

Polaroid and partially exposed photographic film were used as beam attenuators in the light-scattering experiments. It was found that if the laser beam was focussed onto them or they were close to the focal point, and if, in the case of polaroid, the angle was such that a large proportion of the laser light was absorbed in the polaroid, the attenuators were melted. The "liquid lens" formed showed similar time-dependent interference fringes to those described above for liquids. The melting caused permanent damage to the attenuators, which could be seen with the naked eye.

A short study was undertaken of these effects, the results of which are given in ref.(75).

The effects were intensity-dependent, and are attributed to a field-dependent term in the refractive index, which is not one inherent in the material but a term due to the local absorption of power by the medium.

The refractive index may then be written

$$n = n_0 + n_2 |E^2| \quad (\text{AB1})$$

where n_0 is field-independent refractive index. The absorption of power gives rise to a local temperature-gradient, and hence non-linear refraction. Both of these will be time-dependent, until an equilibrium temperature-gradient is reached. This will occur when the power lost due to thermal conduction is equal to that absorbed. If n_2 is less than zero the beam

will be "defocussed". The interference effects are due to aberrations in the resulting "lens", (See ref. (54)), and in a liquid convection currents may cause vertical asymmetry of the pattern if the temperature gradient is high enough.

The absorption coefficients for these liquids were so low ($\sim 10^{-3}$ - 10^{-4} cm^{-1}), that they could not be measured using standard equipment (Unicam SP 600 series 2 spectrophotometer). A formula for evaluating the defocussing, which applies in the case where the radius of the cell is large and boundary effects may be neglected, is given by Akhmanov et al. (76).

$$\theta = \theta_0 + \frac{(\partial n / \partial T) P_0}{\pi n_0 a_0 K} \left[1 - \exp(-\delta l) \right] \dots \dots \dots \text{(AB2)}$$

where $\partial n / \partial T$ is the change in refractive index with temperature (degK^{-1}), P_0 the incident power (W), a_0 the radius of the beam at entry to the cell, (cm), K the thermal conductivity ($\text{W cm}^{-1} \text{degK}^{-1}$), δ the absorption coefficient (cm^{-1}), l the path length of light in the liquid (cm), θ the divergence (rad) (= pattern radius divided by distance from focus to screen) and θ_0 is the original divergence. Akhmanov et al obtained agreement to within 20% between this formula and experiment in the limit of high absorption ($\delta l \rightarrow \infty$).

The above formula was tested under the conditions of low absorption, beam divergence and small cell radius pertaining in our experiments, and it was found that values of δ were predicted which were of the correct order of magnitude. (see Table AB1). For some liquids no thermal conductivity data are available, and this effect could be useful in the determination of thermal conductivities if absorbing impurities were added until the limiting case $\delta l \rightarrow \infty$ were reached.

Table AB1.

Liquid	$\frac{\delta n}{\delta T}(40)$ ($\times 10^{-4}$)	$K(17)$ ($\frac{W}{cm \cdot degK}$)	$n_o(40)$	a_o (cm)	P_o (mW)	δ (cm^{-1})
$C_6H_5NO_2$	4.6	1.5×10^{-3}	1.55	0.03	74	0.99×10^{-3}
C_6H_5Br	4.8	1.1×10^{-3}	1.56	0.03	74	0.67×10^{-3}
C_6H_5F	4.9	1.3×10^{-3}	1.47	0.03	74	2.2×10^{-3}
$C_6H_5NH_2$	5.1	1.72×10^{-3}	1.59	0.03	70	4.9×10^{-3}
p-xylene	5.2	1.3×10^{-3}	1.49	0.03	74	0.86×10^{-3}

Thermal defocussing was also observed in benzonitrile, and very strongly in benzoyl chloride, but thermal conductivity data were not available for these liquids.

The presence of absorbing impurities can greatly increase the amount of thermal defocussing. The temperature change produced by the effect in a liquid has been estimated by Gordon et al (78) to be of order 0.1 degK. under conditions similar to those pertaining in these scattering experiments. This is by no means insignificant in very accurate work.

The interference patterns seen in the light passed through polaroid and photographic film was not reproducible if the beam was intercepted and reintroduced, except after the melting had taken place. This indicates that even if the power absorbed is not great enough to melt the solid, a small amount of permanent damage takes place which is not perceptible to the naked eye.

This effect could possibly be used to measure small absorption coefficients, of liquids, and thermal conductivities as mentioned above.

